UNIVERSITY OF CALIFORNIA
RIVERSIDE

Investigation of Solid Particle Number Measurement of Engine Emissions

A Dissertation submitted in partial satisfaction
of the requirements for the degree of

Doctor of Philosophy

in

Mechanical Engineering

by

Zhongqing Zheng

June 2012

Dissertation Committee:

Dr. Heejung Jung , Chairperson
Dr. Hideaki Tsutsui
Dr. Masaru Rao

The Dissertation of Zhongqing Zheng is approved:

Committee Chairperson

University of California, Riverside

Acknowledgments

Without the support from many people, it would have been impossible for me to finish my study and dissertation at the College of Engineering - Center for Environmental Research and Technology (CE-CERT), University of California Riverside.

I would like to express my deepest gratitude to my advisor, Dr. Heejung Jung, for his excellent guidance, caring, and providing me with an excellent atmosphere for doing research. His wide range of knowledge, innovative ideas, and kindness gave me the best support I can have to succeed on both academical and personal sides in the past 5 years.

Drs. Tom Durbin, Kent Johnson, Wayne Miller, David Cocker, and Akua Asa-Awuku helped me develop many skills necessary for working at CE-CERT and for surviving in my career. Dr. Paul Ziemann at the Chemistry Department of University of California Riverside provided insightful comments on the study. Drs. David Kittelson and Jacob Swanson at University of Minnesota are gratefully appreciated for their comments and suggestions on this study. I would also like to thank Drs. Alberto Ayala, Jorn Herner, Shaohua Hu, Tao Huai, Ajay Chaudhary, and William Robertson at California Air Resources Board for their help. Dr. Martyn Twigg at Johnson Matthey is also acknowledged for the catalyst he provided for the catalytic stripper. I also appreciate the help from Dr. Georgios Karavalakis, Mr. Donald Pacocha, Mr. Joe Valdez, Mr. Bill Welch, Mr. Edward O' Neil, Mr. Kurt Bumiller, and Mr. Chuck Bufalino at CE-CERT.

Many students and colleagues at CE-CERT were a great resource for me to get different perspectives. A non-exhaustive list of students and postdoc scholars whom I have enjoyed working with includes Dr. Manishkumar Shrivastava, Haowei Wu, Anh Nguyen, Ehsan Hosseini, Zhihua Liu, Mike Grady, Yusuf Khan, Sam (Tanfeng) Cao,

Shunsuke Nakao, Xiaochen Tang, Ping Tang, Li Qi, Maryam Hajbabaei, Nick Gysel, Dr. George Scora, and Dr. Guoyuan Wu.

My parents and my parents-in-law are always supportive. My daughter always brings me joy. I would also like to thank the numerous help I and my family get from my granduncle and his family. My special thanks belong to my wife, without whom I could not be where I am now.

To My Wife

Huihui Lv

ABSTRACT OF THE DISSERTATION

Investigation of Solid Particle Number Measurement of Engine Emissions

by

Zhongqing Zheng

Doctor of Philosophy, Graduate Program in Mechanical Engineering
University of California, Riverside, June 2012
Dr. Heejung Jung , Chairperson

As diesel PM regulation gets more stringent, the current gravimetric method which has been used for legal determination of PM mass for vehicle emissions will have difficulty accurately quantifying PM mass emissions. Progress in regulating diesel PM emissions by non-gravimetric means has been made in the Europe. The method, so called particle measurement program (PMP) protocol specifies counting solid particles larger than 23 nm. This method has already been adopted for Euro V and VI to regulate light-duty and heavy-duty vehicle emissions and it is also expected to be adopted to regulate emissions for aviation section. However, exclusion of sub-23 nm particles poses some potential issues. In this thesis, the PMP method was investigated with a focus on finding the nature of sub-23 nm particles which are excluded in the current PMP protocol.

A PMP-compliant system, an AVL advanced particle counter (APC) and an alternative volatile particle removal system, a catalytic stripper (CS) were evaluated and compared for measuring solid particle number emissions in chapters 2 and 3. The evaluations and comparisons were conducted using sulfuric acid and hydrocarbon particles as model volatile particles in laboratory tests, and diluted exhaust from a diesel par-

ticle filter (DPF)-equipped heavy-duty diesel vehicle operated on a heavy-duty chassis dynamometer under steady speed conditions at two different engine loads. This study also compared particulate matter (PM) mass and particle number (PN) emissions from a heavy-duty diesel vehicle operating over the urban dynamometer driving schedule (UDDS) and actual on-road flow-of-traffic driving conditions, including two uphill (phases 1 and 2) and two downhill (phases 3 and 4) segments. The UDDS and on-road flow-of-traffic tests represent a broader engine operating conditions than those currently certified emissions testing cycles.

For the laboratory test, both the APC and CS removed more than 99% of the volatile particles in terms of PN when using aerosols composed of pure sulfuric acid or hydrocarbons. When using laboratory test aerosols consisting of mixtures of sulfuric acid and hydrocarbons more than 99% of the particles were removed by the APC but the surviving particles were no longer entirely volatile, with 12–14% being solid.

For the chassis dynamometer test, PN emissions of particles between 3 and 10 nm downstream of the APC were $\sim$2 and 7 times higher than the PN emissions of particles above 10 nm at the 74 and 26% engine load, respectively. At the 26% engine load, PN level of the 3 to 10 nm particles downstream of the APC were significantly higher than that in the dilution tunnel, demonstrating that the APC was making 3 to 10 nm particles. The PN emissions of 3 to 10 nm particles downstream of the APC were related to the heating temperature of the APC evaporation tube, suggesting these particles are artifacts formed by renucleation of semivolatiles. Considerably fewer particles between 3 to 10 nm were seen downstream of the CS for both engine loads due mainly to removal of

semivolatile material by the catalytic substrates, although some of this difference could be attributed to diffusion and thermophoretic losses.

Chapter 4 provides an evaluation of the nature of sub 23 nm particles downstream of the European PMP methodology with prescribed cycles and on-road flow-of-traffic driving conditions. Particle number concentrations and size distributions were measured using two PMP measurement systems in parallel. For this analysis, the focus is on the real-time results from multiple instruments. The results revealed that a significant fraction of particles downstream of both PMP systems for all tested cycles were below 11 nm. The fraction of sub 11 nm particles observed downstream of the PMP system decreased when the overall dilution ratio of one PMP system was increased from 300 to 1500, suggesting those sub 11 nm particles were formed through re-nucleation of semivolatile precursors. When the evaporation tube temperature was increased from 300 to 500°C, no difference in particle number concentrations was observed, suggesting incomplete evaporation of semivolatile particles did not contribute to those sub 11 nm particles. Particle emissions were about one order of magnitude higher during flow-of-traffic driving along a highway with a steep grade than during the prescribed driving cycles. During the same flow-of-traffic condition, a sudden jump of PMP operationally defined solid particle concentration was observed, while the accumulation mode particle concentrations in the constant volume sampling (CVS) tunnel measured by engine exhaust particle sizer (EEPS) only showed a slight increase. This discrepancy was attributed to the extensive growth of the re-nucleated particles downstream of the PMP systems.

In chapter 5, the PMP system was evaluated over a standard laboratory testing cycle and uphill and downhill on-road, flow-of-traffic driving conditions. The PM mass emissions for the UDDS and on-road tests were more than 6 times lower than the U.S. 2007 heavy-duty PM mass standard. The PM mass emissions for the UDDS fell between those for the uphill and downhill driving on-road driving conditions. The PN emissions of particles larger than 23 nm for the UDDS and downhill on-road driving conditions were $\sim$3 times lower than the Euro VI heavy-duty PN limit for transient cycles, while the PN emissions from the uphill on-road driving conditions were $\sim$4 to 5 times higher than the Euro VI PN limit. The PN emissions of particles larger than 23 nm for the UDDS (with an average engine load of 38%) were comparable in magnitude to those for the phase 3 downhill segment (with an aveage engine load of 40%) of the on-road test, and were 25% lower than those for the phase 4 downhill segment (with an avearage engine load of 18%) of the on-road test. The variability of the PN emissions of particles larger than 23 nm ranged from 10 to 40% for the UDDS and on-road tests, comparable to that found in the European PMP study.

Contents

List of Figures

List of Tables

1 Introduction

1.1 Diesel particulate matter

Diesel engines are widely used in the United States (U.S.) for transportation to power trucks, buses, and trains. It is known that diesel engines have higher thermal efficiencies than gasoline engines. Diesel engine particle emissions have been of great concern to researchers, engine manufacturers, and regulatory agencies due to their adverse health effects. Many studies have associate diesel engine particle emissions with acute and chronic health effects in human beings [4, 5, 6, 7].

Diesel engine emitted particles are mainly consisted of elemental carbon (i.e., soot), ash, volatile organics, and sulfur-containing compounds. Figure 1.1 shows a artist's conception of diesel engine emitted particles. Soot are fractal-like agglomerates. Volatile organics and sulfur-containing compounds are typically condensed on the surface of soot particles.

Diesel particles can range from below 10 nm to 10 μm. It is usually described by a lognormal, trimodal particle size distribution. A typical and generic diesel particulate matter size distribution is shown in Figure 1.2. The figure shows three distinctive modes: nucleation, accumulation, and coarse mode.

Nucleation mode particles are primarily in the size range of below 30 nm [8]. They are consisted of volatile organics and sulfur-containing compounds and formed during the dilution and cooling process of diesel engine exhaust. The formation of nucleation mode particles is a nonlinear function of temperature and dilution ratio of the exhaust

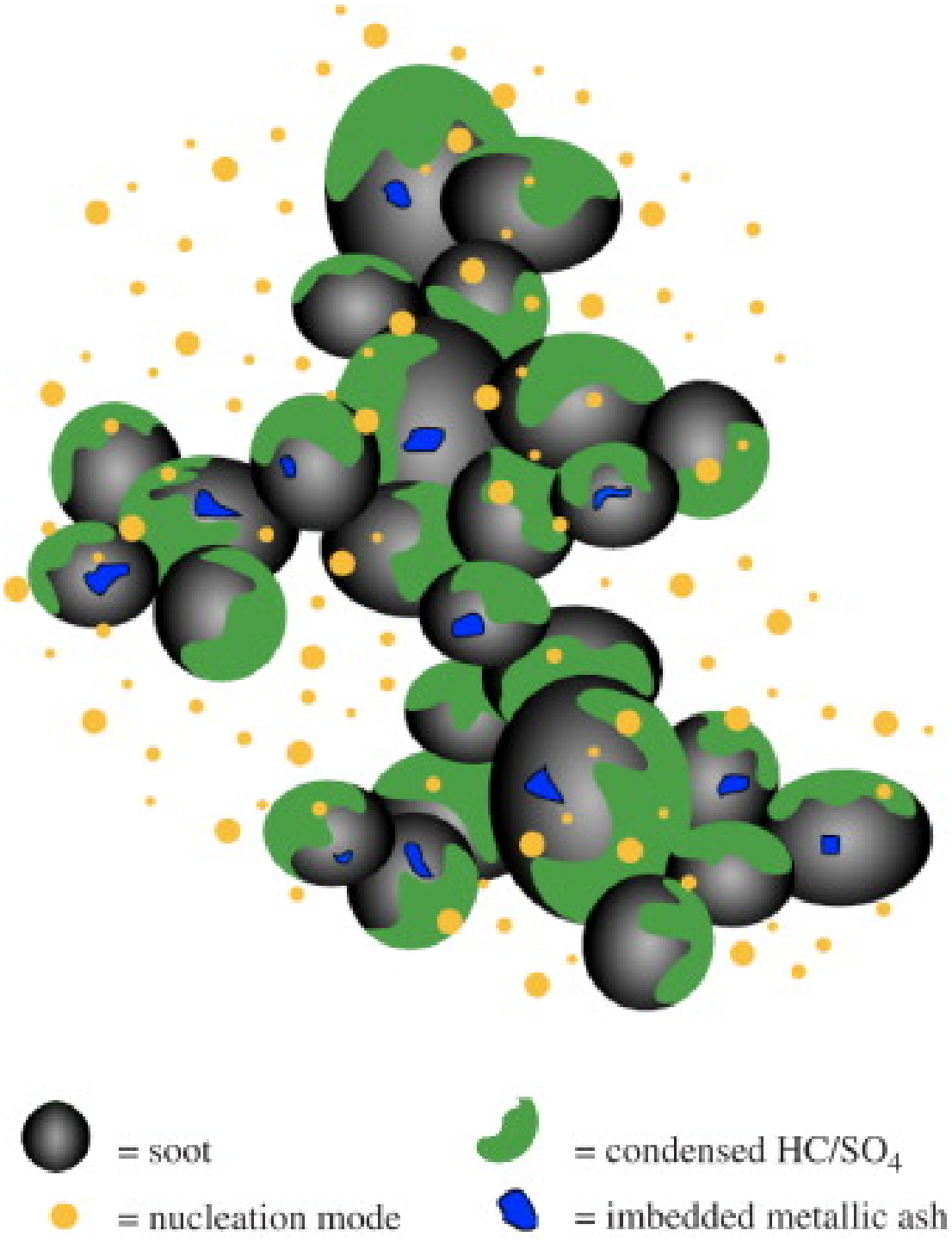

Figure 1.1: Artist's conception of diesel particulate matter [1].

and it can be strongly affected by the use of diesel emissions aftertreatment systems. The nucleation mode particles usually consist of 1–20% of the particle mass and more than 90% of the particle number [2] of total diesel particulate matter emissions.

Accumulation mode particles are mainly soot particles with some condensed volatile hydrocarbons and sulfur containing compounds. Typical size ranges of soot particles are between 30 nm and 1 μm. Soot particles are fractal like agglomerates made of primary soot particles, which typically have diameters of 20–30 nm. Accumulation mode particles usually consist of less than 15% of the particle number and more than 80% of the particle mass of total diesel particles emissions.

Coarse mode particles are mostly wearing metals and re-entrained agglomerates.

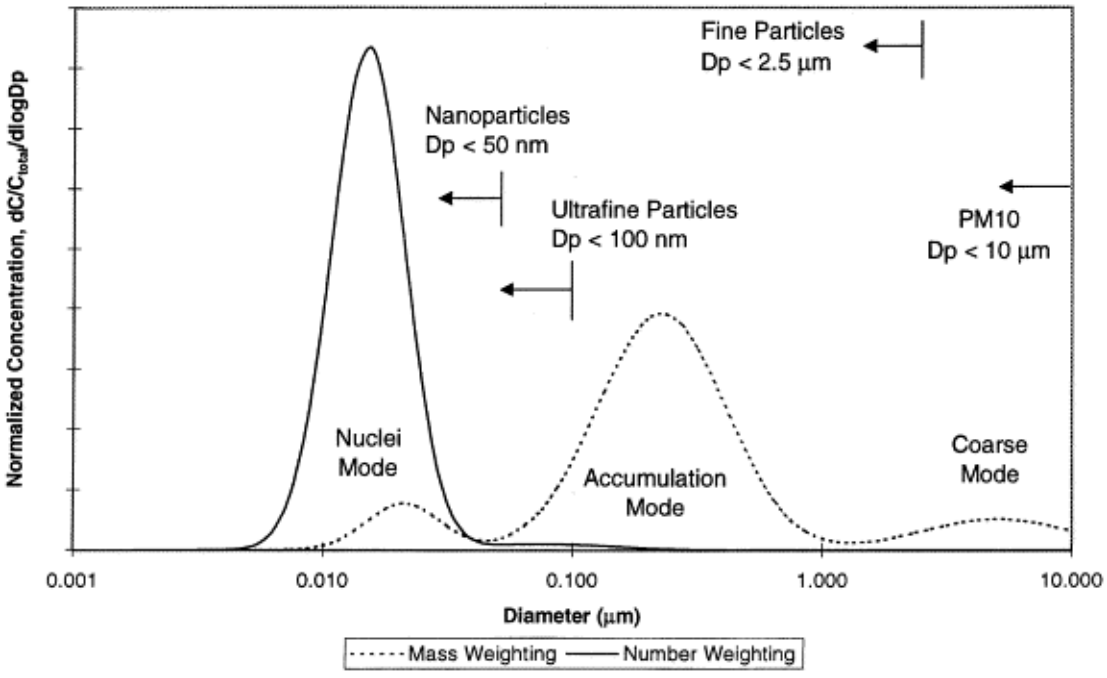

Figure 1.2: Typical diesel particulate matter size distribution [2].

1.2 Diesel particulate matter regulations

Traditionally, diesel particulate matter is regulated by the gravimetric method. Figure 1.3 shows a typical sampling setup for measuring PM emissions from an engine. Engine exhaust is first introduced to a constant volume sampling system (CVS), where the exhaust is diluted by filtered air. The typical dilution ratio of the CVS is below 10:1. Then a portion of the diluted exhaust is extracted from the CVS and diluted a second time, after which PM is collected onto a filter. The filter is weighted before and after collecting PM samples to determine the PM emissions from the engine.

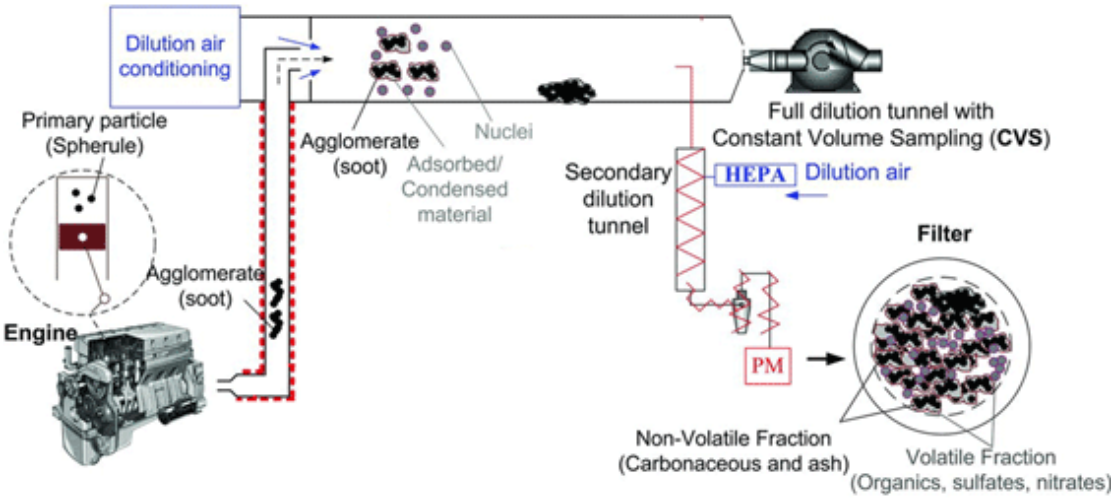

Figure 1.3: Diesel particulate matter sampling by gravimetric method, modified from [3].

Figure 1.4 shows the PM regulations in the United States (U.S.). The U.S. started regulating diesel PM in 1988, when the diesel PM standard was 0.6 g/hp-h. Since then, the PM regulation has become more and more stringent. The latest diesel PM standard was implemented in 2007 and it was 0.01 g/hp-h, which is a 98% reduction from the

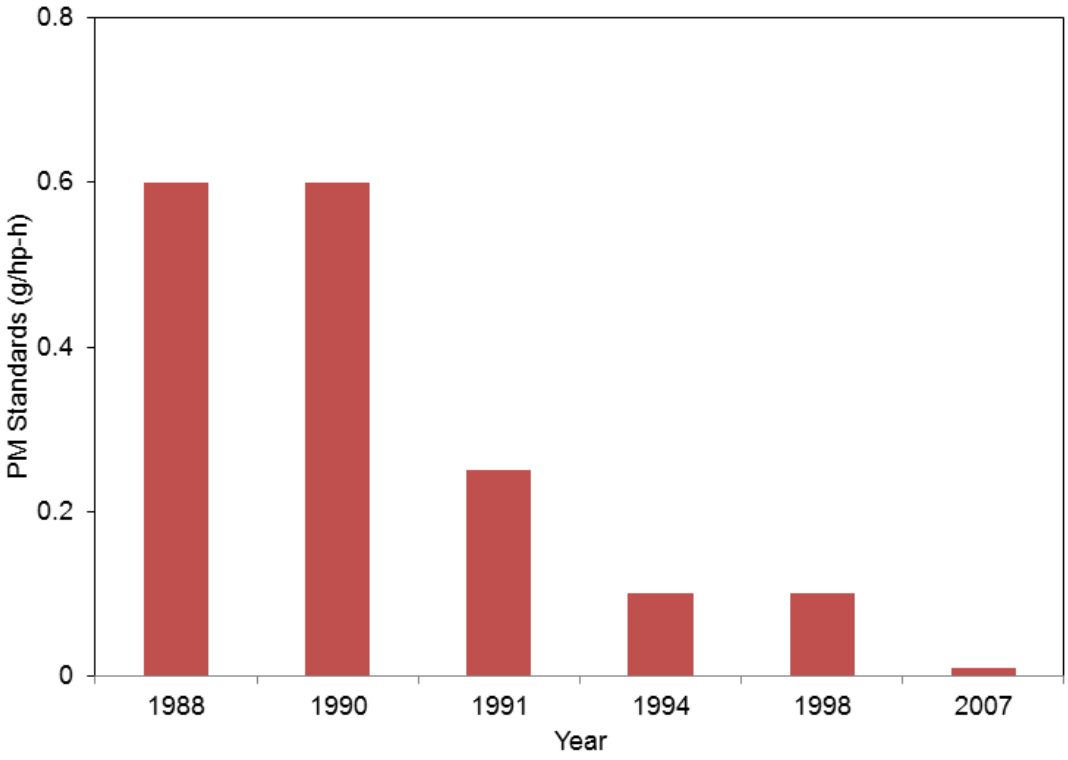

Figure 1.4: US diesel particulate matter regulations.

1988 standard. The European Union has a diesel PM standard at the similar level to that of the U.S..

1.3 Motivation and significance

As regulation of diesel particulate matter mass gets more stringent, the current gravimetric method for the legal determination of emissions will have difficulty accurately quantifying particulate matter mass emissions. Although the U.S. Environmental Protection Agency (EPA) issued an improved protocol for the gravimetric method [9], accuracy will continue to be an issue at the very low emission levels of new diesel vehicles equipped with aftertreatment systems. At the Euro IV heavy-duty engine limit of 0.02 g/kWh, for example, the variabilities of the repeatability and reproducibility of the current gravimetric method are more than 20 and 50%, respectively [10].

Progress in regulating diesel particle emissions by non-gravimetric means has been made in Europe. The United Nations Economic Commission for Europe-Group of Experts on Pollution and Energy (UNECE-GRPE) initiated the Particle Measurement Programme (PMP) working group to develop new particle measurement techniques to supplement or replace the current gravimetric method. The PMP protocol specifies measuring solid particles larger than 23 nm. Solid particles are operationally defined by the PMP as particles that can survive after passing through an evaporation tube (ET) that has a wall temperature of 300–400°C [11, 12].

A solid particle number concentration limit of 6×10^{11} particles/km has been included in the Euro 5/6 standards for light-duty diesel vehicles [13]. The Euro VI standard for heavy-duty diesel vehicles includes a solid particle number concentration limit as well, with the proposed limits of 8×10^{11} particles/kWh for stationary cycles and 6×10^{11} particles/kWh for transient cycles [14].

Volatile particles in the nucleation mode are very difficult to measure in a repeatable manner [2, 15]. To enhance the repeatability and accuracy of the particle number measurement, the PMP group decided to eliminate the volatile particles and measure only solid particle number emissions. The PMP protocol also specifies that only particles larger than 23 nm are measured to eliminate any possible contribution from nucleation mode particles.

Exclusion of sub 23 nm particles may have some potential issues, since not all sub 23 nm or nucleation mode size range particles are volatile. Some studies have found that solid particles in the nucleation mode from heavy-duty diesel vehicles operating at idle or low loads [16, 17]. Even at high load operating conditions, solid particles in the

nucleation mode have been observed for heavy-duty diesel vehicles [18, 19, 20]. These references [16, 17, 18, 19, 20] also define non-volatile or solid particles as particles that can survive after passing through a thermodenuder [21], but with a slightly larger temperature operating range of 270–400°C compared with the PMP. By excluding these sub 23 nm solid particles, the full impact of solid particles is not characterized by the PMP standard [22]. Regulating particle number emissions for other sectors (aviation, off-road) is under discussion [23]. If the current PMP protocol were applied to other sectors, further caution should be taken in excluding sub 23 nm solid particles. For example, solid nucleation mode particles have been found for a gasoline vehicle, when some anti-knock metal additives were used [24]. Lead anti-knock additives are also still used in gasoline for general aviation. Czerwinski et al. [25] even found solid particles below 23 nm emitted from 2-stroke mopeds.

It is also reported that the PMP can remove almost all volatile components of diesel vehicle emissions, and that no nucleation can occur downstream of the PMP [23]. However, during previous California Air Resource Board/University of California Riverside (CARB/UCR) studies of the PMP, a significant number of appeared-to-be solid sub 23 nm particles were found downstream of the PMP volatile particle remover under conditions that were thought to be unlikely to form sub 23 nm solid particles [26, 27]. In the exploratory work for applying the current PMP protocol to heavy-duty diesel engines, Giechaskiel et al. [28] also found apparently non-volatile sub 23 nm particles downstream of the PMP system. Thus, it is important to investigate whether these sub 23 nm particles observed downstream of the PMP system are solid or volatile, and if they are solid, whether they come from the exhaust or are artifacts of the measurement system.

An alternative system commonly used by researchers to remove volatile particles is a catalytic stripper (CS) [29, 30, 31, 32, 33]. In contrast to the PMP system, the CS uses a different approach to remove volatile particles. It removes all volatile hydrocarbon components and sulfur components by catalytic reactions at an elevated temperature. Therefore, the chance of renucleation is much lower downstream the CS. A study comparing the volatile removal efficiency of a CS with a thermal denuder, which is another type of volatile particle remover, showed that the CS has a higher efficiency for removing volatile particles [32]. However, no studies have been conducted to compare the PMP system with a CS in terms of volatile particle removing efficiency.

This study presents a comprehensive investigation of two solid particle number measurement systems, the PMP system and the CS system. An overview of this thesis is given in the following section.

1.4 Overview

Chapter 2 presents laboratory experiments of volatile particle penetration/formation in the PMP system and the CS. The effectiveness of the European PMP system and the CS in removing volatile aerosols using volatile aerosols generated in the laboratory were investigated and compared. Chapter 2 advances our understanding of the nature of sub 23 nm particles downstream of the PMP system in a controlled laboratory environment. Chapter 3 presents diesel vehicle particles penetration/formation in the PMP system and the CS, using diluted exhaust from a heavy-duty diesel vehicle, equipped with a Johnson Matthey Continuously Regenerating Trap (CRT™), operating over various cycles on a chassis dynamometer. Chapter 4 presents a unique study to evaluate the performance of the PMP methodology over a wide range of on-road driving conditions.

Chapter 4 aims to evaluate the PMP methodology based on real-time data to answer the following questions: 1) How do sub 23 nm particle concentrations vary over different testing conditions? 2) What is the nature of sub 23 nm particles? Embedded in the answers to these questions is a suggestion that, with currently available instrumentation, such as CPCs with cut off diameters smaller than 23 nm, the fraction of the emission aerosol that is smaller than 23 nm can be measured and, hence, evaluated. Findings from this study also provide information on why it is difficult to obtain repeatable sub 23 nm particle measurements with the PMP protocol, on instrument comparisons, and on the nuances of constant volume sampling (CVS) and the two PMP systems. Chapter 5 examined PM and PN emissions from a heavy-duty diesel vehicle equipped with a Johnson Matthey Continuously Regenerating Trap (CRT™) over well-designed on-road flow-of-traffic driving conditions and a standard testing cycle, the urban dynamometer driving schedule (UDDS). The main objective is to answer how PM and PN emissions vary under on-road driving and a standard testing cycle. The changes in PN emissions of particles larger than 23 nm, as well as of particles smaller than 23 nm, were characterized for different driving conditions in chapter 5.

2 Evaluating the solid particle number measurement systems using volatile particles

2.1 Solid particle measurement systems

2.1.1 PMP measurement system

The PMP system used in the current study was an AVL particle counter advanced (APC), a commercial solid particle measuring system developed by AVL LIST GmbH. A schematic of the APC is shown in Figure 2.1. The APC fulfills the most recent requirements of the PMP protocol [11, 12]. A brief description of the APC is provided here. More detailed schematics and descriptions of the APC can be found in reference [34] and the manual of the APC. The sample enters the system with a typical flow rate of 5 Lpm (liters per minute) and is diluted by a primary chopper diluter, which has a rotating disk diluter with a dilution ratio ranging from 10 to 1000. The diluted sample has a flow rate of 1 Lpm, and is transferred to the ET through a 2 m line. The dilution air, the primary chopper diluter, and the 2 m line are all operating at 150°C. The ET has a wall temperature of 350°C. A secondary, perforated, tube diluter that dilutes the sample with ambient temperature air follows the ET. The secondary dilution ratio is usually set at 10. A TSI 3790 condensation particle counter (CPC), with a lower 50% cut off diameter (D50) of 23 nm, then measures the particle number concentration of the sample. The outlet flow rate of the APC was $\sim$8.5 Lpm.

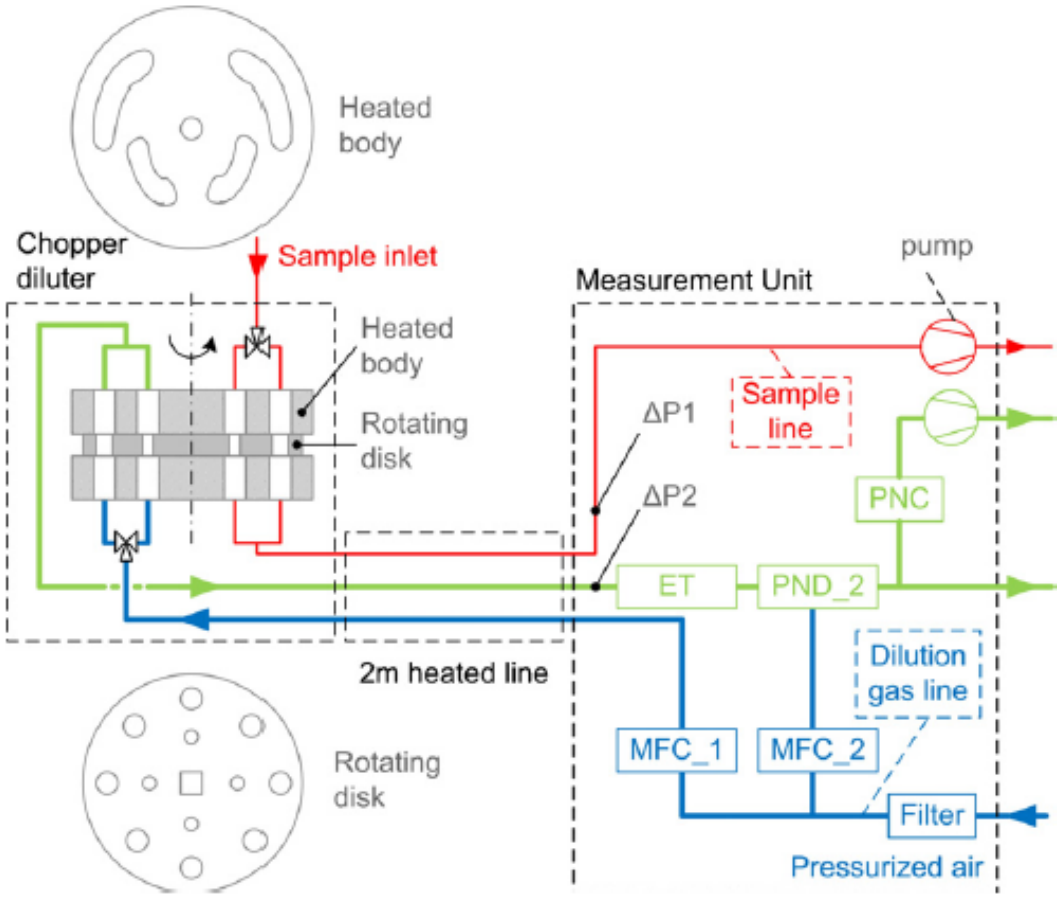

Figure 2.1: Schematic of the APC from the instrument manual.

2.1.2 Catalytic stripper

The catalytic stripper (CS) used in the current study is similar to others described elsewhere [29, 35]. Stenitzer [35] provides a more complete description of the theory, design, and operation of the CS. A brief description of the CS is provided here and a schematic of the CS is shown in Figure 2.2. The CS uses two different catalysts, provided by Johnson Matthey, to remove sulfur components and hydrocarbon components, respectively, from the diesel exhaust. The catalyst that removes hydrocarbon components by oxidation is called an Oxicat and the catalyst that adsorbs sulfur components is called a S-trap. The sample passes by the Oxicat first and then S-trap. Both the S-trap and Oxicat are heated to 300°C. Afterwards, a cooling coil cools down the sample to ambient temperature. There are no specific requirements on the flow rate through the CS. In the current study, a flow rate of 10 Lpm was used.

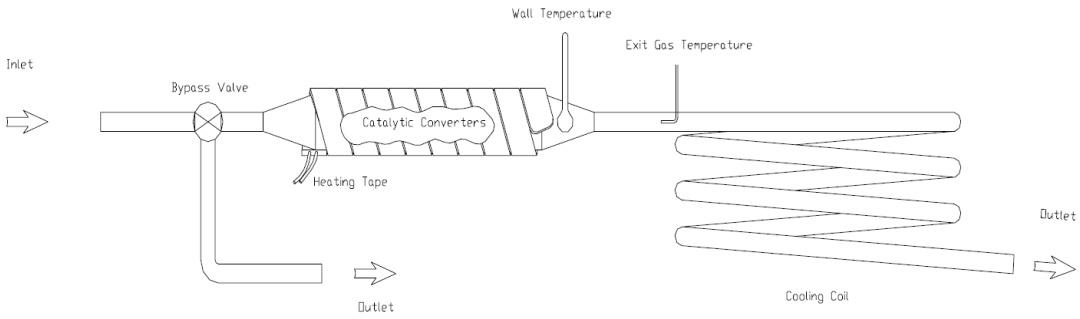

Figure 2.2: Schematic of the CS.

2.2 Test aerosols

For the laboratory tests, aerosols with four different compositions were utilized to evaluate the response of the APC and CS systems under controlled conditions. The aerosol compositions included pure sulfuric acid, pure tetracosane (C_{24} n-alkane), a

mixture of sulfuric acid and tetracosane, and a mixture of sulfuric acid and tetracontane (C_{40} n-alkane). These aerosols were chosen as model aerosols to allow comparisons with the PMP protocol for determining volatile removal efficiency, and to mimic real diesel particulate filter (DPF)-out semivolatile diesel particles. The PMP protocol specifies tetracontane (C_{40} n-alkane) particles as the model aerosol to evaluate the volatile removal efficiency of PMP compliant systems [34]. Biswas et al. [36] reported semivolatile particles downstream of a DPF are mainly composed of sulfate, hydrocarbons, and some ammonium, the source of which could not be identified. It was expected that the particles seen downstream of the continuously regenerating trap (CRT™) in the chassis dynamometer tests here would also have a similar composition. Sulfuric acid and hydrocarbons are model aerosols that have been used by other researchers to evaluate the volatile removal efficiencies of PMP-like systems [37, 32].

2.3 Experimental setup

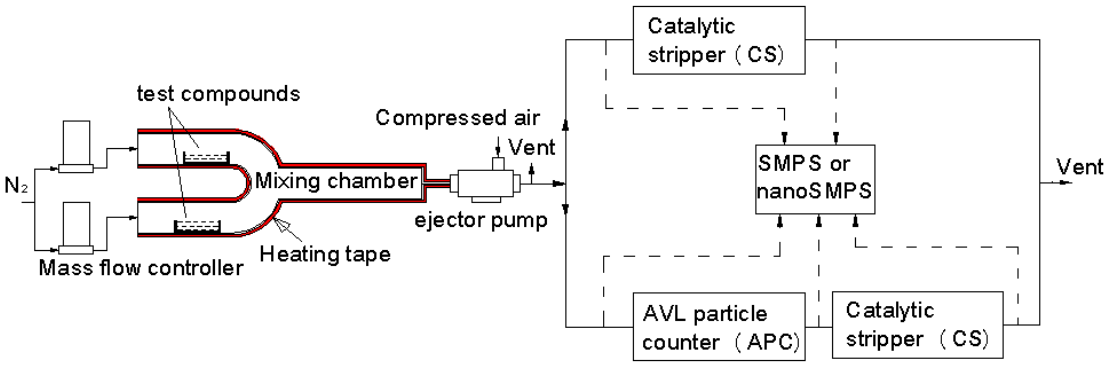

Figure 2.3: Schematic of laboratory test setup

Test aerosols were generated using an evaporation and condensation method [32], as shown in Figure 2.3. Liquid sulfuric acid (73–98%, Fisher Scientific), tetracosane powder (99%, Acros Organics), or tetracontane (90–100%, MP Biomedicals) powder were placed in an alumina crucible, which was then placed in the two parallel stainless steel tubes of a Y shaped apparatus. These compounds were heated to temperatures sufficient to evaporate them, which were 121, 150, and 160°C for sulfuric acid, tetracosane, and tetracontane, respectively. The temperatures were chosen to provide stable and appropriate mass concentrations. Nitrogen gas with a flow rate of 0.5 Lpm carried vapors of these compounds to a mixing chamber that was heated to 250°C. The actual mass ratio of mixtures of different compounds was unknown, however. The vapors were cooled and diluted by an ejector pump (TD 110H, Air-Vac Engineering) after the mixing chamber. Compressed air with a gauge pressure of 30 pound-force per square inch (psi) was supplied to the ejector pump. The compressed air was conditioned by a TSI filtered air supply (model 3074B) to remove oil droplets, moisture, and fine particles. Nanoparticles were formed by nucleation and grew by condensation of the cooled vapors.

These nucleated aerosols were then fed into the APC and CS to evaluate their performances in removing volatile particles. Three setup configurations were employed, the APC alone, the CS alone, and the APC-CS in combination. For the APC-CS configuration, aerosols passed through the APC and CS in series. In the APC-CS configuration, the volatile particle removing efficiency of the APC and the volatility of the particles exiting the APC were evaluated. Particle size distributions were measured by either a nano scanning mobility particle sizer (nanoSMPS) or a regular SMPS. The nanoSMPS

consists of a TSI 3085 nano differential mobility analyzer (nanoDMA) and a TSI 3776 condensation particle counter (CPC), and the SMPS consists of a TSI 3081 DMA and a TSI 3776 CPC.

2.4 Results

The laboratory experiments are an important part of this study, because they allow the formation process of sub 23 nm particle to be investigated using model aerosols under well-controlled conditions. This provides an important link to the vehicle exhaust testing with the chassis dynamometer and on-road flow-of-traffic testing portions in this study and the on-road testing in our previous study [27], both of which showed that a significant fraction of the particles downstream of the PMP were in the sub 23 nm size range.

The number concentrations with 95% confidence limits for all the laboratory tests are summarized in Table 2.1. Total particle number concentrations were obtained by integrating the particle size distributions over all size bins. The size ranges were 3–70 nm and 7–191 nm for nanoSMPS and SMPS, respectively. For all the tests, the upstream aerosol mass concentrations were on the order of 100 $\mu g/m^3$, assuming a particle density of 1 g/cm^3. The upstream particle size distributions had peaks around 15, 60, and 40 nm, respectively, for aerosols composed of pure sulfuric acid, pure tetracosane, and the mixture of sulfuric acid and tetracosane. Particle size distributions for the APC-CS test using a mixture of sulfuric acid and tetracontane are also shown in Figure 2.4. Background concentrations for the laboratory test were checked by turning the heater off and

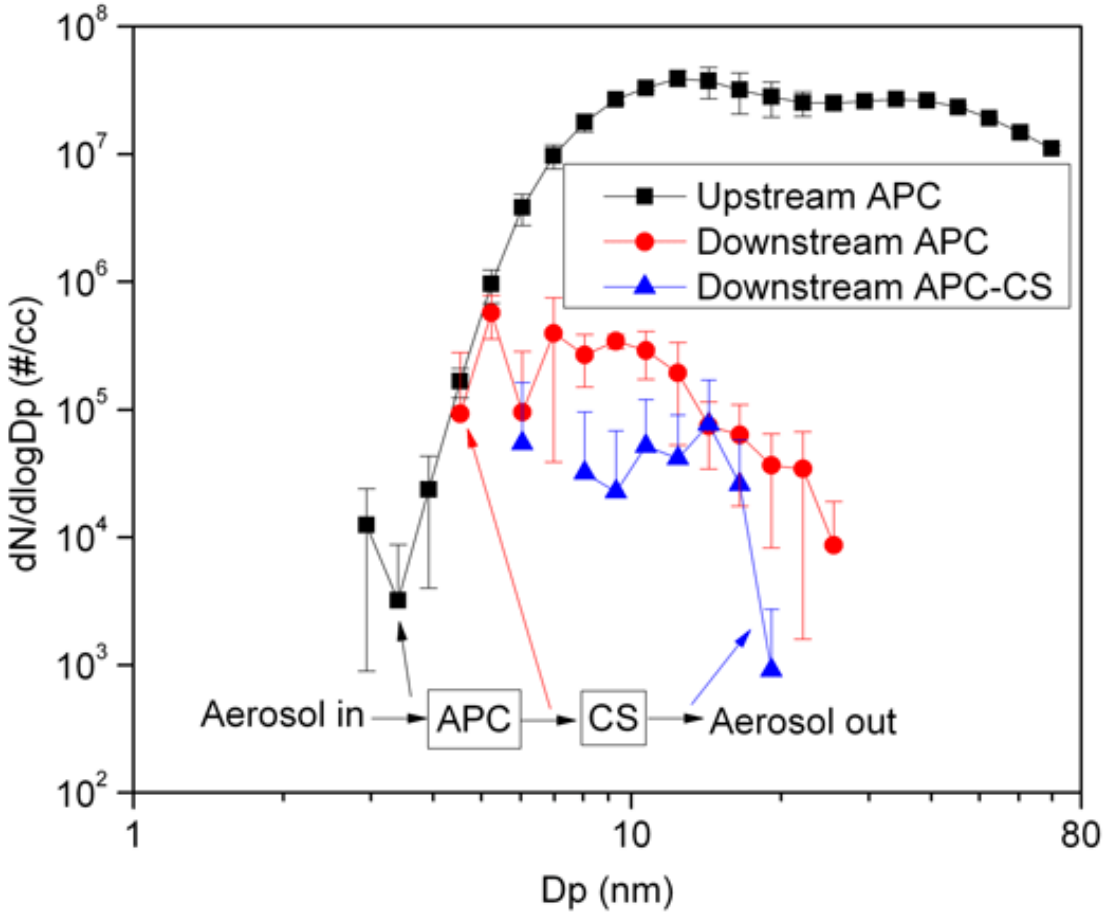

Figure 2.4: Particle size distributions from the laboratory test using mixture of sulfuric acid (H_2SO_4) and tetracontane (C_{40} n-alkane).

measuring the particle size distributions. No particles were seen under this condition for either the CS or APC-CS configurations.

When aerosol composed of pure sulfuric acid was used, both the APC and CS removed more than 99.9% particles by number concentration. When using aerosols composed of pure tetracosane, the APC and CS removed 98.9 and 99.9% particles, respectively. When aerosol composed of a mixture of sulfuric acid and tetracosane was used, the APC and CS removed 99.8 and 99.4% particles, respectively.

For the APC-CS test, no particles were seen downstream of the APC-CS when an aerosol composed of pure sulfuric acid or pure tetracosane was used. When using aerosol composed of a mixture of sulfuric acid and tetracosane for the APC-CS test, a small number of particles were found downstream of both the APC and the APC-CS. As discussed above, the APC removes 99.8% of these particles, of the remaining 0.2% that is then put through the CS, 14.2%, on a number concentration basis, were also observed downstream of the CS or APC-CS combination. This suggested that at least 14.2% of those particles downstream of the APC were non-volatile for the following reasons. First, the concentration of volatile material in the gas phase downstream of the APC was greatly reduced by dilution. Secondly, volatile particles that survive the APC will be reduced in size and easier to evaporate than the upstream particles. Thirdly, the CS has been shown to remove volatile materials effectively even with high inlet concentrations [32]. Finally, the penetration of solid particles through the CS is less than 100%, so that if 14.2% of the particles penetrates, the actual solid fraction must be greater than that. The remaining 85.8% of the particles downstream of the APC, were

likely predominately volatile, and could be due to renucleation of volatile particles in the APC.

The APC-CS test was also carried out using an aerosol composed of a mixture of sulfuric acid and tetracontane. Like the mixture of sulfuric acid and tetracosane test, the APC removed nearly all of the particles, in this case 99.4%. Particles exiting the APC were then fed into the CS and of these, 12.4% penetrated through the CS, indicating at least 12.4% of those particles exiting the APC were non-volatile. The fact that non-volatile particles were observed downstream of the APC when aerosols composed of mixtures of sulfuric acid and hydrocarbons, which are both volatile, were used suggests that non-volatile particles were formed in the APC from volatile species. This result was similar to what Swanson and Kittelson [32] reported in their thermal denuder and CS study, where they found solid particles were formed in the thermal denuder from sulfuric acid and hydrocarbons.

In our previous study [27], the majority of particles downstream of the PMP were in the sub 23 nm size range. Based on the operational definition of solid particles for the PMP method, this means the PMP method is not counting the majority of solid particles, which could be problematic. The laboratory tests show that solid particles are formed with mixtures of sulfuric acid and hydrocarbons that are likely found in real exhaust, but would not be characterized in the tetracontane only volatile removal efficiency tests that are currently in the PMP legislation [34]. The results from the lab experiments also showed that a majority of sub 23 nm particles below the APC are likely re-nucleated semivolatile particles, with some non-volatile solid particles, based on the APC-CS study.

Table 2.1: Summary of laboratory test results. *Note*: particle number concentrations are shown with 95% confidence limits.

Aerosol	Config.	Concentration (particles/cm^3)				Dilution ratio		Instrument
		Upstream	Downstream APC	Downstream CS	Downstream APC-CS	Primary	Total	
H_2SO_4	CS	$3.4 \times 10^7 \pm 2.5 \times 10^5$	-	$2.3 \times 10^2 \pm 2.2 \times 10^2$	-	-	1	SMPS
	APC-CS	$2.4 \times 10^7 \pm 2.3 \times 10^6$	$1.9 \times 10^3 \pm 3.7 \times 10^3$	-	$0.0 \times 10^0 \pm 0.0 \times 10^0$	50	500	SMPS
C_{24}	CS	$5.3 \times 10^6 \pm 3.4 \times 10^6$	-	$4.4 \times 10^3 \pm 3.8 \times 10^3$	-	-	1	SMPS
	APC-CS	$8.9 \times 10^5 \pm 5.4 \times 10^5$	$1.3 \times 10^4 \pm 1.3 \times 10^4$	-	$0.0 \times 10^0 \pm 0.0 \times 10^0$	50	500	SMPS
$H_2SO_4 + C_{24}$	CS	$9.3 \times 10^6 \pm 3.1 \times 10^5$	-	$5.7 \times 10^4 \pm 3.0 \times 10^4$	-	-	1	SMPS
	APC-CS	$3.3 \times 10^7 \pm 7.9 \times 10^6$	$2.5 \times 10^4 \pm 2.4 \times 10^4$	-	$9.2 \times 10^3 \pm 3.8 \times 10^3$	20	120	SMPS
	APC-CS	$2.6 \times 10^7 \pm 1.3 \times 10^7$	$5.0 \times 10^4 \pm 1.8 \times 10^4$	-	$7.2 \times 10^3 \pm 3.9 \times 10^3$	20	120	nanoSMPS
$H_2SO_4 + C_{40}$	APC-CS	$2.7 \times 10^7 \pm 2.4 \times 10^6$	$1.5 \times 10^5 \pm 4.4 \times 10^4$	-	$1.9 \times 10^4 \pm 5.8 \times 10^3$	20	120	nanoSMPS

2.5 Discussion

The nature of the solid particles found by using the CS to treat the aerosol downstream the APC is worth more discussion. The mechanism of this type of solid particle formation is not clear yet. It is known that n-alkanes, such as tetracontane and tetracosane, do not react well with sulfuric acid in gas phase [38], but Swanson and Kittelson [32] have proposed such reactions to explain this type of solid particle formation. Another hypothesis is that n-alkanes were oxidized on the hot metal tube walls heterogeneously and then reacted with sulfuric acid to produce a non-volatile salt. More studies are needed to thoroughly understand the mechanism of particle formation in the ET of the APC.

3 Evaluating the solid particle number measurement systems over steady state engine operating conditions

3.1 Setup

For the chassis dynamometer tests, the APC and CS were tested with exhaust generated by driving a heavy-duty truck on a chassis dynamometer. This provided actual exhaust to test the response of the systems, but under more controlled conditions than would be found under in-use driving. A schematic of the chassis dynamometer test set up is shown in Figure 3.1. The setup can be divided into two parallel systems, the CS system and the APC system. Both the CS and APC systems took samples from the same inlet. A cyclone was used on this inlet to remove particles bigger than 2.5 μm, in accordance with the PMP protocol. After the cyclone, tubes leading to the CS and APC were heated to 150°C, the same temperature used for the primary diluter of the APC. The APC was used following manufacturer's recommendations, as discussed earlier. On the CS side, an ejector pump (TD110H, Air-Vac Engineering) was used to pull exhaust through the CS. A 1 mm critical orifice and compressed air with a gauge pressure of 55 psi produced a flow rate through the CS of 10 Lpm. The exhaust was further diluted by a venturi pump after the ejector pump to avoid saturating the measurement instruments. The flow rate of the compressed air for the venturi pump was controlled by a mass flow controller, which was preinstalled in CE-CERT's Mobile Emissions Laboratory (MEL) [39]. The compressed air was produced by compressing ambient air with an Ingersoll Rand (Davidson, NC) OL5D5 oilless compressor. The compressed

air was further conditioned by a Speedaire refrigerated compressed air dryer (5UZ85, Grainger), a HANKiSON DHW series dryer system, and a HEPA filter. It should be pointed out that there was a difference between the APC and CS dilution systems. For the APC, exhaust in the constant volume sampling (CVS) dilution system was first diluted by the primary diluter, and then went into the ET, which is the key component of the APC, and then was diluted again by the secondary diluter. For the CS, exhaust in the CVS was sampled directly into the CS, without any dilution. All dilution on the CS side was done after the CS.

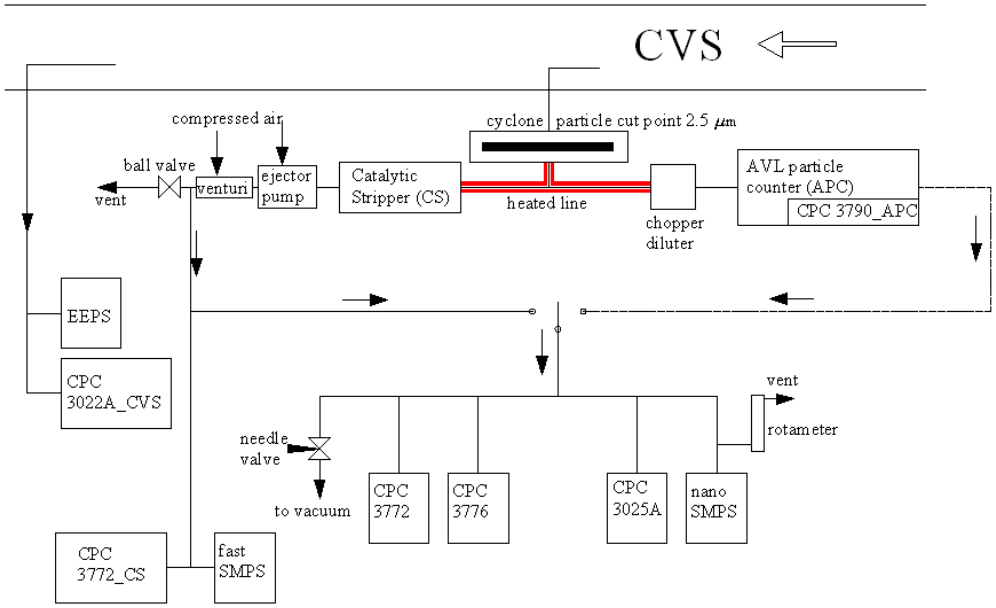

Figure 3.1: Schematic of chassis dynamometer test setup

An engine exhaust particle sizer (EEPS) spectrometer (TSI, 3090) and a 3022A CPC (labeled as CPC 3022A_CVS) were used to measure particle size distributions and total number concentrations of the diluted exhaust in the CVS tunnel. A 3790 CPC (labeled as CPC 3790_APC) is built into the APC by the manufacturer and it always sampled from the APC side. Similarly, a 3772 CPC (labeled as CPC 3772_CS) and

CE-CERT's fast-SMPS (labeled as fast-SMPS) were fixed to always sample from the CS side. One nanoSMPS and three CPCs with different cut off sizes were switched alternatively between the CS side and the APC side to measure size distributions and number concentrations. For the purpose of this report, this set of instruments is called the "alternating set". The three CPCs were a 3025A CPC, a 3776 CPC, and a 3772 CPC. The specifications of all these instruments are summarized in Table 3.1, including cut off sizes, maximum concentrations, and sample locations. All of the condensation particle counters (CPCs) used in this study were TSI products.

Table 3.1: Specifications of instruments used in this study.

Instrument	Cut off size (nm)	Max. Conc. (#/cc)	Sample location
CPC 3022A_CVS	7	9.99×10^6	Always at CVS
EEPS	5.6	-	Always at CVS
CPC 3790_APC	23	1×10^4	Always at APC
CPC 3772_CS	10	1×10^4	Always at CS
fast-SMPS	3	-	Always at CS
CPC 3025A	3	9.99×10^4	Switch either for CS and APC
CPC 3772	10	1×10^4	Switch either for CS and APC
CPC 3776	2.5	3×10^5	Switch either for CS and APC
nanoSMPS	3	-	Switch either for CS and APC

To minimize the effects of diffusion losses on the comparison between systems, efforts were made to equalize the diffusion losses among all the instruments. The EEPS and CPC 3022A_CVS shared one sample line and the split point was connected as close to the instruments'inlets as possible. The same plumbing configuration was applied to the CPC 3772_CS and fast-SMPS. A stainless steel manifold with six equal distance outlets was used in connecting the alternating set of instruments, so that the CPC 3776

and CPC 3025A had the same sample line lengths and flow rates. As mentioned earlier, the outlet flow rate of the APC was 8.5 Lpm, which was also the flow rate passing through the manifold. The flow rate through the manifold was controlled to 8.5 Lpm on both the APC and CS sides, which is the same as the outlet flow rate of the APC.

3.2 Test vehicles, fuels, lubricants

The vehicle and aftertreatment system used for the chassis dynamometer tests were the same as those used for the on-road test in CARB/UCR's previous study [27]. It was a 14.6 liter, 2000 Caterpillar C-15 engine equipped, Freightliner class 8 truck. A Johnson Matthey continuously regenerating trap (CRT™) was installed on the vehicle. The CRT™ is a passive DPF system that had previously been shown to provide sufficient levels of particles over driving conditions similar to those used in this experiment [27]. The truck was tested at a load of 65,000 lbs, which corresponds to the same load as for the on-road testing. The truck had a mileage of 41,442 miles at the beginning of the testing. CARB Ultra Low Sulfur Diesel (ULSD) fuel (S = 8 ppmw) and standard lubricating oil with sulfur level of 0.29% were used.

3.3 Test cycles

Two cruise cycles with extremely different nucleation mode particle number concentrations were tested. The two cycles both used a constant speed of 56 mph, one with a 26% engine load and the other with a 74% engine load. The 74% engine load cycle was performed right after the 26% engine load cycle.

3.4 Results

3.4.1 Particle measurements from the CVS

As the aerosol in the CVS was the source aerosol being fed into the APC and CS, it is important to characterize the CVS aerosol. Contour plots of particle size distributions in the CVS, as shown in Figure 3.2, showed a distinctive bimodal pattern of accumulation mode and nucleation mode particles for the 74% engine load condition. The number concentrations of both nucleation mode and accumulation mode particles were stable at the 74% engine load, while particle number concentrations were near the EEPS's detection limit for the 26% engine load. The observation of higher number concentrations of nucleation mode particles at the higher engine load is consistent with previous studies [40], which have shown the formation of nucleation mode particles for vehicles with aftertreatment is a strong function of temperature.

Total particle number concentrations in the CVS measured by the CPC 3022A and the EEPS are shown in Figure 3.3 for the 74% engine load. Since the EEPS and CPC 3022A have similar cut off sizes, 5.6 and 7 nm, similar total particle number concentrations were expected. The two instruments tracked closely up to about 4×10^5 particles/cm^3, but diverged above that concentration. Above 1×10^4 particles/cm^3, the CPC 3022A utilizes a photometric particle counting method that becomes increasingly non-linear as concentration increases. We attribute the discrepancy in particle concentrations above 4×10^5 particles/cm^3 to the fact that the CPC 3022A was not calibrated for these high concentrations before the test. Thus, the EEPS should be con-

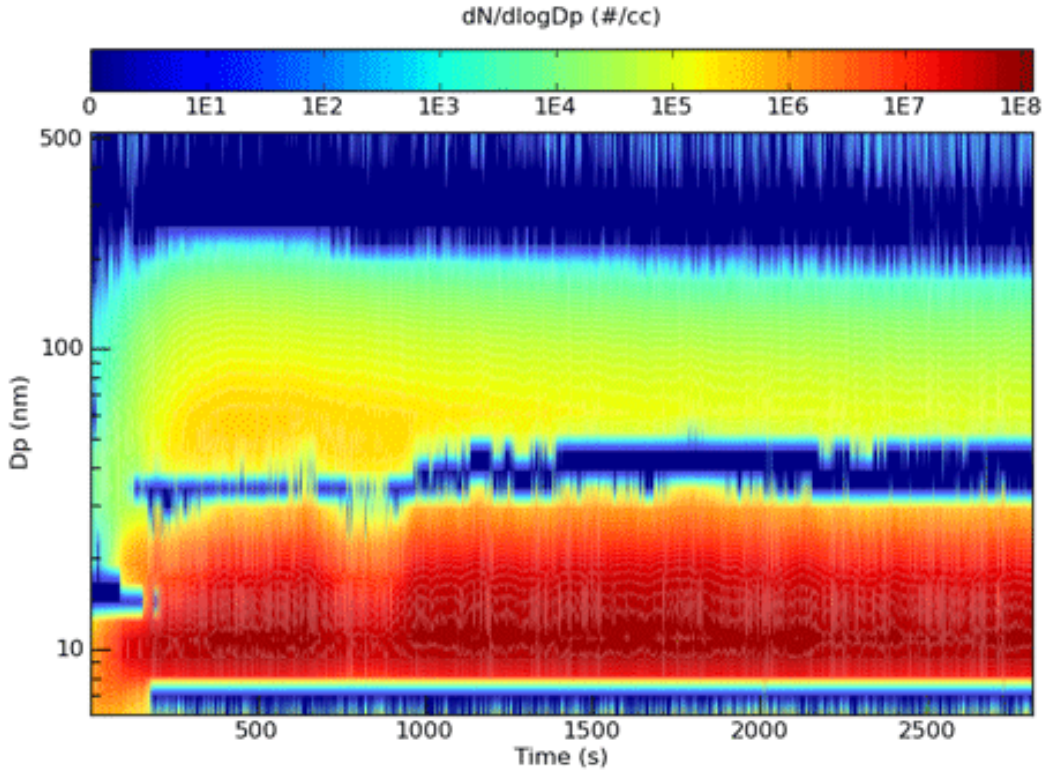

Figure 3.2: Contour plots of real-time particle size distributions measured by the EEPS in the CVS at the 74% engine load.

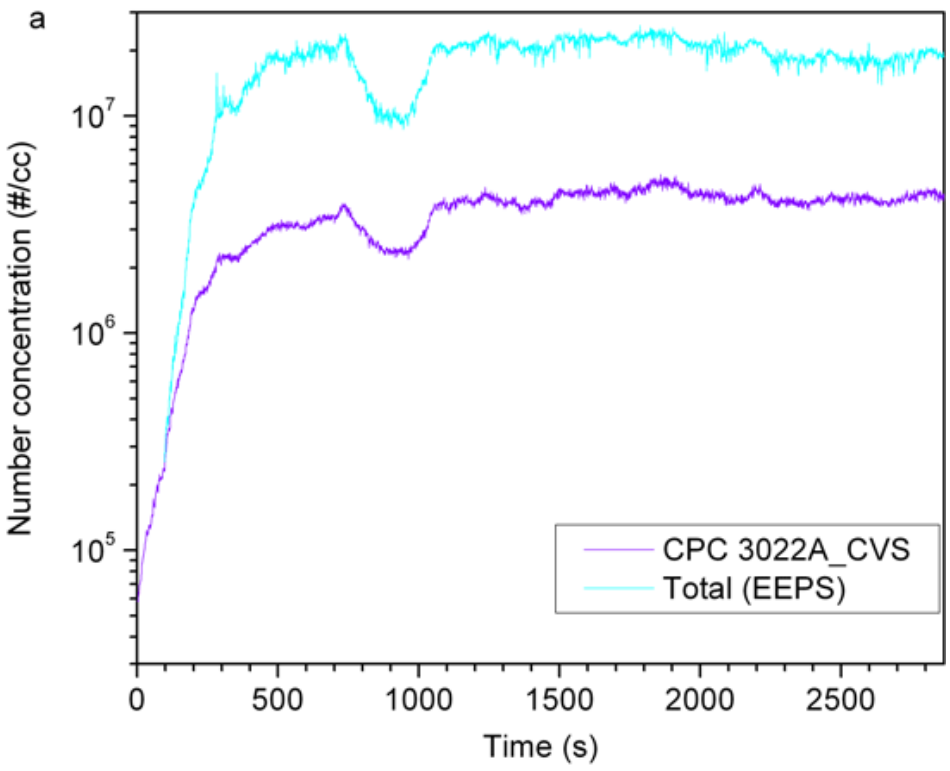

Figure 3.3: Total particle number concentrations in the CVS at the 74% engine load.

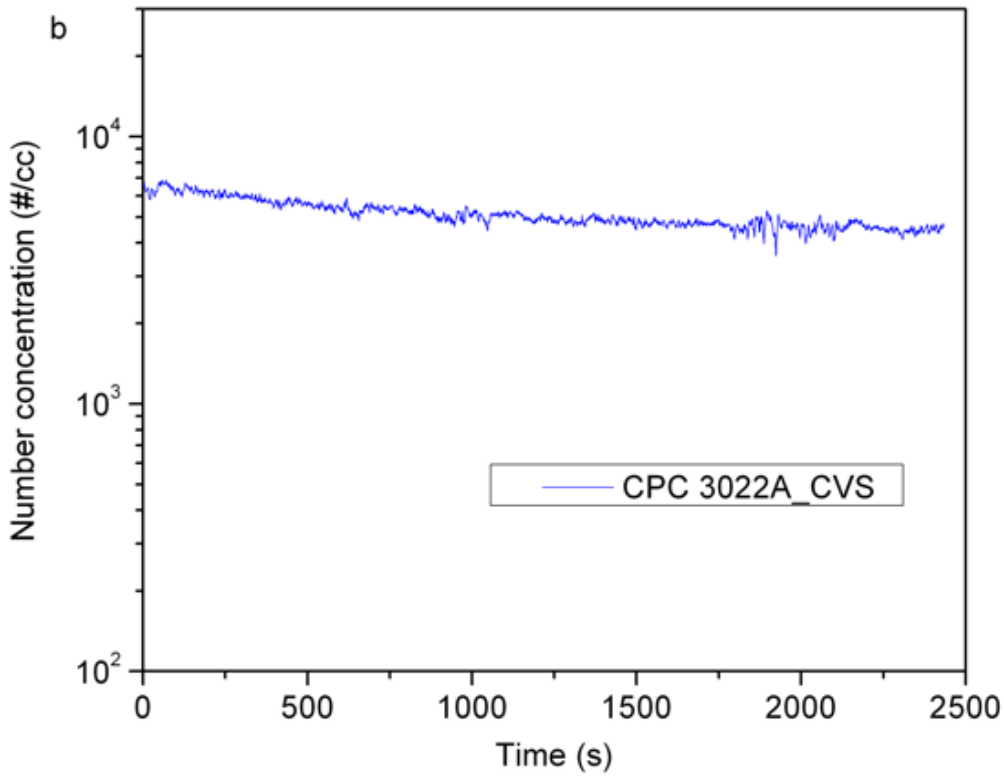

Figure 3.4: Total particle number concentrations in the CVS at the 26% engine load.

sidered more accurate at the higher concentrations in Figure 3.3. Figure 3.4 shows particle concentrations at the 26% engine load. EEPS data is not shown, as the concentrations were near the detection limit. Particle concentrations at the 26% engine load were steady and lower by three orders of magnitude compared to 74% load.

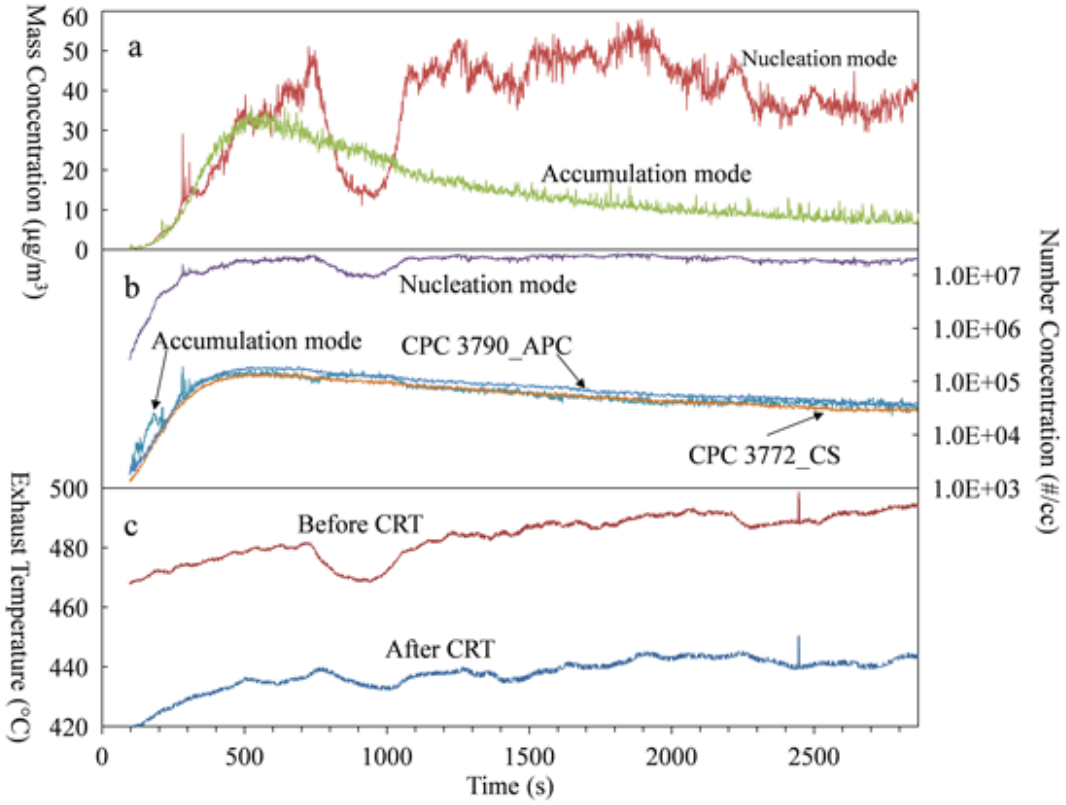

Figure 3.5: (a) CVS particle mass concentrations of nucleation mode and accumulation mode particles; (b) CVS particle number concentration of nucleation mode and accumulation mode particles; (c) Exhaust temperatures before and after the CRT™.

Figure 3.5 shows number concentrations and estimated mass concentrations determined using the EEPS for the 74% load condition. The mass concentrations were calculated assuming that the nucleation mode consists of spherical hydrated sulfuric acid particles with a density of 1.46 g/cm^3, which corresponds to the ambient relative humidity ($25 \pm 3\%$) and temperature (33 ± 1°C) in the current study, and the accumulation

mode particles were assumed to have an effective density of 1.0 g/cm^3 following the manufacturer's recommendations. The number concentrations of nucleation mode and accumulation mode particles were determined by fitting the EEPS size distributions to a bimodal, log normal distribution. The nucleation mode concentrations increase as exhaust temperature increases due to the increase of SO_2 to SO_3 conversion. The dip in number concentration between 700 and 1000 seconds is associated with a dip in exhaust temperature related to a change in engine coolant temperature, which is utilized as a heat exchanger for engine intake air. This only influences the nucleation mode and does not impact the accumulation mode concentration. The decrease in accumulation mode particle concentrations as a function of time suggests the CRT™ is becoming more efficient as it loads with soot, although the exhaust temperatures are high enough for passive regeneration to be occurring simultaneously.

3.4.2 Particle number emissions under the APC and CS

Figures 3.6 and 3.7 show the number concentrations measured by various means plotted against time for the two engine operating conditions. Number concentrations have been corrected for dilution ratio (DR) to reflect the concentrations that would be seen in CVS. The APC DR used for the concentration correction was the ratio of the total sample plus dilution air mass flow rate to the sample flow rate based on the settings of the APC mass flow controller. The actual DR of the APC varied only about 1% due to flow and pressure variations during the test. The primary and secondary DRs of the APC were 50 and 10 for a total DR of 500, and 10 and 10 for a total DR of 100. Based on our preliminary tests, a DR of $\sim$20 on the CS side was necessary to avoid saturating the particle counting instruments. The actual CS DR was determined by two independent

methods, a flow rate measurement and CO_2 measurement. These two methods agreed well, and the CS DR was monitored continuously during the test. It had an average value of 21, and the variations over a test were less than 1%. Therefore, the average value of 21 was used for all calculations.

For both engine loads, the tests with the "alternating set" of instruments (i.e., the 3025A CPC, the 3776 CPC, the 3772 CPC, and the nanoSMPS) were performed in the following sequence; the APC with a DR of 500, the APC with a DR of 100, and the CS. At the 26% engine load, this test sequence was conducted twice and then the instruments were directly connected to the CVS. At the 74% engine load, this test sequence was conducted three times without directly connecting to the CVS. The direct connection to the CVS was done for the 26% engine load, but not for the 74% engine load, because the particle number concentrations were much lower at the 26% engine load. When the CPCs were switched to the CS side or the CVS, the APC DR was set at 500. As discussed previously, the CPC 3772_CS and the CPC 3790_APC were dedicated to the CS and APC, respectively.

Figure 3.6 shows the results for the 74% load condition. The load was increased rapidly to 74% after the vehicle was started. Number concentrations rise rapidly after the load is increased as the engine and CRT™ adjust to the new operating condition. Several things are happening simultaneously: engine out emissions are adjusting to the new operating condition, and the CRT™ is simultaneously loading and undergoing passive regeneration. After the operation is stabilized at the 74% engine load, the exhaust temperatures are well over 400°C. The catalysts used for passive regeneration not only

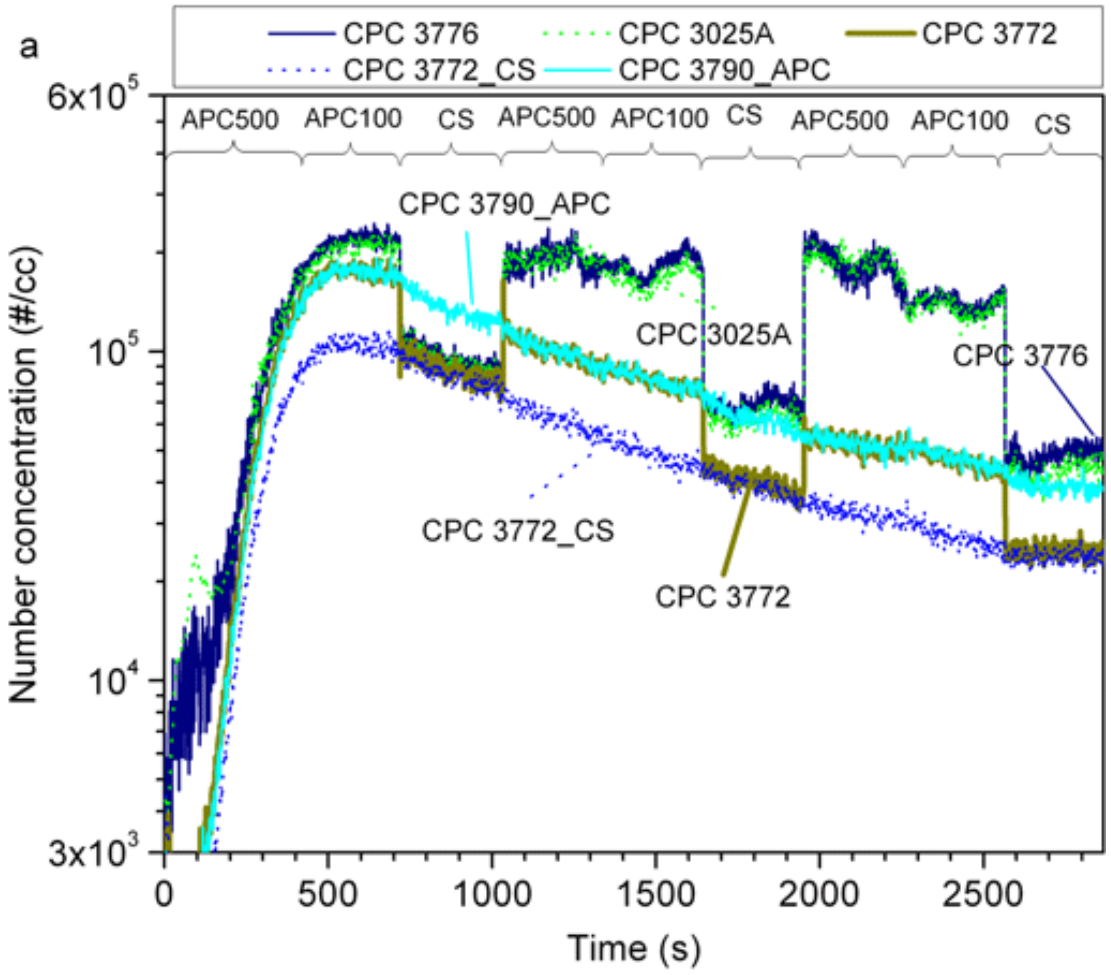

Figure 3.6: Real-time particle number concentrations measured by different CPCs at the 74% engine load. Note: The sampling locations and conditions were: the APC side with a DR of 500 (labeled as APC500), the APC side with a DR of 100 (labeled as APC100), the CS side (labeled as CS).

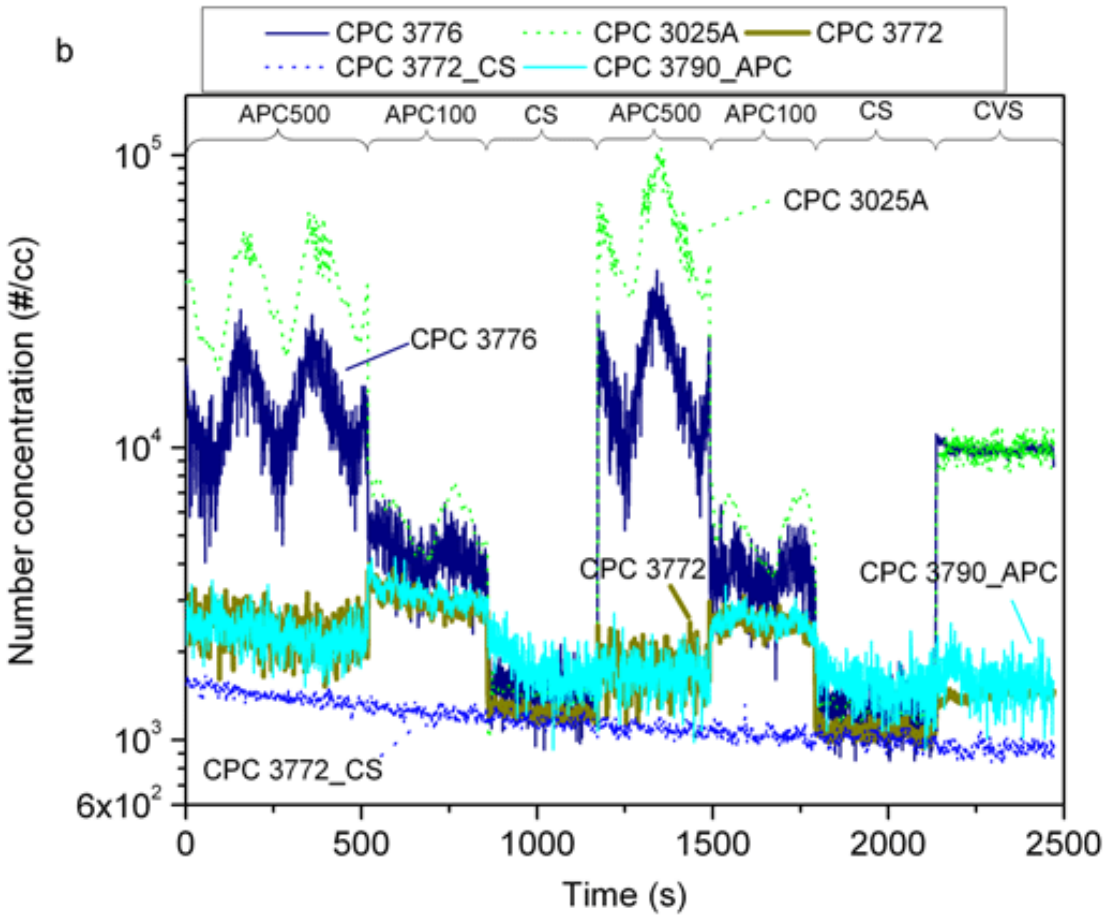

Figure 3.7: Real-time particle number concentrations measured by different CPCs at the 26% engine load. Note: The sampling locations and conditions were: the APC side with a DR of 500 (labeled as APC500), the APC side with a DR of 100 (labeled as APC100), the CS side (labeled as CS), and the CVS directly (labeled as CVS).

oxidize NO to NO_2 but also oxidize SO_2 formed from sulfur in the fuel or lubricating oil to SO_3, especially at temperatures above 350°C [41]. The SO_3 emissions are likely associated with the increase in nucleation mode particles seen in Figure 3.5.

"Solid" particle emissions measured with the CPC 3790_APC and CPC 3772_CS follow a smooth trend of increases and decreases very much like that of accumulation mode particles in Figure 3.5b. This consistency suggests that these CPCs are accurately tracking the accumulation mode particles penetrating the CRT™. Engine out accumulation mode number concentrations are typically larger than 10^7 particles/cm^3, and the concentrations observed here were less than 2×10^5 particles/cm^3, suggesting removal efficiencies greater than 98.5%. Peak concentrations are reached at about t = 500 second. Here, the peak concentration measured with the 3790_APC and the CPC 3772 downstream of the APC agree well, and are about 60% higher than the 3772_CS. The agreement of the CPC 3790_APC and the CPC 3772 downstream of the APC indicates that there were no particles present between 10 and 23 nm, the respective cut sizes of the CPCs, while the disagreement with the 3772_CS is consistent with the expected losses in the CS due mainly to thermophoretic deposition in the cooling section of the CS. On the other hand, downstream of the APC, the 3776 and 3025A CPCs show about 30% higher concentrations than the 3790_APC and 3772, indicating particles between 3 and 10 nm.

Moving to the next time window, where most of the instruments are downstream of the CS, agreement is found between the 3772, 3025A and 3776, indicating no particles between 3 and 10 nm. During the next two windows, APC500 and APC100, the low cut size instruments, the 3025A and 3776, essentially agree as do the higher cut size in-

struments, the 3790 and 3772, but the ratio of low cut to high cut number count grows. The agreement between the 3790 and 3772 suggests that there are few particles between 10 and 23 nm so that the increasing ratio is primarily due to relatively more particles between 3 and 10 nm. During the next window when the instruments are switched downstream of the CS, particles below 10 nm begin to appear, as the 3025A and 3776 show higher concentrations than the 3772. The trend of increasing fractions of particles below 10 nm continues both downstream of the APC and CS in subsequent time windows. The last time windows downstream of the APC and CS show, respectively, 70 and 50% of the observed particles between 3 and 10 nm.

It is not likely that these particles represent penetration through the CRT™. The most penetrating particle size for typical filters ranges from 100 to 300 nm, with particles either larger or smaller than that size removed more efficiently. In the case of sub 23 nm particles, although there is some evidence that under some conditions tiny solid nanoparticles are emitted, there is no evidence in the literature of formation of high enough concentrations of these particles to offset the decreased penetration through the DPF. The only exception to this might be the case when an excess of a metallic fuel additive, like a fuel borne catalyst, is used. Thus, it is extremely unlikely that these particles are due to penetration of solid particles through the DPF. Rather they are likely formed by renucleation downstream of the APC and CS. The question is why the fraction of these particles increases during the run. The accumulation mode particle concentrations, and corresponding solid particle concentrations, decrease continuously after 500 s, while the fractions below 10 nm increase, although the absolute concentration between 3 and 10 nm changes little. These particles could be formed by nucleation

of sulfuric acid. In which case, it would require conversion of only 0.02% of the sulfur in the fuel to account for all the particles observed between 3 and 10 nm below the APC, even making the worst assumption that they are all 10 nm in diameter.

Figure 3.7 shows the results of particle number measurements at the 26% load condition. Here, particle number concentrations are much lower than for the higher load condition and the structure is even more complex. As with the high load, measurements are made below the APC at two overall dilution ratios, 100 and 500. The first time window is APC500, i.e., instruments below the APC with a dilution ratio of 500. Here we see the 3772 and 3790 in good agreement but the 3025A and 3776 read more than 15 and 6 times higher, respectively, indicating that most of the particles are below 10 nm. All these instruments have been calibrated and agree well for calibration aerosols so the difference between the 3025A and 3776 is likely due to slight differences in the lower cutoff behavior of the two instruments which are specified to have 50% counting efficiency cut points of 3.0 and 2.5 nm, respectively. Although it would be expected that the 3776 would read higher than the 3025A, actual instrument cut points may vary from manufacturers'specifications, especially at the extremes of the operating range. In any case, these differences suggest that most of the particles are below the lower counting limits of these instruments, about 3 nm. The large swings in concentrations seen with the 3025A and 3776 are associated with temperature swings in the evaporation tube. This is discussed later in this chapter of the report.

The results are even more difficult to understand when the APC dilution ratio is reduced to 100. Here, we see a relatively sharp drop in the CPC 3776 and CPC 3025A counts when normalized to the CVS concentrations. This can probably be attributed

to differences in nucleation between the two different dilution ratios. In this regard, it should be noted that the particle concentrations in the evaporation tube are a factor of 5 higher at the lower dilution ratio than the higher dilution ratio. It would be expected that the lower dilution ratio would lead to more particle nucleation and growth downstream of the evaporation tube, but this is only partly true. Actually, there is apparently less nucleation as indicated by the reduced concentrations for the 3025A and 3776, but more growth as indicated by agreement between the 3025A and 3776, showing that the particles have grown to well beyond 3 nm, and the increase in the particle concentration indicated by the 3772 and 3790, showing that some particles have even grown above 23 nm. One might argue that the combination of a lower concentration of very small particles and overall growth is due to coagulation, but the low concentration in the evaporation tube, a few hundred particles/cm^3, makes this unlikely.

In the first time window, comparing the CPCs 3025A, 3776, and 3772 below the CS, the 3025A and 3776 are about 20% higher than the 3772 and 3772_CS, indicating some particle formation between 3 and 10 nm, while the 3772s below the CS are about 40% lower than the 3790_APC. This is the difference expected from thermophoretic losses in the CS. If the 3772s were less than 40% lower than the 3790, it would suggest particles between 10 and 23 nm below the CS, but this is not the case. The same trends continue for the rest of the run until the last condition, where all the instruments, except the 3772_CS and the 3790_APC, are connected directly to the dilution tunnel, so that all particles, both solid and volatile, are being counted. Under these conditions, the 3025A and 3776 are in good agreement, suggesting that most of the particles are above 3 nm. These two instruments also show about 7 times higher concentrations than

the 3772, suggesting that most of the particles are between 3 and 10 nm. The average concentration measured by the 3025A during the last APC500 time window case (1200–1500 second) is more than 5 times higher than for the same CPC sampling directly from the CVS. This is further evidence significant creation of sub 10 nm particles below the APC.

The results for the 26% load condition are quite surprising, and are hard to understand in terms of aerosol physics and chemistry. The concentration of sulfuric acid downstream of the CRT™ would be expected to be lower because of lower exhaust temperatures, and thus less oxidation of SO_2 to SO_3. Fuel is being burned at a lower rate so the concentration of SO_2 should also be lower. All of this should lead to a lower driving force for the nucleation of sulfuric acid. On the other hand, the total "solid"particle concentrations are also very low, about one and one half orders of magnitude lower than for the high load case, so that there is less surface area available to suppress nucleation by adsorption. Other species may be involved in the nucleation process. Arnold (2006) has shown that nucleation downstream of catalyzed DPFs is sometimes associated with organic acids. Of course questions could be raised about the accuracy of the dilution ratio measurements and the calibration of the CPCs at very low concentrations. In most cases, particle concentrations downstream of the APC and CS were below 100 particles/cm^3, and they were often below 10 particles/cm^3. However, great care was taken in calibrations of the CPCs and in dilution ratio determinations. Clearly, more work needs to be done to understand PMP type measurements for heavy-duty diesel engines. The results indicate great care should be taken in interpreting the results of so-

called solid particle measurements, especially if the measurements are to be extended to sizes below 23 nm.

The CS showed much less of a tendency to form particles downstream than the APC, but still appeared to form particles in the 3 to 10 nm range under some conditions but there was no evidence of formation of particles larger than 10 nm. Presumably the reduced tendency of the CS to form tiny particles is due to removal of semivolatile materials by the catalytic substrates, although diffusion and thermophoretic losses also play a role. During the higher load chassis test the APC did not appear to be making particles between 10 and 23 nm. For these conditions, the number concentrations of particles above 10 nm found downstream of the CS were about 40% less than number concentrations of particles above 23 nm found downstream of the APC, which was mainly due to the expected thermophoretic losses in the CS. Although the tests here were not

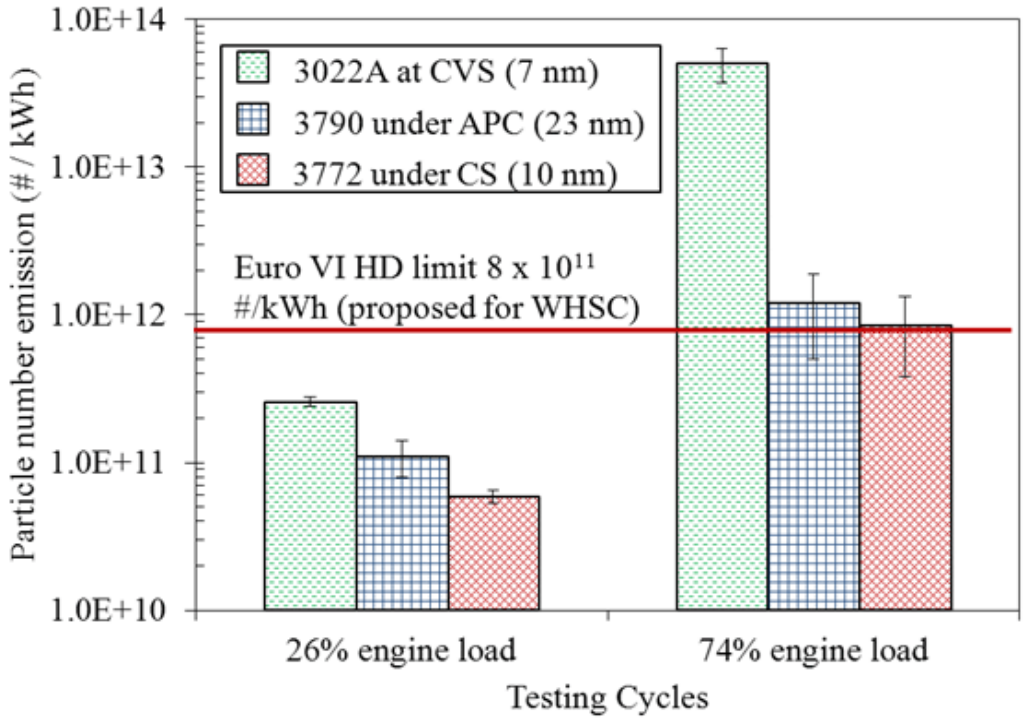

Figure 3.8: Integrated particle number emissions for the chassis dynamometer test.

performed over a standard regulatory cycle, it is of interest to compare with proposed EU number standards. Comparisons to the proposed World Harmonized Stationary Cycle (WHSC) are shown in Figure 3.8. At the 74% engine load, the particle number emissions under the APC and CS were both slightly higher than the proposed Euro VI particle number emission limit for heavy-duty (HD) diesel vehicles for the WHSC. At the 26% engine load, particle number emissions under the APC and CS were both below the proposed Euro VI HD limit. This is not surprising since the average load of the WHSC is between a 26% and 74% engine load.

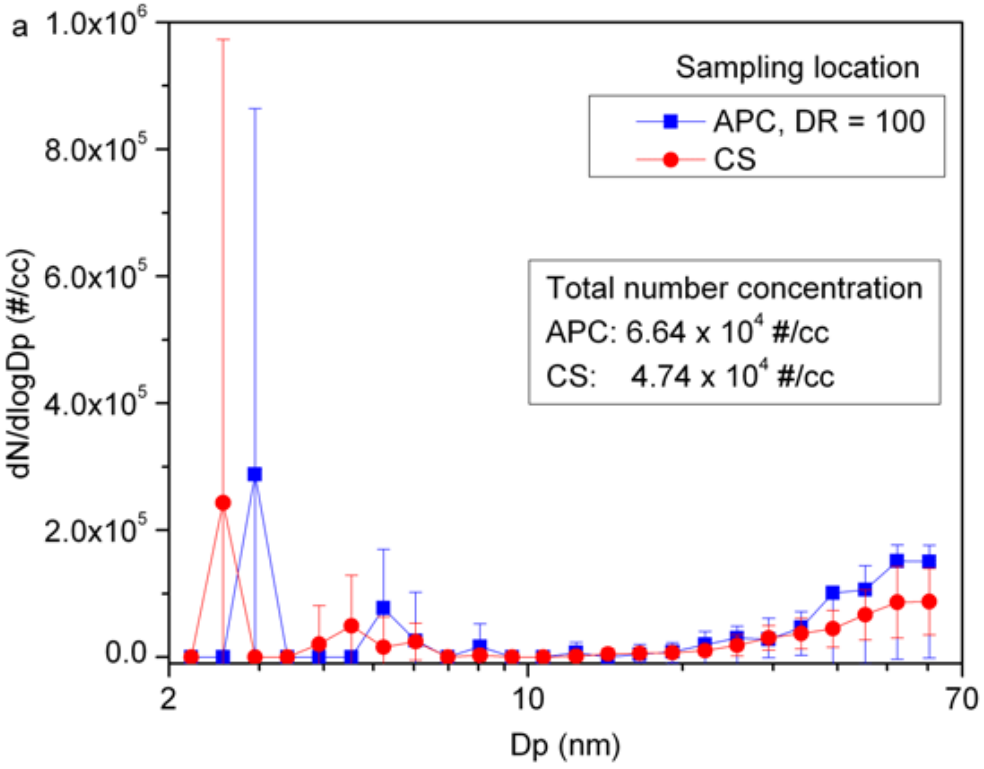

Figure 3.9: Particle size distributions measured by the nanoSMPS downstream of the APC and CS at the 74% engine load.

Particle size distributions downstream of the APC and CS from the nanoSMPS for the two engine loads are shown in Figures 3.9 and 3.10. As seen in the Figures 3.9 and

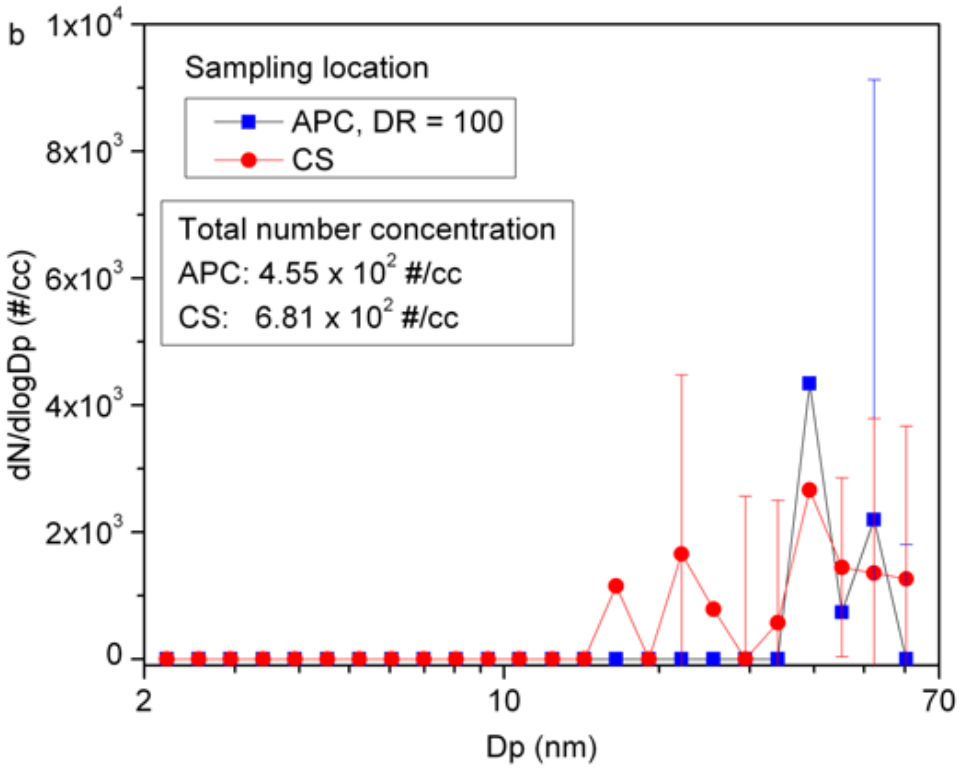

Figure 3.10: Particle size distributions measured by the nanoSMPS downstream of the APC and CS at the 26% engine load.

3.10, the count rates for the size distributions are relatively low, but they still represent important information in understanding the aerosol physics. At the 74% engine load (Figure 3.9), particles below 10 nm were seen by the nanoSMPS on both the APC and CS sides, which is consistent with the results suggested by the CPC measurements. At the 26% engine load (Figure 3.10), no particles below 10 nm were observed in the particle size distributions. The differences between the higher number concentrations of sub 10 nm particles seen by the CPC 3776 and CPC 3025A and the number concentrations seen by the nanoSMPS suggest that these particles were extremely small, making them difficult to be seen by the nanoSMPS due to high diffusion losses and a low charging efficiency. Although the ET wall temperature of the APC was set at 350°C, the actual

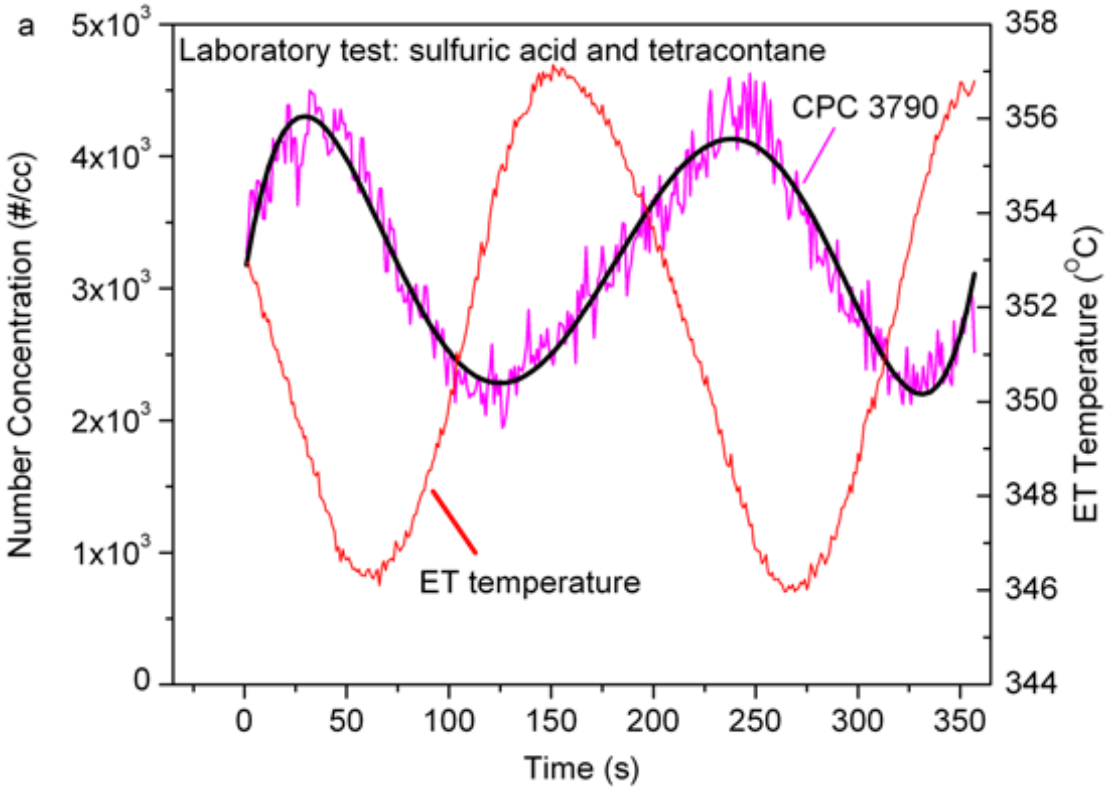

Figure 3.11: Real-time ET wall temperature and CPC concentrations for the laboratory test using aerosol composed of mixture of sulfuric acid and tetracontane. Wide solid lines are the polynomial fits to the individual curves.

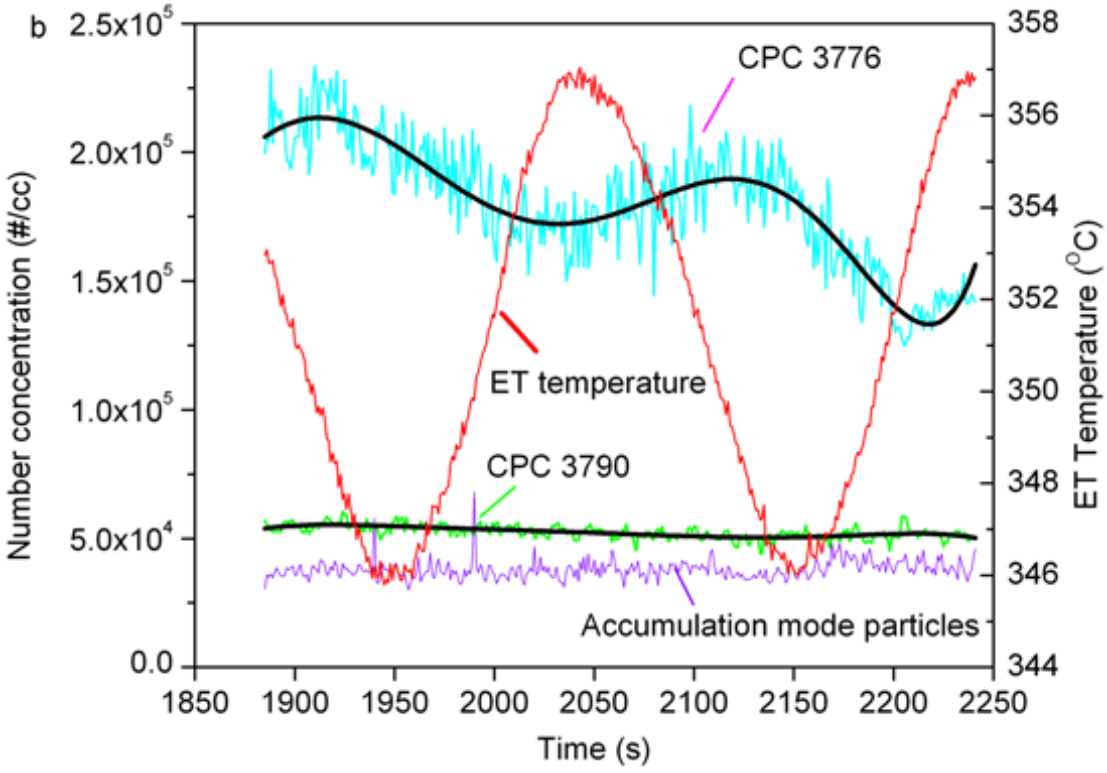

Figure 3.12: Real-time ET wall temperature and CPC concentrations for the chassis dynamometer test at the 74% engine load, time scale is the same as Figure 3.6. Wide solid lines are the polynomial fits to the individual curves.

wall temperature oscillated between approximately 345 and 357°C. Interestingly, CPC particle number concentrations for both the laboratory test and the chassis dynamometer test also showed oscillations that were related to temperature oscillations of the ET, as shown in Figures 3.11 and 3.12. In the laboratory test, the concentration of the CPC 3790 oscillated with the same frequency as the oscillation of ET wall temperature (Figure 3.11). In the chassis dynamometer test, the CPC 3776 oscillated, as did the 3025A, which is not shown, but the 3790 did not (Figure 3.12). The oscillation curves of the ET wall temperature were identical, and the oscillating patterns of the CPC 3790 in the laboratory test and of the CPC 3776 in the chassis dynamometer test were similar too. These observations suggest that particles found downstream of the APC in the laboratory test and particles below 23 nm found downstream of the APC in the chassis dynamometer test were all formed as a function of ET temperature, through similar, if not the same, mechanisms. The CPC 3790 did not oscillate in the chassis dynamometer test because it only measured solid particles above 23 nm, which were mostly accumulation mode soot particles that had passed through the CRT™ that were not influenced by the ET temperature. The number concentrations of accumulation mode particles are also shown in Figure 3.12 for comparison. The accumulation mode particle concentrations were determined by fitting the EEPS size distributions assuming lognormal bimodal size distribution. Although the aerosol mass concentration upstream the APC of the laboratory test was about 10 times higher than that of the chassis test, the number concentration measured by the CPC 3790 for the laboratory test was about 2 orders of magnitude lower than the number concentration measured by the CPC 3776 in the chassis test. This was because only a small portion of particles were measured by the

CPC 3790 due to its large cut off size, i.e., the 3790 was only seeing the upper edge of the size distribution that was moving back and forth with temperature changes. The integrated nanoSMPS number concentration downstream the APC for the same test was about 2 orders of magnitude higher than the CPC 3790 concentration (Figure 2.4 and Table 2.1).

4 Evaluating the solid particle number measurement systems over various driving cycles

4.1 Experimental approach

4.1.1 Test vehicle, fuels, and lubricants

The test vehicle was the College of Engineering-Center for Environmental Research and Technology (CE-CERT)'s in-house Freightliner Class 8 truck, equipped with a 2000 Caterpillar C-15 engine (14.6 liter, 6 cylinders, and 475 hp). This vehicle is certified to EPA 2000 model year standards, with a NOx certification level of 3.7 g/hp-h and a PM mass certification level of 0.08 g/hp-h.

For this study, the vehicle was retrofitted with a Johnson Matthey CRT™. The CRT™ is a passive, wall-flow type DPF, which regenerates continuously when the exhaust temperature is above ∼250°C. Platinum is used in the first chamber of the CRT™ as the catalyst to oxidize NO to NO_2. The mileage accumulated on the DPF was about 2700 miles prior to this study.

The vehicle had a mileage of 18,000 miles and was loaded by CE-CERT's Mobile Emissions Laboratory (MEL) trailer, which included all the emissions analyzers. The weight of the tractor and the MEL was 65,000 lbs. Emission tests were conducted using California Air Resources Board (CARB) ultra low sulfur diesel (ULSD) fuel (S < 15 ppm). The lubrication oil used was a SAE 15W-40 formulation, with a sulfated ash content of 1.35% by weight.

4.1.2 Test cycles

Testing was performed on road using the motorway segment of the European Transient Cycle (ETC), the Urban Dynamometer Driving Cycle (UDDS), and two flow-of-traffic tests. The ETC motorway cycle is a highway cruise cycle with a speed of approximate 50 mph. The cycles were conducted on highways and farm roads near Thermal, CA in the Palm Springs/eastern Coachella Valley area of California. This area is remote, lightly trafficked, and, hence, makes for a suitable test track for vehicle emissions testing. Descriptions of the ETC and UDDS cycles are provided in the Supplemental Information of [27]. Note that the UDDS cycle results presented in this paper represent only the first 700 s of the cycle and there was a break during one of the UDDS tests due to limitations on the length of the test road. The average speed of the first 700 s of the UDDS was $\sim$8 mph. For the ETC motorway cycle, the vehicle was accelerated to reach a cruise speed of 50 miles per hour (mph) prior to starting the cycle. The flow-of-traffic test denoted as route 1 was conducted under freeway driving conditions that included long climbs in elevation (grade of 2.9%, defined as the ratio of rise to run), where the engine was subjected to higher loads than those in the standard cycles. The route 2 flow-of-traffic test was conducted on a long arterial road with stops about every 2 miles.

4.1.3 PMP measurement systems

Two PMP measurement systems were used for this study. One, which is denoted as PMP system-A, was assembled to clone the first commercially available PMP measurement system at the time (circa 2007) when these experiments were performed. The PMP system-A is composed of a pre-classifier/cyclone sampling directly from the CVS

tunnel with a 2.5 μm size cut, a volatile particle remover (VPR) for volatile species control, and a condensation particle counter (CPC, TSI 3790) with a 23 nm cut-off diameter. The VPR includes an initial hot dilution (150°C) stage with a rotating disk type diluter (MD-19, Matter Engineering), followed by an evaporation tube (ET) heated to a 300°C wall temperature, followed by a second diluter (Ejector diluter, Dekati) at room temperature. The sequence of hot dilution, followed by an ET, and then cold dilution is designed to lower volatile concentrations and to suppress re-nucleation. The primary and secondary dilution ratios of the PMP system-A were 30:1 and 10:1, respectively, during the ETC cycle. For the UDDS cycle, the primary dilution ratio was varied between 30:1 and 150:1, while the secondary dilution was fixed at 10:1. The ET temperature was maintained at 300°C for all test cycles.

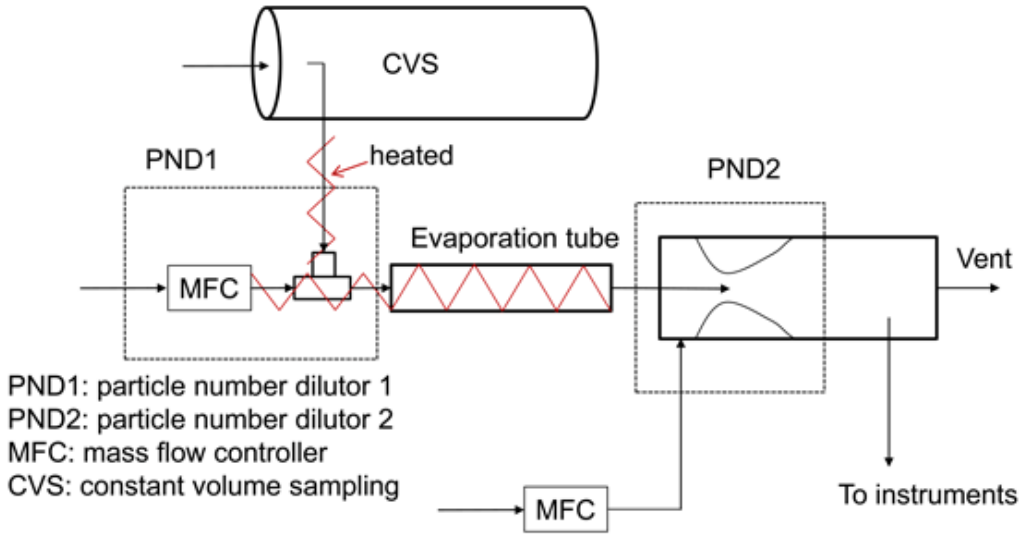

Figure 4.1: Schematic diagram of the PMP system B.

The other PMP system, denoted as PMP system-B, was designed to provide a comparison with the PMP system-A. The PMP system-B utilizes a modified design of an ISO 8178 partial flow single venturi fractional flow sampler (as shown in Figure 4.1). The venturi creates a negative pressure causing the sample to flow from the CVS to the ET. A Swagelok© tee, which serves as the first particle number diluter (PND1), was placed upstream of the evaporation tube. Both the heated dilution air (150°C) and exhaust sample were introduced into the tee by the negative pressure created by the venturi. The mixed flow of dilution air and exhaust sample then flowed into the ET and the venturi, which serves as the second particle number diluter (PND2). The ET maintained a residence time of 0.2 seconds. The flow rate of the clean air into the venturi

was 100 liter per minute (lpm), resulting in a 10 lpm flow through the ET, as determined by calibration. Therefore, the dilution ratio of PND2 was 11:1. The flow rate of the PND1 dilution air was controlled at 9 lpm so that the exhaust sample flowing into the tee was 1 lpm, making the dilution ratio of PND1 to be 10:1. The ET temperature of the PMP system-B was maintained at 300°C for the ETC motorway cycle and the two flow-of-traffic tests, and was varied between 300 and 500°C for the UDDS cycles. PMP system calibrations according to the regulations (i.e., UNECE Regulation 49 and Regulation 83) were not performed because the regulations were yet to be published at the time of testing. All CPCs, however, were calibrated following CPCs' manuals to assure measurement quality [42].

CPCs with different cut-off diameters were used below the PMP system-B, as shown in Figure 4.2. Three CPCs were sampling on the PMP system A, they were a TSI 3790 CPC with a cut-off diameter of 23 nm (labeled as CPC_23_PMPA), a TSI 3760A CPC with a cut-off diameter of 11 nm (labeled as CPC_11_PMPA), and a TSI CPC 3025A with a cut-off diameter of 3 nm (labeled as CPC_3_PMPA). Since only a single TSI 3790 CPC was available for this project, the PMP system-B utilized a TSI 3760A (labeled as CPC_11_PMPB) and a TSI 3025A (labeled as CPC_3_PMPB) for particle number measurements.

Additional measurements were also made at the CVS using an engine exhaust particle sizer (EEPS) with a lower size cut of 6 nm (labeled as EEPS_6_CVS) and a TSI 3022A CPC with a cut-off diameter of 7 nm (labeled as CPC_7_CVS) to measure particle size distributions and number concentrations. A fast scanning mobility particle sizer (fSMPS) with a lower size cut of 8 nm (labeled as fSMPS_8) (Shah and Cocker

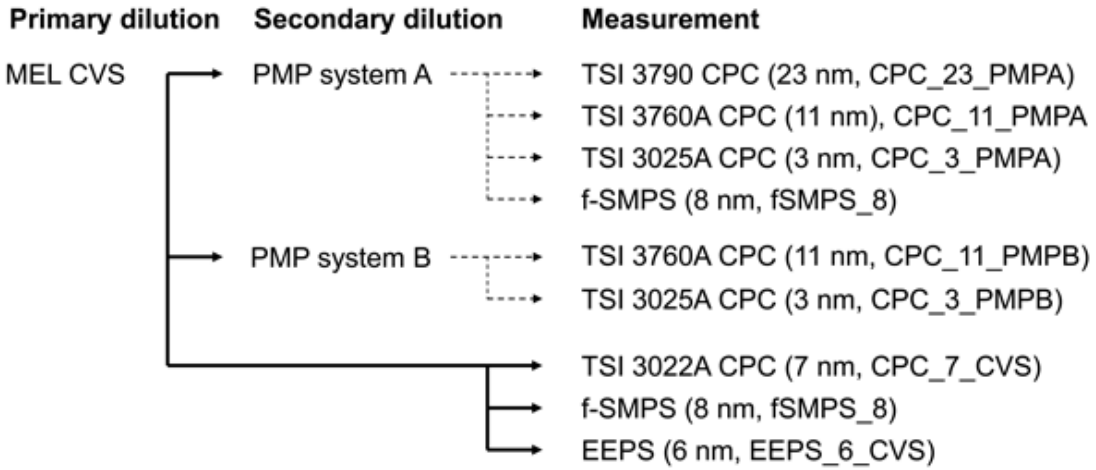

Figure 4.2: Flow diagram of PM sampling system off the primary dilution tunnel. Solid and dotted lines show measurement off the primary and secondary dilution respectively. Numbers within parentheses are D50 cut-off diameter of the instruments. The fSMPS was switched between both the CVS and PMP systems.

2005) was switched between the CVS and the PMP system-A to measure particle size distributions.

4.2 Results

4.2.1 Particle size distributions and particle number concentrations in the CVS

As the PMP systems sample from the CVS, it is important to characterize the CVS aerosol. Figures 4.3 and 4.4 show the results of particle measurements made for the ETC motorway cycle. Figure 4.3 shows particle size distribution contours measured with the fSMPS_8 while Figure 4.4 shows total number concentrations measured in the CVS tunnel with the EEPS_6_CVS and CPC_7_CVS, as well as particle number measurements made downstream of the PMP system A with the CPC_23_PMPA, CPC_11_PMPA, and CPC_3_PMPA. Exhaust temperature and road speed are also shown. For this cycle, the test vehicle was accelerated to reach a cruise speed of 50 mph prior to the beginning of the ETC motorway cycle, resulting in the higher exhaust temperature at the start (t = 0) of the cycle. The accumulation mode particles are at their highest level at the start of the cycle and gradually decrease throughout the test, as may be seen from the fSMPS_8_CVS data in the 40 to 200 nm range. The fSMPS_8_CVS data show initial formation followed by quick decay of a nucleation mode in the CVS tunnel in the 8 to 30 nm region. This is also apparent in Figure 4.4 in the EEPS_6_CVS and CPC_7_CVS data. For most of the first $\sim$80 s of the test CPC_7_CVS reads higher than EEPS_6_CVS. The lower counting limit of the EEPS_6_CVS (EEPS 3090) is 5.6 nm and it counts nothing below that size. On the other hand, the CPC_7_CVS (TSI model CPC 3022A) has a broad counting efficiency curve and a 10% nominal counting efficiency for 4 nm particles. The higher counts with the CPC_7_CVS suggest a nucleation mode

with significant particle concentrations below 6 nm. This is consistent with the results shown by Zheng et al. [43], where they found a significant number of particles between 3 and 7 nm in the CVS by comparing various CPCs with different cut-off diameters all sampling directly from the CVS.

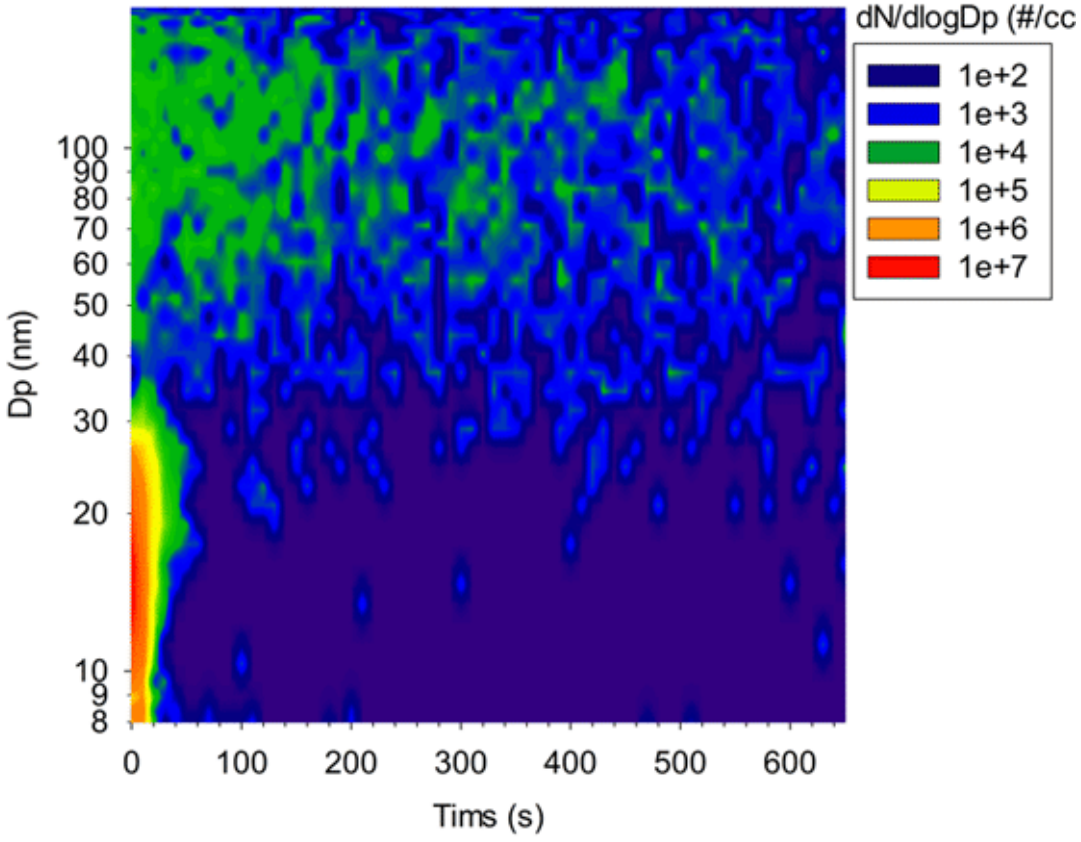

Figure 4.3: Particle size distribution spectrum at the CVS measured by the fSMPS over the ETC.

The formation of a semivolatile nucleation mode, as measured at the CVS, is most likely due to SO_2 to SO_3 conversion over the DPF. This conversion is temperature dependent, with higher conversion found for higher temperatures [40]. Figure 4.4 shows a decrease in exhaust temperature with time, and this is associated with a reduction in

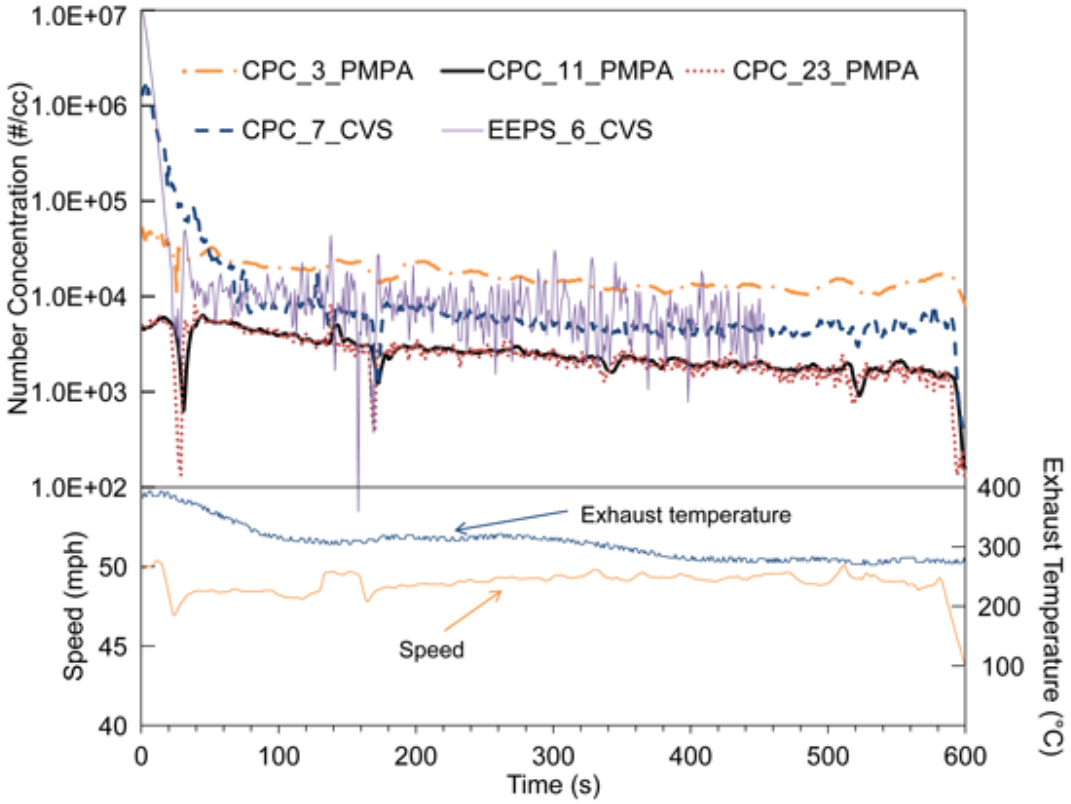

Figure 4.4: Particle concentrations measured by CPCs along with exhaust temperature over the ETC.

the concentration of the nucleation mode particles. The slow decrease of the CPC_7_ CVS concentration tracks the exhaust temperature curve.

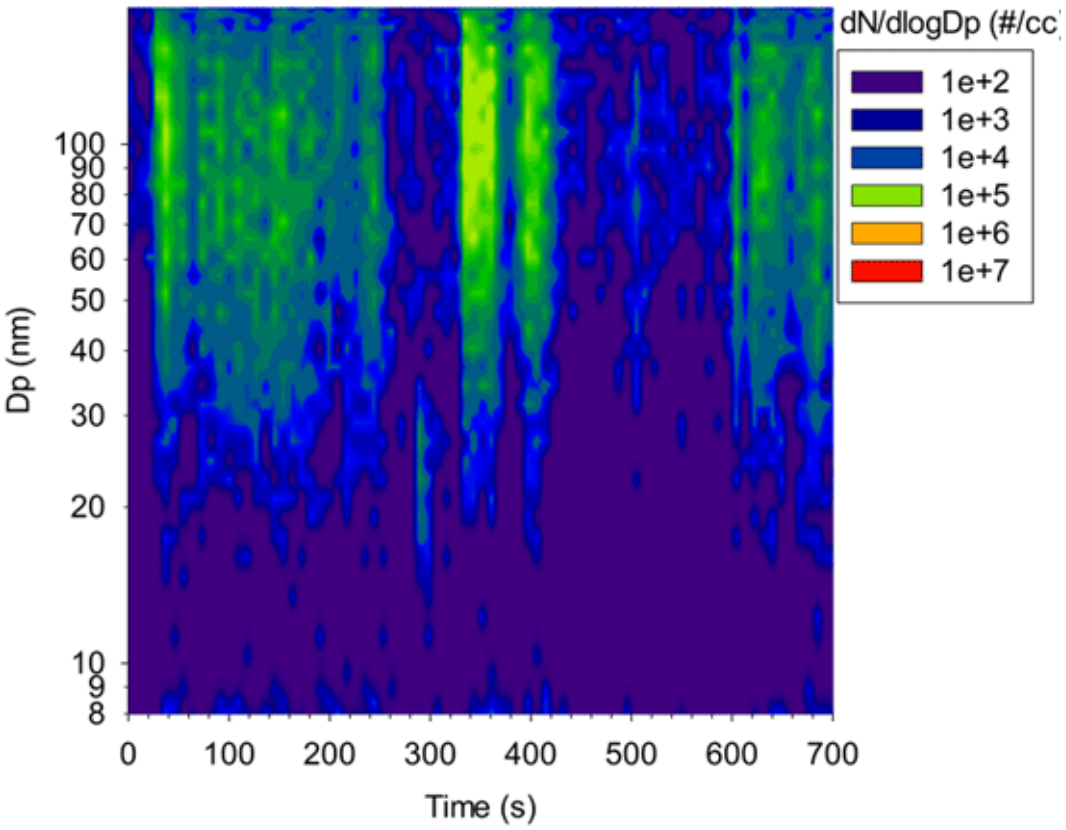

Figure 4.5: Particle size distribution spectrum at the CVS measured by the fSMPS over the UDDS.

Results of the UDDS cycle are shown in Figures 4.5 and 4.6. Particle size distribution spectra of the fSMPS_8 shown in Figure 4.5 reveal the dominance of accumulation mode particles. Since it is likely that most of the particles in the accumulation mode are solid, and since the fSMPS_8_CVS data shows no significant particles between 8 and 11 nm, the differences between the CPC_7_CVS and CPC_11_PMPA data (Figure 4.6) suggest the presence of sub 8 nm nucleation mode particles in the CVS for the

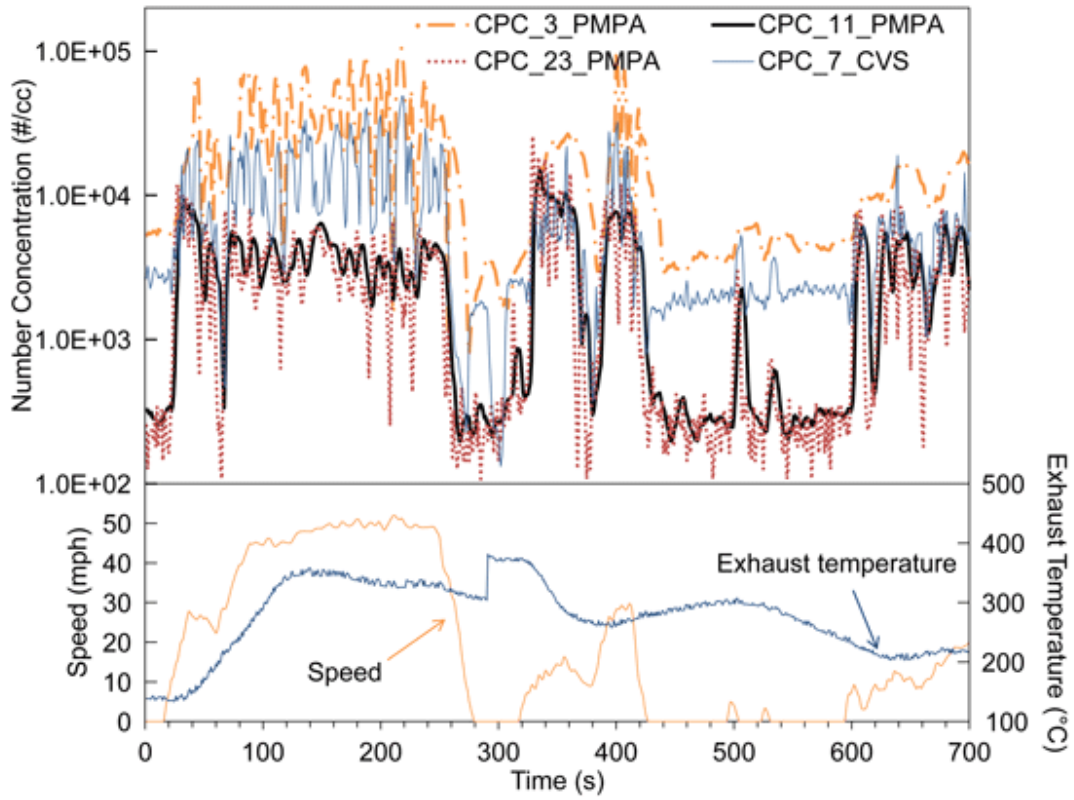

Figure 4.6: Particle concentrations measured by CPCs along with exhaust temperature over the UDDS.

UDDS cycle, similar to the ETC motorway cycle. It should be noted that there was a discontinuation at about t = 300 s for this UDDS cycle due to a stop sign on the testing road.

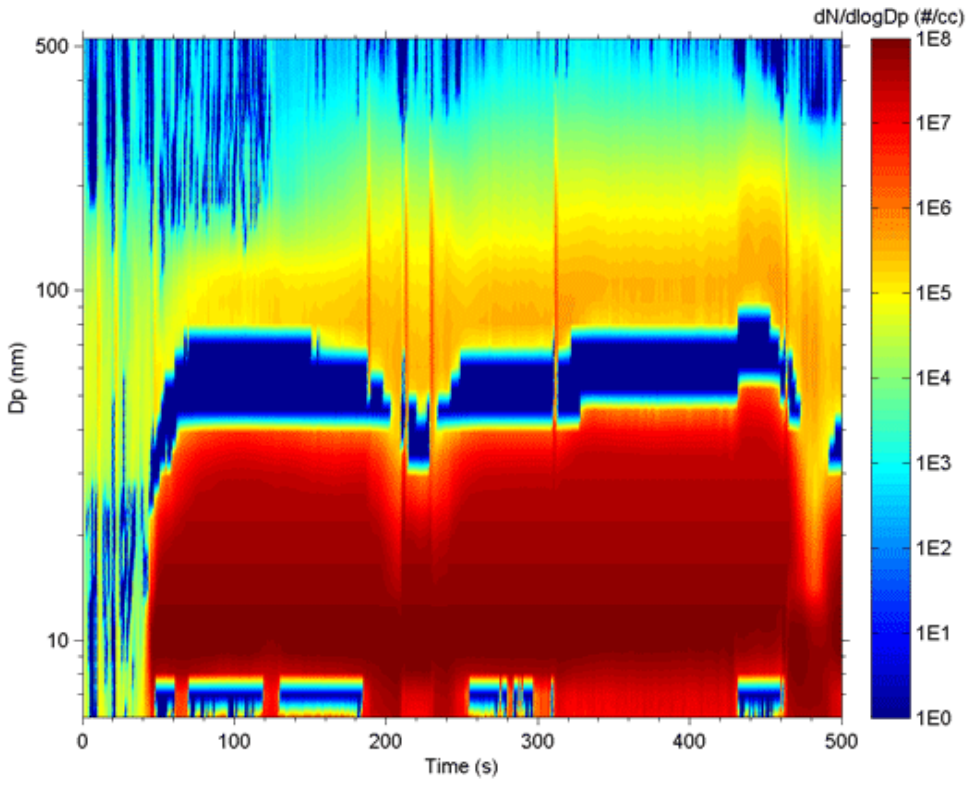

Figure 4.7: Particle size distribution spectrum at the CVS over the route 1 flow-of-traffic testing.

Figure 4.7 shows particle size distributions measured with the EEPS_6_CVS in the CVS for the route 1 flow-of-traffic test. The route 1 flow-of-traffic test had a number of long climbs in elevation, so the average engine load on the route 1 was higher than that of the UDDS or ETC motorway cycle. The total particle number emissions were dominated by the nucleation mode particles after about 50 s, when the exhaust temperature exceeded 350°C, as shown in Figure 4.8. The CPC_7_CVS was saturated throughout

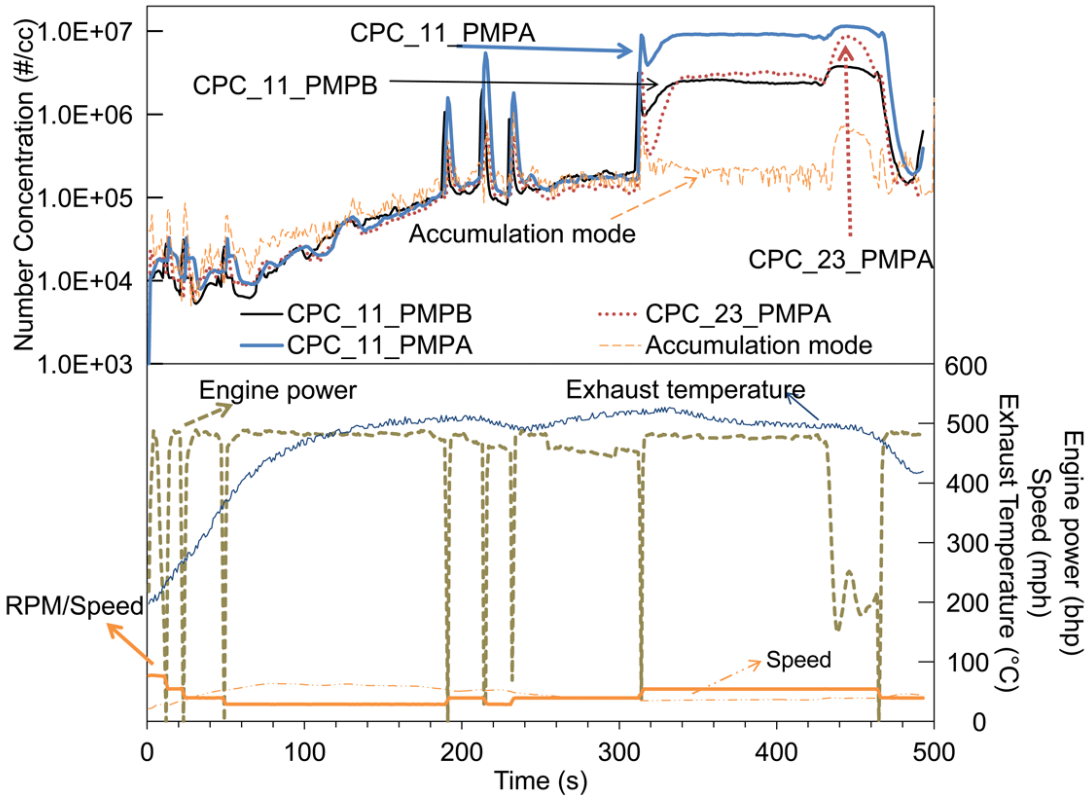

Figure 4.8: Particle concentrations measured by CPCs along with exhaust temperature over the route 1 flow-of-traffic testing.

the entire test due to the high concentration of nucleation mode particles in the CVS, so these data are not shown. The EEPS was also saturated between about 11 and 26 nm, so concentrations shown in this range are underestimated.

4.2.2 Particle number concentrations downstream of the PMP systems

Particle number concentrations downstream of the PMP systems are shown in Figures 4.4, 4.6, and 4.8, for the ETC motorway cycle, the UDDS cycle, and the route 1 flow-of-traffic test, respectively. Particle number concentrations downstream of the PMP systems were all corrected for dilution ratio to reflect the concentrations that would be seen in the CVS.

During the ETC motorway cycle, as shown in Figure 4.4, the CPCs downstream of the PMP system-A showed a significant number of particles below 11 nm. This can be seen by the nearly an order of magnitude higher concentrations for the CPC_3_PMPA compared to those of the CPC_11_PMPA and CPC_23_PMPA. The CPC_11_PMPA and CPC_23_PMPA tracked each other very well, indicating there was a negligible number of particles between 11 and 23 nm, the respective cut-off diameters of the two CPCs.

During the UDDS cycle, the CPCs that measured particle concentrations downstream of the PMP systems, as shown in Figure 4.6, gave results similar to those of the ETC motorway cycle. The CPC_3_PMPA measured $\sim$3 to $\sim$30 times higher concentrations than the CPC_11_PMPA and the CPC_23_PMPA, showing that most of particles present were smaller 11 nm. The CPC_11_PMPA and the CPC_23_PMPA tracked each other very well, showing no, or negligible, particles present between 11 and 23 nm. The differences between the CPC_3_PMPA and the CPC_11_PMPA and

the CPC_23_PMPA varied, and seemed to be smaller when the accumulation mode was more prominent (e.g. t = 350 - 450 s). This is consistent with suppression of nucleation by adsorption onto the accumulation mode particles.

Although particle number concentrations downstream of the PMP system-B are not presented for the ETC motorway and the UDDS cycles to reduce the complexity of the figures, it is worth mentioning that particle number concentrations downstream of the PMP system-B were similar to those downstream of the PMP system-A. Specifically, the CPC_3_PMPB concentrations agreed well with those for the CPC_3_PMPA for both the ETC motorway and the UDDS cycles, and the CPC_11_PMPB concentrations agreed well with the CPC_11_PMPA concentrations. The agreement between the two PMP systems suggests that the performance of the PMP is insensitive to the dilution method employed.

Figure 4.8 shows particle number concentrations downstream of the PMP systems during the route 1 flow-of-traffic test. Particle concentrations were orders of magnitude higher than those from the standard driving cycles (i.e., the ETC motorway cycle and the UDDS) presented earlier in this section. Only the three high cut-off diameter CPCs, i.e., the CPC_11_PMPA, the CPC_23_PMPA, and the CPC_11_PMPB, are shown in the figure because both the CPC_3_PMPA and the CPC_3_PMPB were saturated throughout the test. The saturation of the low cut-off diameter CPCs (i.e., the CPC_3_PMPA and the CPC_3_PMPB) indicates very high concentrations of sub 11 nm particles downstream of both the PMP systems. The integrated particle number (PN) emissions as measured by the CPC_11_PMPA, the CPC_23_PMPA, and the CPC_11_PMPB were 2.3×10^{12}, 9.7×10^{11}, and 1.5×10^{12} particles/kWh, respectively. Even

the high cut point CPCs (i.e., the CPC_11_PMPA, the CPC_23_PMPA, and the CPC_11_PMPB) were saturated for about 140 s from t = 320 to 460 s during the route 1 test, so that this time windows was excluded from the emission calculation.

Particle concentrations showed a steady increase from t = 60 to 180 s while the engine load is nearly constant. This is likely due to the gradual decrease of the DPF filtration efficiency, which is in turn due to the consumption of the soot cake as the DPF regenerates. There were a few spikes at about t = 190, 210, 230, and 320 s, which tracked well with vehicle gear shifts. From t = 230 to 320 s, particle concentrations were relatively steady, and in the range of 10^5 particles/cm^3. Note the 10^5 particles/cm^3 is PMP dilution corrected, and as such is still an order of magnitude lower than the saturation levels of the instruments.

Accumulation mode particle concentrations were calculated in the CVS by a least square fit of the EEPS_6_CVS accumulation mode particle size distributions to a log-normal unimodal distribution, using only channels above 50 nm. EEPS nucleation mode particles were excluded from the fitting process since some of these channels were saturated and did not represent real values. In the fitting process, the lower and upper constraints of the geometric mean diameter were set as 30 and 200 nm, respectively. The broadness of the distribution is defined by the geometric standard deviation, which is the ratio of the diameter below which 84.1% of the particles are found to the geometric mean diameter [44]. The geometric standard deviations from the fitting process ranged from 1.4 to 1.9. The geometric mean diameters of the accumulation mode particles from the fitting process ranged from $\sim$50 to 127 nm. The three CPCs below the PMP tracked well with the accumulation mode concentrations of the EEPS_6_CVS un-

til t = 320 s, indicating both the PMP systems remove semivolatile nucleation mode particles larger than 11 nm effectively.

The CPCs and the EEPS_6_CVS accumulation mode particle concentrations started to show discrepancies past the 320 s spike. While accumulation mode particle concentrations measured by the EEPS_6_CVS showed a minor increase from t = 325 to 460 s, the CPC concentrations increased more than 10 times. These discrepancies will be discussed further in the discussion section of this manuscript.

4.2.3 Particle size distributions upstream and downstream of the PMP system

It would also be very informative if particle size distributions could be measured downstream of the PMP. However, such measurements are extremely difficult to make due to the low particle concentrations under most conditions and the transient nature of the size distributions. Fortunately, particle size distributions upstream and downstream of the PMP system were measured simultaneously using two fast response sizing instruments during the route 2 flow-of-traffic test in this study. The EEPS_6_CVS and f-SMPS_8 took samples at the CVS and downstream of the PMP system-A, respectively. Although the particle counts are at low levels, Figures 4.9 and 4.10 show that the measurements were well above the lower limits of detection for the instruments. Particle size distributions measured at the CVS showed a bimodal distribution due to the presence of a nucleation mode, as shown in Figure 4.9. It should be noted that the EEPS size channels from 9 to 20 nm were saturated during the three nucleation mode particle formation events (i.e., t = 360, 840, and 1320 s). Particle size distributions downstream of the PMP system-A showed that accumulation mode particles passed through the PMP system, while semivolatile nucleation mode particles larger than 8 nm

were effectively removed, as shown in Figure 4.10. The vehicle speed is also plotted in Figure 4.11. For the route 2 flow-of-traffic test, the fSMPS_8 data did not show a significant concentration of sub 11 nm particles downstream of the PMP, which is due to its relatively large cut-off diameter, 8 nm. The CPC_3_PMPA data, which is not presented here, but is reported in [27], did show the presence of sub 11 nm particles downstream of the PMP system. There was a slight difference in the geometric mean diameter of the accumulation mode measured by the two instruments. This is due to differences in the inversion algorithm between two instruments, multiple charge effects for a fractal-like aggregate [45], and the saturation of the EEPS channels in the nucleation mode size range.

4.3 Discussion

4.3.1 Nature of sub 23 nm particles downstream of the PMP systems

The fact that there are a substantial number of sub 11 nm particles downstream of the PMP systems is consistent with the findings of [40]. They found 25 to 75% of the operationally defined solid particles under the PMP measured by the EEPS to be below 20 nm. Giechaskiel et al. [28] also reported that the concentration of the non-volatile particles below 23 nm was 15-45% higher than the non-volatile particles greater than 23 nm. These sub 23 nm particles found downstream of the PMP system are defined operationally as solid by the VPR's ability to remove semivolatile particles. However, the actual physical state of these operationally defined solid particles is unknown. It is important to understand the nature of these sub 23 nm particles to make sure that

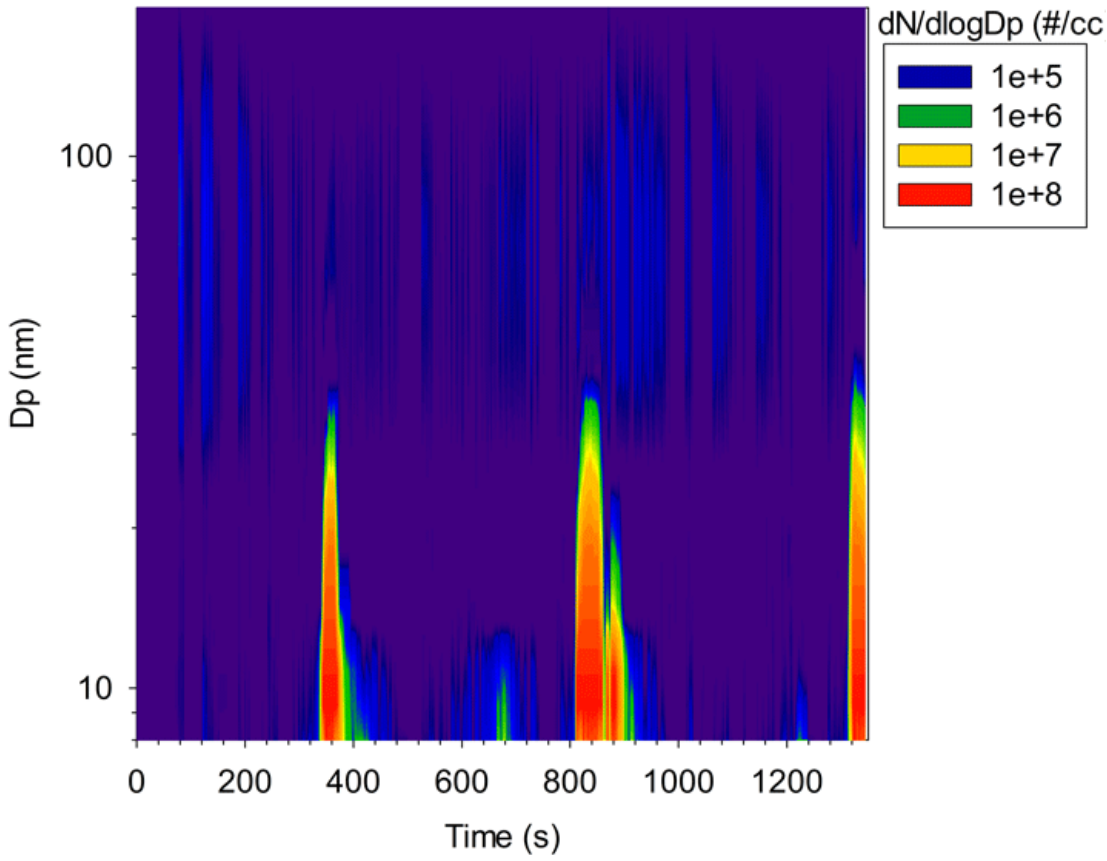

Figure 4.9: Particle size spectrum from the CVS over the route 2 flow-of-traffic testing.

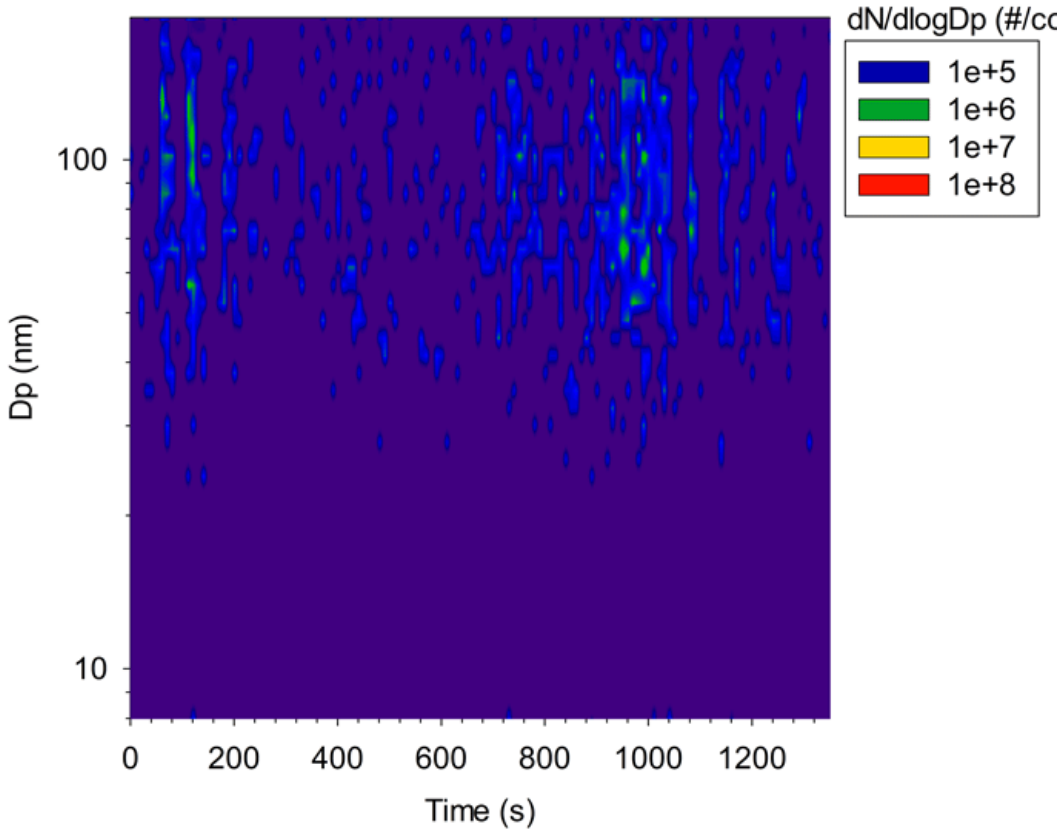

Figure 4.10: Particle size spectrum downstream of the PMP over the route 2 flow-of-traffic testing.

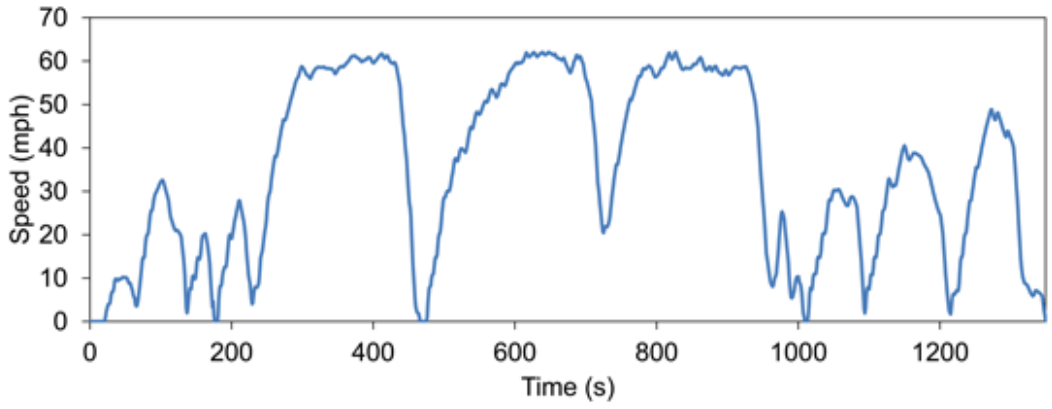

Figure 4.11: Real-time vehicle speed over the route 2 flow-of-traffic testing.

the PMP methodology counts majority of solid particles. There are several possible explanations for our observation of operationally defined solid particles. Three such hypotheses are discussed below.

The first hypothesis is solid particle penetration. Hu et al. [46] reported that DPFs reduced emissions of total trace elements by 85 and 95% for cruise and UDDS cycles, respectively. The highest total metal emission rate was 0.06 mg/km in Hu et al. [46]'s study, which was from the Veh1-DPF1 configuration (i.e., a class 8 tractor with a 1998 Cummins M11 diesel engine (11 L) with a CRT™) and the UDDS cycle. In this case, the metal emissions were dominated by calcium (Ca) and zinc (Zn) based on their high-resolution inductively-coupled plasma mass spectrometer analysis. Ash particle number emissions from the engine used in this study were estimated using the total metal emission rate from Hu et al. [46]'s study. Assuming the worst case scenario, the ash particle number emission rate was calculated to be only 5.5×10^{10} particles/km, if all particles were spherical with a diameter of 3 nm and were composed of only $CaSO_4$ (which has a smaller density than $ZnSO_4$). In this scenario, the ash particle number concentration is the highest. The calculated ash particle emission rate for this scenario was 2 orders of magnitude less than the total particle number emission rate downstream of the PMP system-A, 4.6×10^{12} particles/km, as measured by the CPC_3_PMPA. Since the number of particles that could be solid ash particles is relatively small, this hypothesis does not seem plausible.

The second hypothesis is re-nucleation of semivolatile particles downstream of the PMP systems, most likely made of sulfur compounds. This hypothesis suggests these

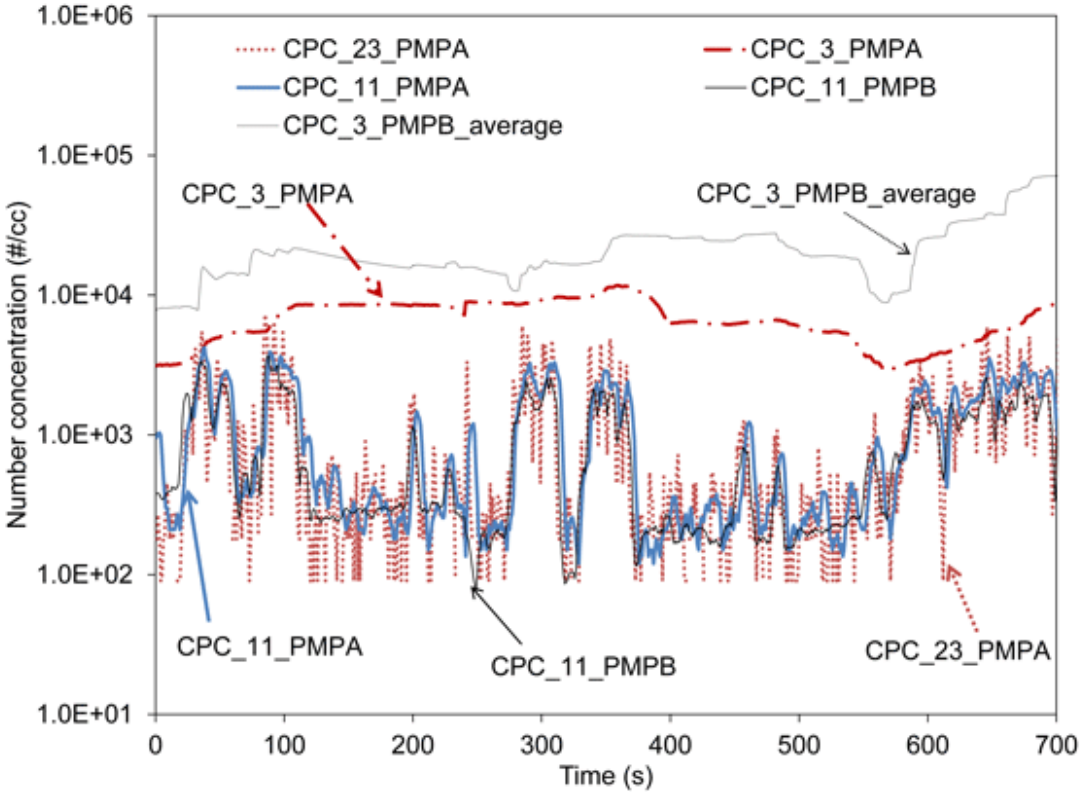

Figure 4.12: Particle concentrations under the high dilution condition for the UDDS, PMP system-A at 1500 DR, PMP system B at 110 DR, a manual 200 second running average was performed for the CPC_3_PMPB to facilitate comparisons with the CPC_ 3_PMPA.

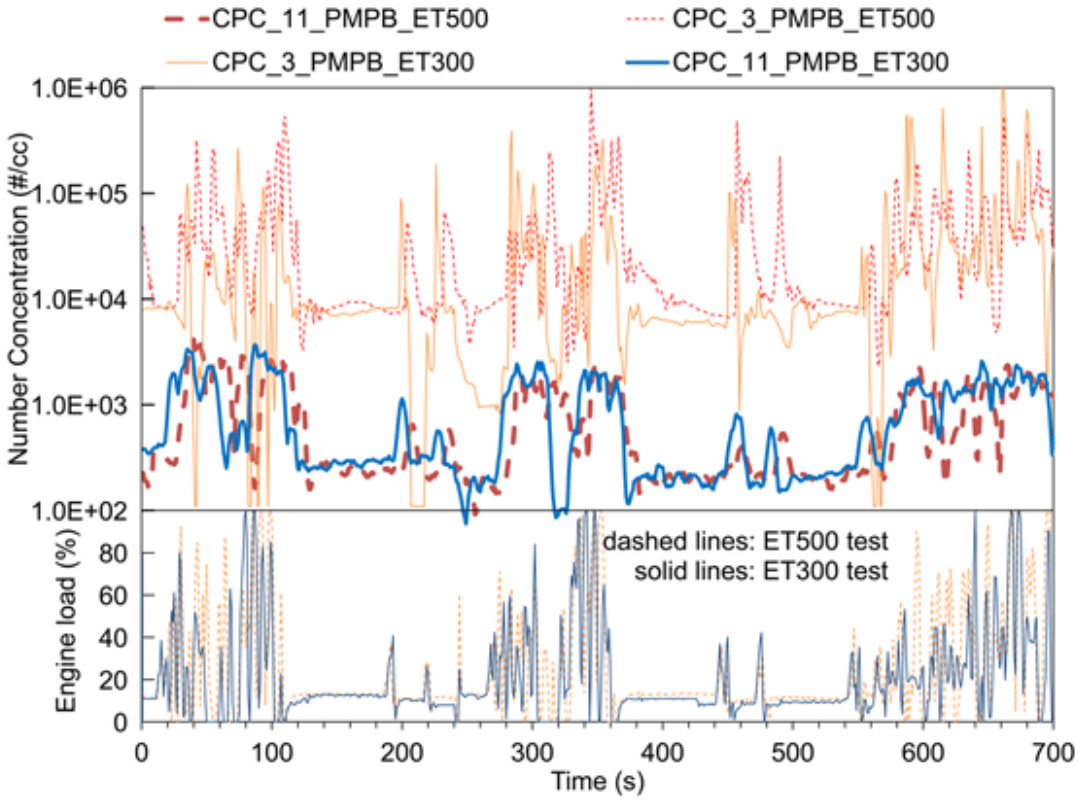

Figure 4.13: Particle concentrations under the high temperature condition for the UDDS, PMP system-B at VPR=500°C and PMP system-A at VPR = 300°C.

semivolatiles evaporate at the VPR and re-nucleate downstream of the PMP system. Biswas et al. [36] and Grose et al. [47] reported significant changes in particle composition due to DPFs. Sulfate compounds and hydrocarbons dominated the particle mass for a catalyzed DPF-equipped engine in their studies, while elemental carbon or soot was found at much lower levels. Zheng et al. [43] calculated the sulfuric acid vapor concentration in the CVS needed to form 10^5 particles/cm^3 10 nm particles downstream of the PMP system for the same vehicle and aftertreatment systems as used in the present study. They showed that only a 0.02% conversion of the fuel sulfur would provide high enough sulfuric acid vapor concentrations.

The primary dilution ratio of the PMP system-A was varied to examine the hypothesis of re-nucleation of semivolatile particles over different UDDS cycles, since nucleation by sulfur compounds is a steep non-linear function of dilution ratio. Prior studies [48, 49, 15, 50] have shown that a small change in dilution ratio can have a significant change in nucleated particle size distributions.

The overall dilution ratio of the PMP system-A changed from 300 to 1500, over the test sequence. A corresponding increase in the dilution ratio of the PMP system-B could not be achieved due to its inherent design, so the PMP system-B was used with its standard operating conditions. It was expected that some change in re-nucleation could occur over this dilution ratio range. The results for the high dilution test are shown in Figure 4.12. Note the CPCs with larger cut-off diameters (i.e., the CPC_11_PMPA, the CPC_23_PMPA, and the CPC_11_PMPB) tracked each other well, which was expected. The CPC_3_PMPA showed a much smoother response than the three high cut-off diameter CPCs (i.e., the CPC_11_PMPA, the CPC_23_PMPA, and the

CPC_11_PMPB). This is due to the fact that the CPC_3_PMPA performs auto running average depending on the concentration. The lower the concentration (due to higher dilution ratio), the longer the running-average time, and correspondingly the slower the instrument response [51]. In this particular test, a 200-second running average was performed by the CPC_3_PMPA built-in software. The CPC_3_PMPB did not fall into the auto running average concentration range, and tracked the vehicle load change well (not shown in the figure for the sake of readability).

To facilitate the comparison between the CPC_3_PMPA and the CPC_3_PMPB, a manual 200 second running average was performed for the CPC_3_PMPB, labeled as CPC_3_PMPB_average in Figure 4.12. In contrast to the three high cut-off diameter CPCs, which agreed well for PMP system-A and system-B, the concentrations of the CPC_3_PMPB_average were 20 to 90% higher than those of the CPC_3_PMPA, suggesting the re-nucleation of semivolatiles downstream PMP system-A was suppressed by the elevated dilution ratio. This high dilution test indicated that part, if not all, of the sub 23 nm particles downstream of the PMP systems were re-nucleated semivolatiles. It should be noted that vapors of semivolatiles would also condense onto the surfaces of accumulation particles downstream of the PMP systems, but condensation on existing particles does not change the particle number concentration. Thus, this second hypothesis appears to be a plausible explanation.

The third hypothesis is partial evaporation of large, less volatile particles. In another experiment, the ET temperature of the PMP system-B was increased to 500°C to examine this hypothesis (Figure 4.13). The CPC_3_PMPB and CPC_11_PMPB concentrations of the high ET temperature test are labeled as CPC_3_PMPB_ET500

and CPC_11_PMPB_ET500 (dashed lines), respectively, in Figure 4.13. The CPC_3_PMPB and CPC_11_PMPB concentrations from a similar test done at ET temperature of 300°C are also included in Figure 4.13 for better comparisons, labeled as CPC_3_PMPB_ET300 and CPC_11_PMPB_ET300 (solid lines), respectively. Engine loads of the two tests are plotted in Figure 4.13 as well. The CPC_11_PMPB_ET500 agreed well with the CPC_11_PMPB_ET300, indicating the accumulation mode particles are not affected by the ET temperature variation. General agreement was seen between the CPC_3_PMPB_ET500 and the CPC_3_PMPB_ET300 most of the time, except for a few occasions when the CPC_3_PMPB_ET300 concentrations fell to very low levels. It was noted that the CPC_3_PMPB_ET300 even fell below the CPC_11_PMPB_ET300 during these occasions, which is theoretically impossible. This was most likely due to an occasional clog of the aerosol capillary tube of the CPC_3_PMPB_ET300 [52]. If the operationally defined solid particles are due to incomplete evaporation of semivolatile particles, then one would expect a decrease of sub 11 nm particle concentrations when the PMP ET is operated at elevated temperatures. Such a response was not observed in this test, as discussed above. Thus, the partial evaporation hypothesis does not seem possible.

4.3.2 Implications to on-road flow-of-traffic driving

Several other measurements and observations that were made during the test, but not shown in this manuscript, are worth mentioning to fully understand the discrepancy between the EEPS_6_CVS accumulation mode particle concentration and the much higher CPC concentrations from t = 325 to 460 s. These measurements and observations during this time period are (a) the EEPS_6_CVS total particle concentrations were flat;

(b) nine EEPS_6_CVS channels, from 9.3 to 29.4 nm, were saturated; (c) both the TSI Dustrak and Dekati mass monitor (DMM) measuring in the CVS showed about a 50% increase in particle mass concentrations; (d) total hydrocarbon (THC) mass concentrations increased more than one order of magnitude based on the THC measurement. These observations, along with only a slight increase of the EEPS_6_CVS accumulation mode particle concentrations, suggest a large increase in nucleation mode particles that was not captured by the EEPS_6_CVS because some of the nucleation mode size channels were saturated.

Given these observations, the differences between the EEPS_6_CVS accumulation mode particle concentration and the much higher CPC concentrations can be attributed to the growth of re-nucleated semivolatile particles downstream of the PMP systems. After formation by nucleation, some of the particles grew larger than 11 nm and others even grew larger than 23 nm, causing the difference between the three high cut-off diameter CPCs and the EEPS_6_CVS accumulation mode particle concentrations. The differences would have been even greater, but the concentrations of these re-nucleated semivolatile particles were so high that all the three CPCs were saturated during this period of time. It is acknowledged that dilution ratios should have been adjusted to avoid instrument saturation. Resources were not available to repeat the test with higher dilution ratios, however. Dwyer et al. [53] also observed a sharp increase of PMP operationally defined solid particles during an DPF regeneration event for a light-duty diesel vehicle, and proposed the incomplete removal of semivolatile particles by the PMP could contribute to the sharp increase of apparently solid particles. However, as indicated by the current study, and given the existence of large concentrations of

volatile or semivolatile nucleation mode particles during DPF regeneration [54], the sharp increase of the operationally defined solid particles in Dwyer et al. [53]'s study were probably re-nucleated particles that grew larger than the 23 nm sizecut.

5 Evaluating the solid particle number measurement systems under on-road driving and standard testing cycles

5.1 Introduction

In Europe, particle number (PN) emissions are measured under the same testing cycles as particle mass (PM mass) emissions and other gaseous emissions [11, 12], using cycles such as the world harmonized steady cycle (WHSC) and the world harmonized transient cycle (WHTC). These testing cycles were designed to represent on-road driving emission levels. It is uncertain, though, whether laboratory testing cycles reflect on-road driving conditions, especially for the newly regulated PN emissions. Currently, there is no PN regulation in the United States (U.S.). In the on-road testing part of previous CARB/UCR PMP study [27, 55], a very high level of solid larger than 23 nm particles was reported downstream of the PMP under an aggressive on-road flow-of-traffic driving condition. In that study, however, the elevated engine load, on-road flow-of-traffic driving was performed only once. Therefore, no statistical comparisons could be made.

PM mass and PN emissions from the same heavy-duty diesel vehicle used in the chassis dynamomter test were also investigated over well-designed on-road flow-of-traffic driving conditions and a standard testing cycle, the urban dynamometer driving schedule (UDDS). The main objective of the on-road test is to answer how PM mass and

PN emissions vary under on-road driving and a standard testing cycle. The variability of PN emissions of particles larger than 23 nm, as well as particles smaller than 23 nm, was characterized for different driving conditions in this thesis.

5.2 Experimental methods

5.2.1 Setup

The experimental setup is same as that of the chassis dynamometer test presented in Chapter 3, as shown in Figure 5.1.

5.2.2 Test vehicles, fuels, lubricants

The test vehicles, fuels, and lubricants used in the on-road test were same as those used for the chassis dynamometer test. The MEL trailer and truck combined have a weight of approximately 65,000 lbs, including all emission measuring instruments.

5.2.3 Test cycles

5.2.3.1 On-road tests

The on-road flow-of-traffic tests were performed by driving the CE-CERT's MEL at 45 to 70 miles per hour (mph) on the U.S. Interstate-10 (I-10) freeway near Palm Springs, California at flow-of-traffic conditions (Figure 5.2). The driving route consisted of four distinct phases, with average engine loads ranging from 20 to 80%. Phases 1 and 2 were east bound on the I-10, which was mostly uphill providing high engine loads. The overall road grades of phases 1 and 2 are about 2.2 and 1%, respectively, which are calculated as the ratio of rise to run for each phase. Phases 3 and 4 were west bound on the I-10, which was mostly downhill providing light engine loads, and were the return trips corresponding to phases 2 and 1, respectively. The overall road grades of phases 3

and 4 were about -1 and -2.2%, respectively. As shown in Figure 5.2, phase 1 began at point A, where the MEL was accelerated to above 45 mph after it was driven on to the freeway via the ramp at point E. Phase 2 began at point B right after phase 1 ended. The end location of phase 2 was at point C, before the MEL went off-ramp. After being turned around at point D, the MEL was accelerated to above 45 mph, and then phase 3 began at the same location where phase 2 ended, point C. Following phase 3, phase 4 began at the same location where phase 1 ended, point B. Phase 4 ended at point A, the same location where phase 1 began. After the ending of phase 4, the MEL was turned around at point E to start another repeat. The on-road flow-of-traffic test was repeated 4 times.

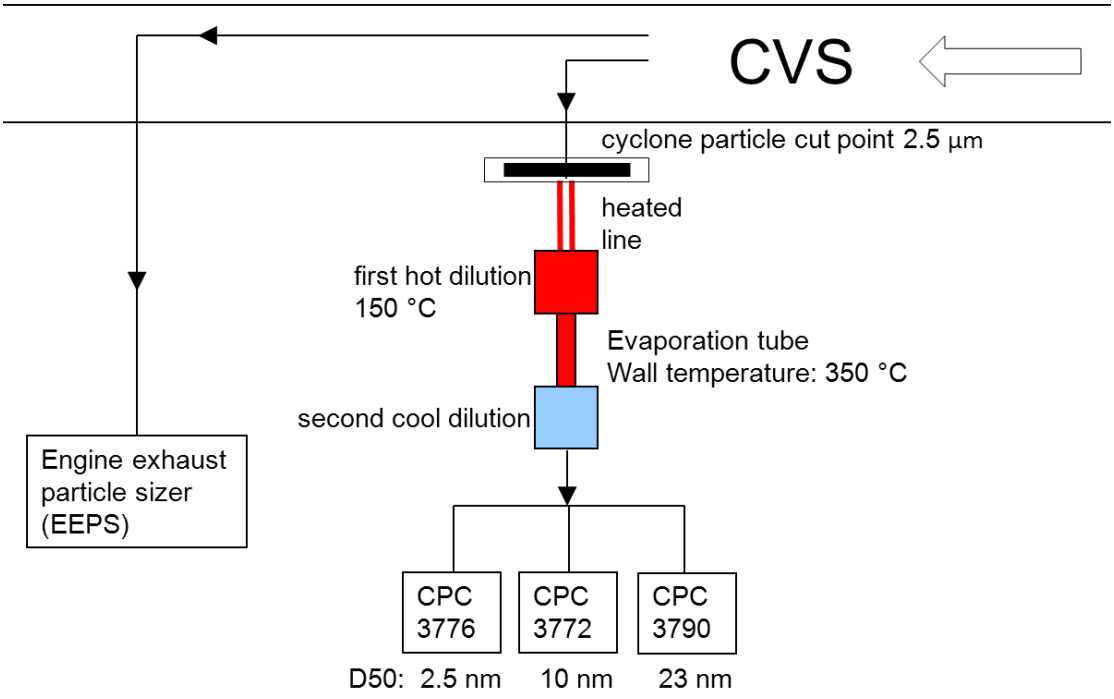

Figure 5.1: Schematic of experimental setup for the on-road test.

Figure 5.2: Map and elevation variation of the on-road test

5.2.3.2 UDDS

The Federal heavy-duty vehicle urban dynamometer driving schedule (UDDS) is a transient test cycle with a short cruise section, and hence exercises both the test vehicle and the PMP system over a fairly wide range of operation. This cycle covers a distance of 5.55 miles with an average speed of 18.8 mph and a maximum speed of 58 mph over 1060 seconds.

5.3 PM mass emissions calculation

There were no stops between different phases to keep the on-road flow-of-traffic driving continuous, as discussed in the previous section, Thus, only one filter sample was taken for each on-road driving test (i.e., including phases 1, 2, 3, and 4). In order to compare PM mass emissions for different phases, PM mass emissions were calculated from the EEPS particle size distributions measured in the CVS, using the Integrated Particle Size Distribution (IPSD) method. The IPSD method was introduced by Liu et al. [56], who showed good agreement between the IPSD and gravimetric filter sample measurements. The IPSD calculates total particle mass from measured particle size distributions using Equation 5.1.

$$M_{IPSD} = \sum_{i} \rho_{eff,i} \times \left(\frac{4}{3}\pi \times \left(\frac{D_{p,i}}{2} \right)^3 \right) \times n_i \tag{5.1}$$

where M_{IPSD} is the total suspended PM, i is the particle size channel, $\rho_{eff,i}$ the effective density of particles falling in the size channel i, $D_{p,i}$ is the mid-particle diameter of the size channel i, and n_i is the total number of particles in size channel i.

The effective density correlation for the accumulation mode (soot) particles was adopted from Maricq and Xu [57] and is defined in Equation 5.2.

$$\rho_{eff,i} = \rho_0 \times \left(\frac{D_{p,i}}{D_{p0e}} \right)^{d_f - 3} \tag{5.2}$$

where ρ_0 is the primary particle density, D_{p0e} is the effective primary particle diameter, and d_f is the fractal dimension. Values of ρ_0, D_{p0e}, and d_f were 2 g/cm^3, 16 nm, and 2.35, respectively. The accumulation mode particles were chosen to be particles larger than 30 nm, which is the cut point between the nucleation mode and accumulation mode defined by Kittelson et al. [8]. For the nucleation mode particles, a density of 1.46 g/cm^3 was used [43], assuming they are composed of mostly spherical hydrated sulfuric acid.

5.4 Results

5.4.1 Real-time PN emissions

Typical real-time PN concentrations downstream of the PMP system for the on-road tests are shown in Figure 5.3 for the UDDS test. Vehicle speed, engine load, and exhaust temperature are also plotted in Figure 5.3. The CPC 3772_10 tracked closely with the CPC 3790_23, indicating a negligible number of particles between 10 and 23 nm present downstream of the PMP system, consistent with the other parts of this study. The CPC 3776_2.5 concentrations were always higher than the concentrations of the other two CPCs, indicating the existence of sub 10 nm particles downstream of the PMP system.

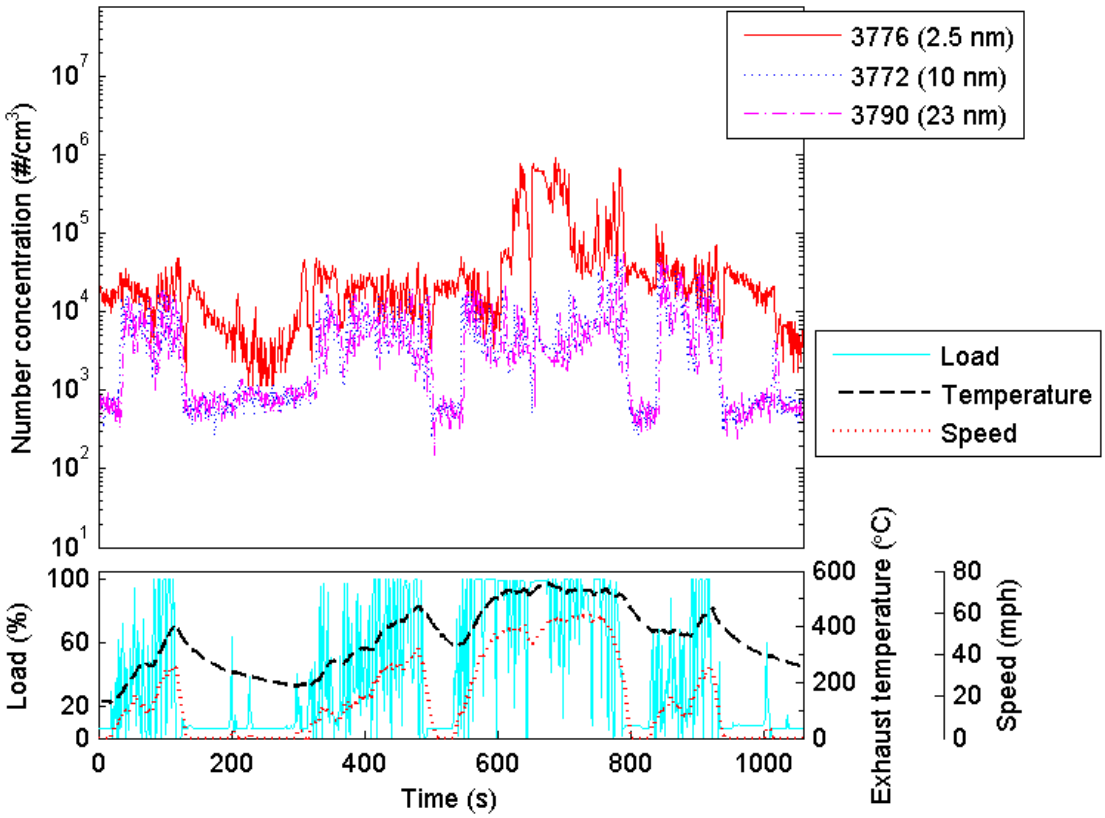

Figure 5.3: Real-time PN concentrations during the UDDS test.

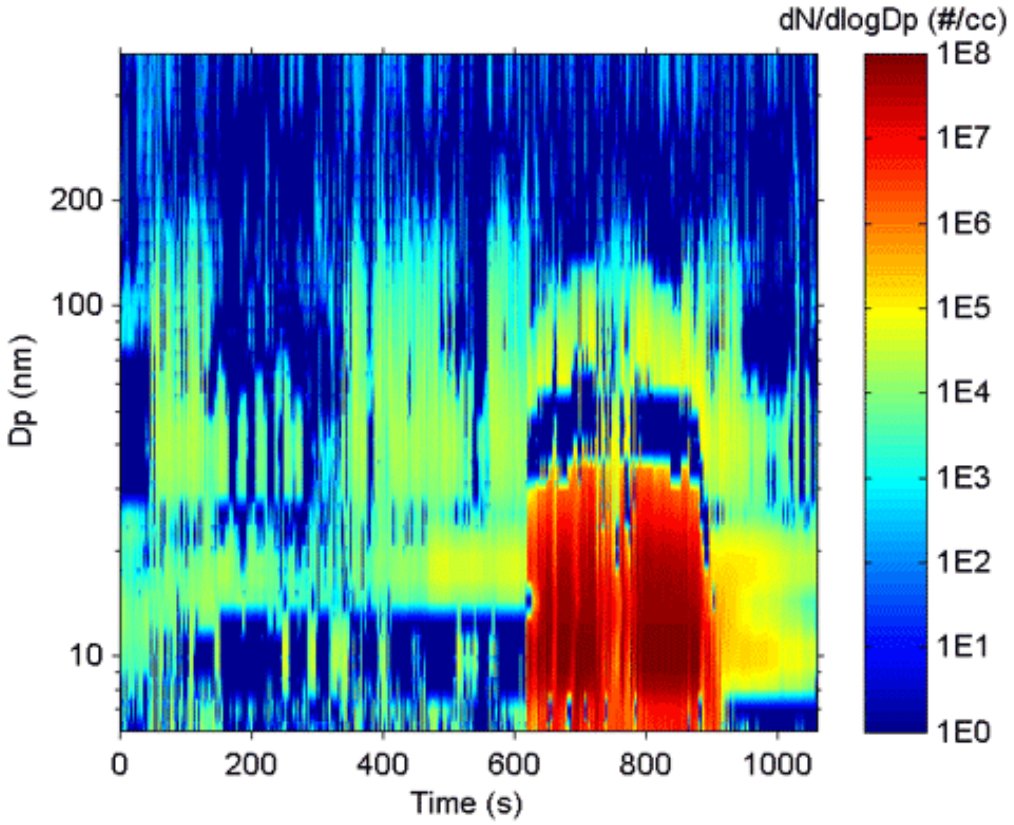

Figure 5.4: Particle size distributions contour in the CVS during the UDDS test.

When the concentrations of the two high cut-off diameter CPCs, the CPC 3772_10 and CPC 3790_23, were relatively high, the differences between the CPC 3776_2.5 and the high cut-off diameter CPCs were generally small. This is due to the competing process between the nucleation of volatile vapors to form new particles and the condensation of volatile vapors onto existing solid soot particles downstream of the PMP system. When more solid soot particles are available (as indicated by the relatively high concentrations of the CPC 3772_10 and CPC 3790_23), more condensation onto existing soot particles will occur, resulting in lower volatile vapor concentrations, and hence less re-nucleated sub 10 nm particles (as indicated by the relatively small differences between the CPC 3776_2.5 concentrations and the CPC 3772_10 and CPC 3790_23 concentrations). Between t = 600 and 800 seconds, though, the CPC 3776_2.5 concentrations were about 2 orders of magnitude higher than the CPC 3772_10 and CPC 3790_23 concentrations, even when the accumulation soot particle concentrations were relatively high. This phenomenon is most likely caused by the extremely high volatile vapor concentrations downstream of the PMP system, which in turn is due to the extremely high concentrations of nucleation mode particles in the CVS tunnel during this period of time, as measured by the EEPS and shown in Figure 5.4.

Figure 5.5 shows the real-time PN concentrations downstream of the PMP system for the on-road flow-of-traffic driving test. Speed, engine load, and exhaust temperature are also shown in Figure 5.5. The dashed horizontal line in Figure 5.5 is the PMP dilution corrected saturation limit of the CPC 3772_10 and CPC 3790_23. The CPC 3772_10 reached its saturation limit during some time periods of phases 1 and 2. The CPC 3790_23 also saturated for a very short period of time during phase 1. It is

worth mentioning that the concentrations of the CPC 3772_10 and CPC 3790_23 are underestimated during the saturation. The CPC 3776_2.5 was under its saturation limit throughout the entire test.

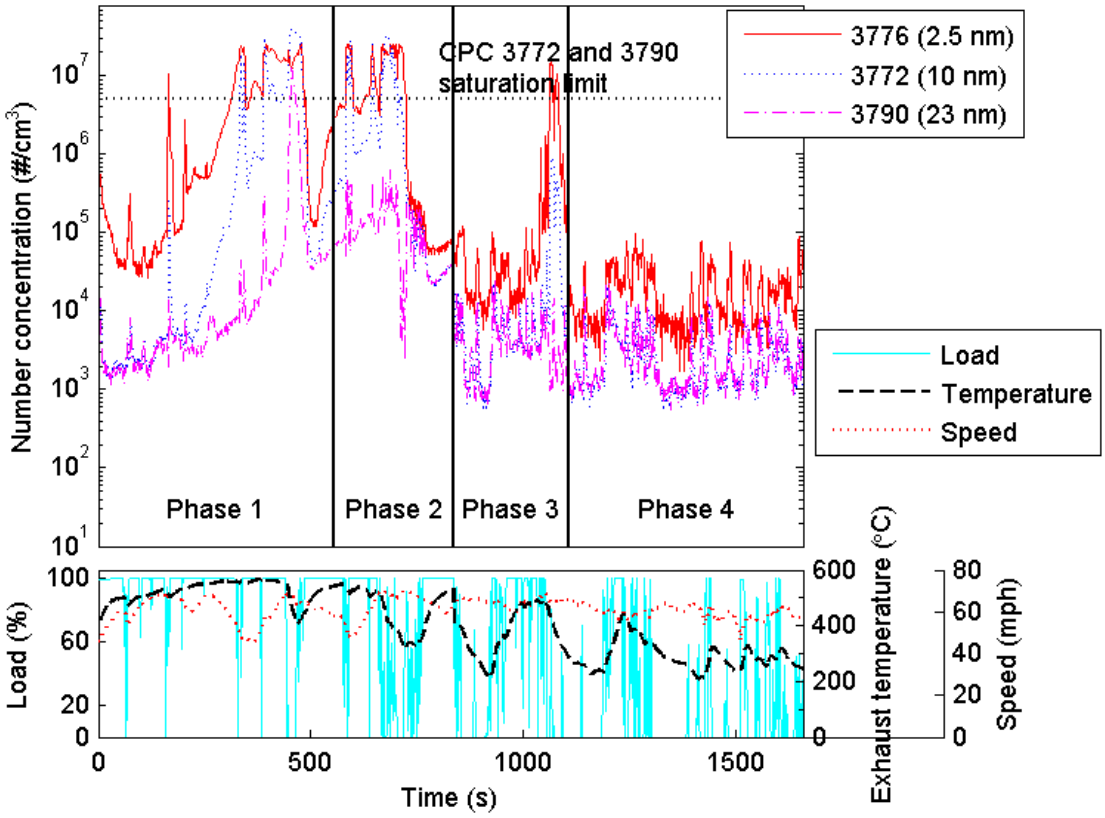

Figure 5.5: Real-time PN concentrations for the on-road flow-of-traffic diriving test.

The CPC 3776_2.5 concentrations were always higher than the CPC 3772_10 and CPC 3790_23 concentrations, which was expected and consistent with the UDDS results. The CPC 3772_10 and CPC 3790_23 agreed well at the beginning of phase 1. As the test proceeded, however, the CPC 3772_10 began to rise relative to the CPC 3790_23 and approach the CPC 3776_2.5. This is attributed to the excessive condensational growth of the re-nucleated particles downstream of the PMP system caused by an increase of the nucleation mode particle concentrations in the CVS, as measured

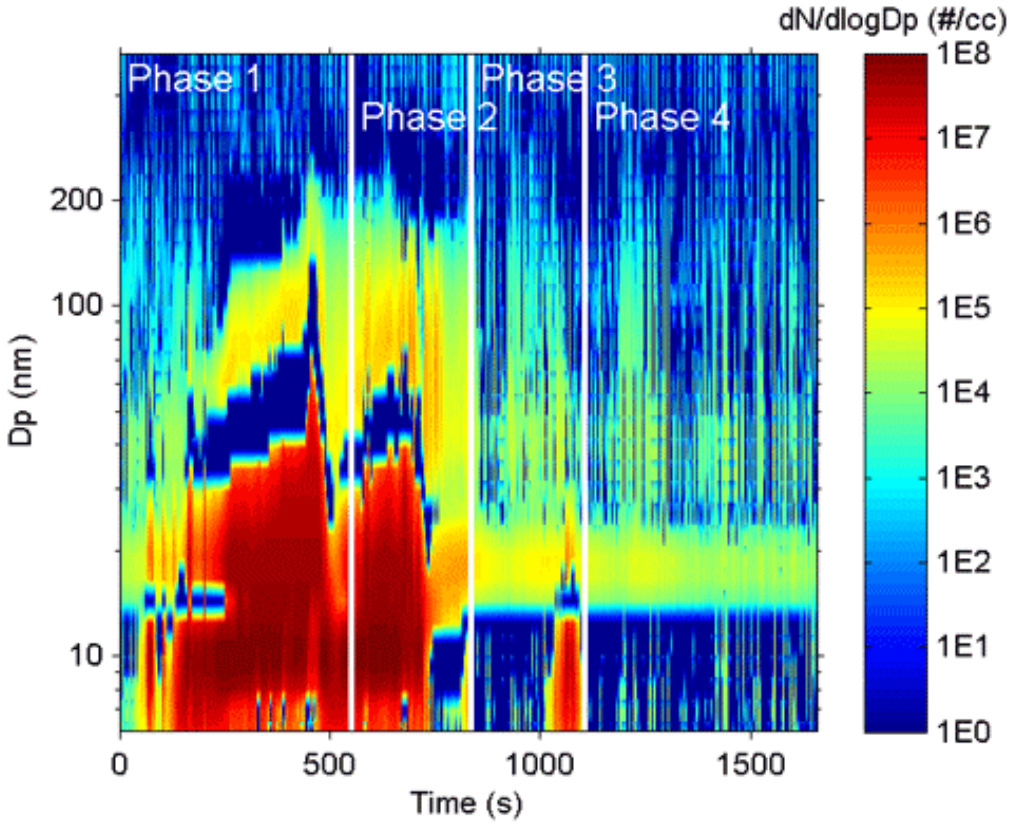

Figure 5.6: Particle size distributions contour in the CVS during the on-road test.

by the EEPS (Figure 5.6). Following their formation through nucleation downstream of the PMP system, particles begin to grow through condensation. If enough volatile vapors are available downstream of the PMP system, caused by high concentrations of the nucleation mode particles in the CVS, the re-nucleated particles will grow to larger than 10 nm and be detected by the CPC 3772_10, which will cause the CPC 3772_10 concentrations to increase relative to both the CPC 3790_23 and the CPC 3776_2.5. The CPC 3772_10 and CPC 3790_23 tracked well again from the end of phase 2 through phases 3 and 4 to the end of the entire test, except for the time period around t = 1050 second, where the excessive growth of the re-nucleated particles downstream of the PMP system was observed again. This excessive growth episode corresponded to high concentrations of nucleation mode particles in the CVS as well (Figure 5.6).

5.4.2 Integrated PM mass and PN emissions

Figure 5.7 shows the average engine loads and average exhaust temperatures for the on-road and UDDS tests. The average engine loads were 88, 72, 40, and 18%, for phases 1, 2, 3, and 4 of the on-road test, respectively. The average exhaust temperatures were 505, 466, 357, and 266°C, for phases 1, 2, 3, and 4, respectively. The average engine load and average exhaust temperature for the UDDS test were 38% and 352°C, respectively, both of which were comparable to those of the phase 3 of the on-road test, which represents downhill driving with an overall road grade of about -1%.

The PM mass and PN emissions for the UDDS test and the four phases of the on-road test are shown in Figure 5.8. Note the left y-axis (PN emissions) is on a logarithmic scale while the right y-axis (PM mass emissions) is on a linear scale to improve the readability of the figure. It should be noted that for the PM mass and PN emissions, an

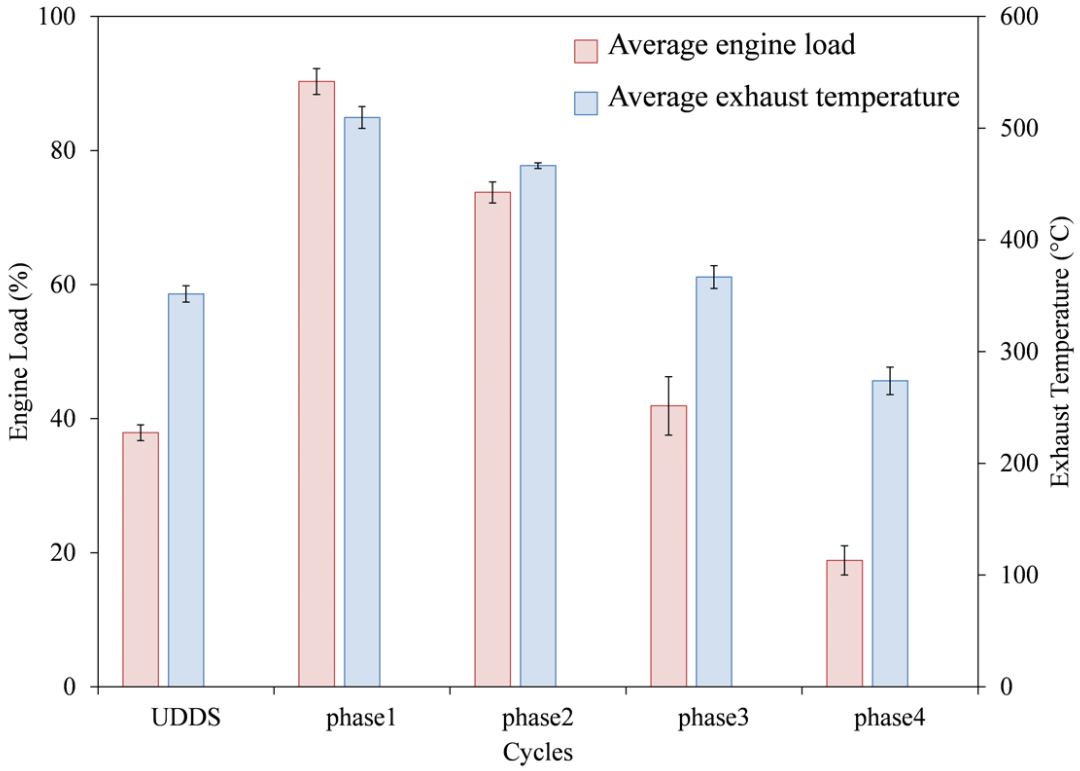

Figure 5.7: Average engine loads and exhaust temperatures for the UDDS and on-road tests.

outlier was identified for the on-road flow-of-traffic test using Dixon's Q test [58] with 99% confidence limits. This outlier was excluded from the calculations presented in this paper. Total PM mass emissions are composed of nucleation mode particles (< 30 nm) and accumulation mode particles (> 30 nm). The total PM mass emissions were dominated by the nucleation mode particles for the UDDS and uphill driving conditions (phases 1 and 2) of the on-road test and by the accumulation mode particles for the downhill driving conditions (phases 3 and 4) of the on-road test. The dominance of nucleation mode particles for the UDDS and uphill driving conditions is most likely due to high sulfur oxide (SO_3) formation at high exhaust temperatures [40]. It should be noted that some of the EEPS channels in the nucleation mode size range were saturated during the UDDS and uphill driving conditions (i.e., phases 1 and 2) of the on-road test. In other words, the PM mass emissions of nucleation mode particles for the UDDS and phases 1 and 2 were underestimated.

Total PM mass emissions for both the UDDS and on-road tests were more than 6 times lower than U.S. 2007 heavy-duty PM mass standard, 13.4 mg/kWh. This is consistent with a previous study using the same engine and aftertreatment system [27] and with other engine studies [59]. The total PM mass emissions for the UDDS test were $\sim$6 times higher than those from the downhill driving conditions (i.e., phases 3 and 4) but $\sim$3 times lower than those from the uphill driving conditions (i.e., phases 1 and 2). On the other hand, the accumulation mode PM mass emissions for the UDDS were comparable to those from phase 3, which has a similar average engine load to the UDDS, and were 33% less than those from phase 4, which has an lower average engine load than the UDDS and phase 3.

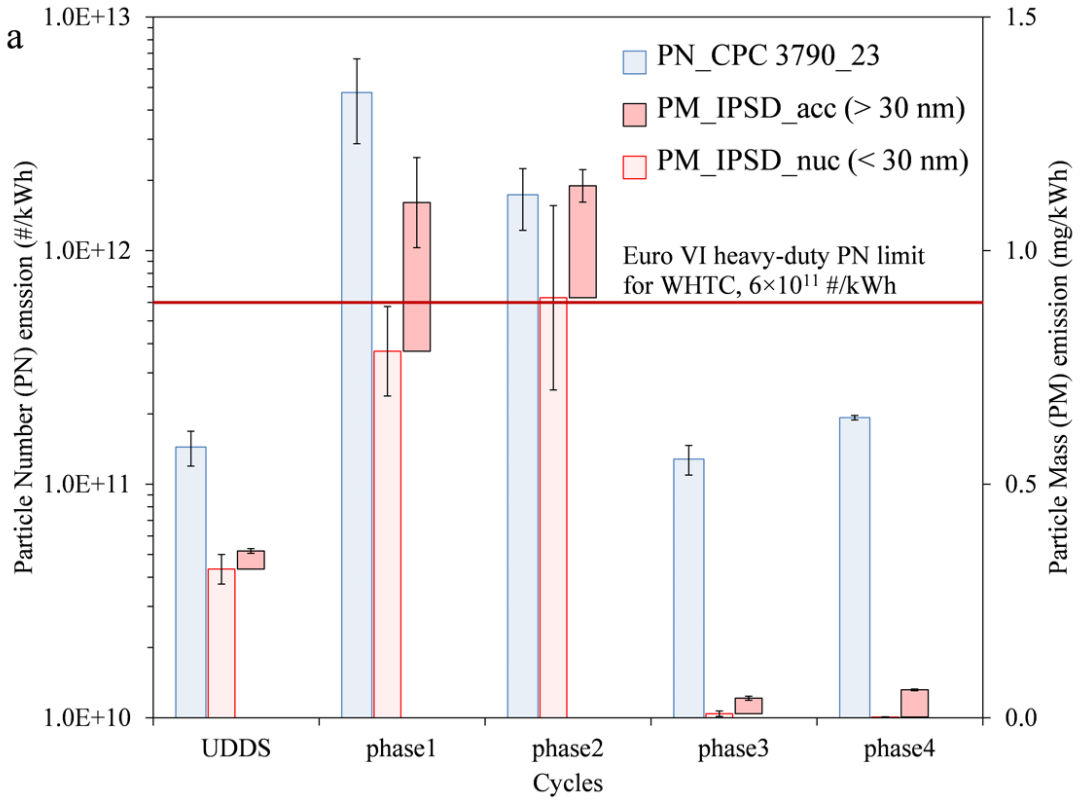

Figure 5.8: Integrated PM mass and PN emissions for the UDDS and on-road tests.

For comparison, PN emissions of particles larger than 23 nm for the UDDS and the downhill driving conditions (i.e., phases 3 and 4) were ∼3 times lower than the Euro VI heavy-duty PN limit for the transient cycle (i.e., WHTC), 6×10^{11} particles/kWh. On the other hand, PN emissions of particles larger than 23 nm for the uphill driving conditions (i.e., phases 1 and 2) of the on-road test were ∼3 to 7 times higher than the Euro VI PN limit. Similar to the accumulation mode PM emissions, PN emissions of particles larger than 23 nm for the UDDS (with the average engine load of 38%) were comparable in magnitude to those for phase 3 of the on-road test, and were 25% lower than those for phase 4 of the on-road test.

5.4.3 Test repeatability

Good repeatability is one of the necessary requirements for any regulatory measurement method. In Europe, repeatability and reproducibility have been the two main properties that both the PMP inter-laboratory correlation exercise and round robin test aimed to evaluate [3]. The Heavy-duty Inter-laboratory Correlation Exercise (ILCE_HD) [60] showed a PN repeatability ranging from 20 to 61% and a PM mass repeatability ranging from 35 to 56% for CVS measurements.

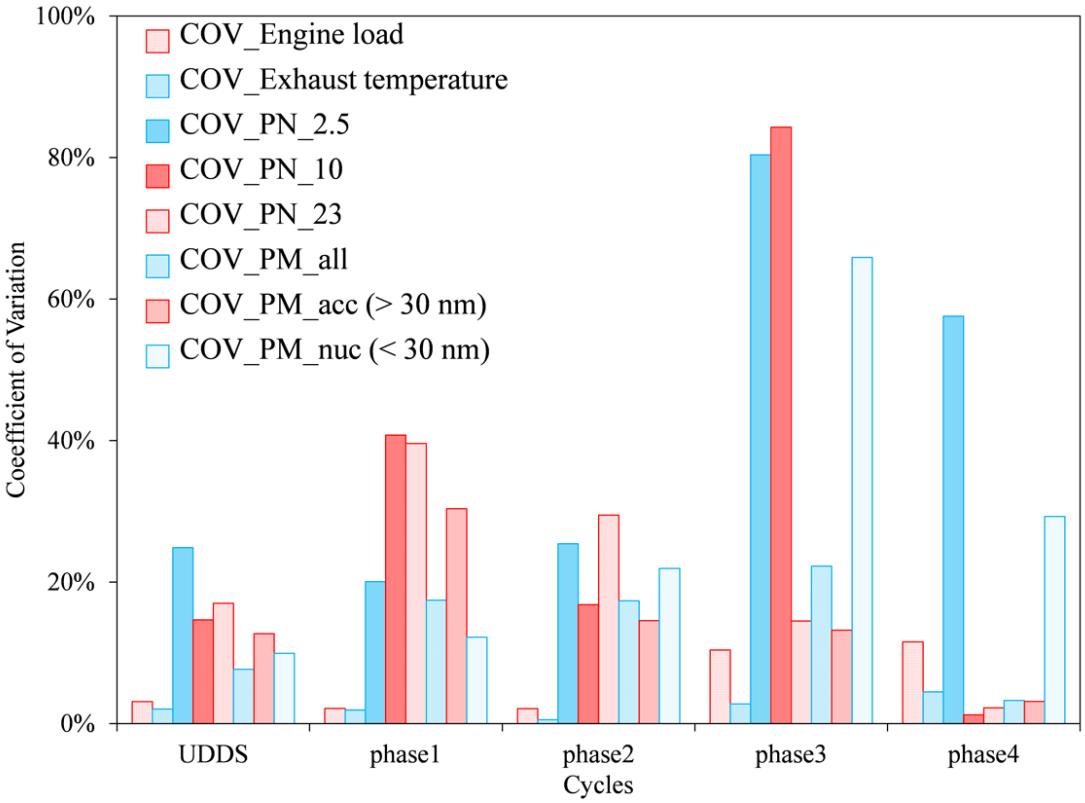

Figure 5.9: Coefficients of variations for the UDDS and on-road tests.

The coefficients of variation (COVs) of average engine loads, average exhaust temperatures, PM mass emissions of accumulation mode particles (COV_PM_acc), total PM mass emissions (COV_PM_all), PN emissions of particles larger than 23 nm

(COV_PN_23), and PN emissions of particles larger than 2.5 nm (COV_PN_2.5) are shown in Figure 5.9. The COVs of the PN emissions of particles larger than 10 nm (COV_PN_10) and of the PM mass emissions of nucleation mode particles (COV_PM_nuc) are also included in Figure 5.9 for completeness. COV_PM_all, COV_PM_acc, and COV_PM_nuc are all measurements from the CVS tunnel, with COV_PM_all representing the variability of both the nucleation and accumulation mode particles and COV_PM_acc representing the variability of the accumulation mode particles in the CVS tunnel, which is upstream of the PMP system. On the other hand, the COV_PN_2.5 represents the variability of both the nucleation and accumulation mode particles and the COV_PN_23 represents the variability of the accumulation mode particles downstream of the PMP system. Therefore, it is interesting to compare the COV_PM_all and COV_PN_2.5 and the COV_PM_acc and COV_PN_23.

For both the UDDS and on-road tests, the variabilities of both nucleation and accumulation mode particles downstream of the PMP system were usually slightly larger than those upstream of the PMP system (i.e., in the CVS tunnel). The COV_PN_23 values were 40, 30, 13, 10, and 18% for phases 1, 2, 3, 4, and UDDS, respectively. In contrast, the COV_PM_acc values were 31, 14, 13, 5, and 13% for phases 1, 2, 3, 4, and UDDS, respectively. The relatively large values of the COV_PN_23 and COV_PM_acc for phases 1 and 2 were likely associated with the elevated levels of DPF regeneration during phases 1 and 2, which can be attributed to the high exhaust temperatures. The COV_PN_2.5 values were 20, 24, 80, 50, and 25% for phases 1, 2, 3, 4, and UDDS, respectively. On the other hand, the COV_PM_all values were 18, 16, 21, 5, and 9% for phases 1, 2, 3, 4, and UDDS, respectively. Phase 3 had the largest COV_PN_2.5

and COV_PM_all values. This was attributed to the spike of sub 23 nm particle concentrations around t = 1050 second (Figure 5.5). The COV_PN_23 for both the UDDS and on-road tests were comparable to the PN emissions variability of the PMP ILCE_HD [60].

Both the UDDS and on-road tests were repeatable in terms of engine parameters. The COVs of the average engine loads and average exhaust temperatures for the UDDS and on-road tests were all below 5%, except the COVs of the average engine loads for phases 3 and 4 of the on-road test, which were 10 and 12%, respectively.

6 Summary

A European PMP compliant particle measurement system, the APC, and an alternative system for removing volatile particles, the CS, were evaluated and compared using laboratory-generated model volatile particles and diluted exhaust of a DPF-equipped, heavy-duty diesel vehicle operated on a heavy-duty chassis dynamometer and on-road in chapters 2 and 3. The goal of this study was to investigate and characterize particles found downstream of the PMP system, with an emphasis on sub 23 nm particles. The well-controlled laboratory experiments provided an important link to the vehicle exhaust testing by evaluating the formation and volatility of the sub 23 nm particles downstream of the APC. The laboratory tests were conducted with pure sulfuric acid and hydrocarbon aerosols separately, and then with mixed sulfuric acid/hydrocarbon aerosols.

Particles were found below the APC and CS for both the laboratory and the chassis tests. In the laboratory tests, the APC and CS eliminated 98.9 to 99.9% of the input particles by total particle number. The remaining particles downstream of the APC were almost entirely volatile when aerosols generated from pure sulfuric acid or pure tetracosane were used. However, for tests where particles were generated using a mixture of sulfuric acid and hydrocarbons, 12–14% of the particles downstream of the APC were non-volatile, and appeared-to-be formed in the APC. The temperature of the evaporation tube in the APC fluctuated by ± 5°C about its 350°C set point, in a roughly sinusoidal manner, and under some conditions in both laboratory and chassis tests, par-

ticle concentrations downstream of the APC fluctuated by up to a factor of two or more at the same frequency, suggesting that a highly nonlinear process like nucleation was responsible.

For the two steady state cycles tested on the chassis dynamometer, particle number concentrations between 3 and 10 nm downstream the APC were $\sim$2 and 7 times higher than the number concentrations of particles above 10 nm at the 74 and 26% engine load, respectively. At the 26% engine load, number concentrations of the 3 to 10 nm particles downstream the APC were more than half an order of magnitude higher than the total (volatile plus solid) number concentration in the dilution tunnel, demonstrating the APC was making 3 to 10 nm particles.

The CS showed much less of a tendency to form particles downstream than the APC, but still appeared to form particles in the 3 to 10 nm range under some conditions. During the higher load chassis test the APC did not appear to be making particles between 10 and 23 nm. For these conditions, the number concentrations of particles above 10 nm downstream the CS were about 40% less than number concentrations of particles above 23 nm downstream the APC, which was mainly due to the expected thermophoretic losses in the CS.

Chapter 4 evaluated the performance of the European PMP methodology for the measurement of solid particle number under different driving conditions. The testing was conducted using a heavy-duty vehicle equipped with a passive DPF and CE-CERT's Mobile Emissions Laboratory (MEL). Emissions measurements were conducted over a series of standard driving cycles, including the UDDS and the motorway cruise segment of the European ETC cycle, as well as under two on-road, flow-of-traffic conditions.

For the ETC motorway cycle, a nucleation event was observed in the CVS near the beginning of the cycle that was attributed to the acceleration prior to starting the test cycle. These nucleation mode particles rapidly decreased as the cycle continued but decreased in size to smaller than 6 nm. Nucleation mode particles smaller than 6 nm were also observed in the CVS during the more transient UDDS cycle. During the route 1 flow-of-traffic test, where the average engine load was higher than that of the standard testing cycle, total particle number concentrations in the CVS were dominated by the nucleation mode particles. For the same flow-of-traffic test, accumulation mode particle concentrations were orders of magnitude higher than those of the standard testing cycles.

Overall, particle concentrations measured by the PMP compliant CPC (model 3790 with a cut-off diameter of 23 nm) corresponded well with different engine loads and accumulation mode particle concentrations for all the testing cycles conducted. The CPCs with cut-off diameters of 11 nm tracked well with the CPC with the cut-off diameter of 23 nm downstream of the PMP systems indicating limited numbers of particles between 11 and 23 nm. However, CPCs with the smallest cut-off diameter of 3 nm always measured higher concentrations than other CPCs, showing the presence of a significant number of sub 11 nm particles downstream of the PMP systems. Two different PMP systems used in this study showed no distinguishable difference in terms of CPC responses.

We hypothesize that the majority of the particles in the sub 11 nm size range were formed from re-nucleation of vaporized semivolatile particles in the ET and were not truly solid, as indicated by the reduced number concentration of sub 11 nm particles

downstream of the PMP system at an elevated PMP dilution ratio. It is worth mentioning that a follow-up study by Zheng et al. [43], which includes more fundamental experiments, did show that some truly solid particles can be formed in the ET from mixtures of semivolatile hydrocarbon and sulfuric acid particles. During a UDDS cycle, when the ET temperature was increased from 300 to 500°C, no difference in particle number concentrations was observed, suggesting incomplete evaporation of semivolatile particles did not contribute to those sub 11 nm particles. It was shown by a calculation based on metal particle emission factors from Hu et al. [46] that worst case metal ash particle concentrations would be $\sim$2 orders of magnitude less than the total particle number concentrations downstream of the PMP system, suggesting these particles were not solid particles with ash origin.

During the route 1 flow-of-traffic test, a sudden jump of about 2 orders of magnitude in particle number concentrations measured by the PMP compliant CPC was observed. This was attributed to the extensive growth of the re-nucleated artifact particles downstream of the PMP systems, which in turn was associated with a very high concentration of hydrocarbons in the exhaust. Although there concentrations are well above typical operating conditions for the PMP, this also suggests that quantifying solid particle concentrations in situations where very high semivolatile particle concentrations might be found, such as regeneration, could be challenging.

Chapter 5 compared PM mass and PN emissions from a heavy-duty diesel vehicle operating under on-road flow-of-traffic driving conditions and the UDDS. The average engine loads for the on-road test were 88, 72, 40, and 18% for phases 1, 2, 3, and 4, respectively. Phases 1 and 2 were uphill driving and phases 3 and 4 were downhill

driving. The UDDS test was comparable to the phase 3 in terms of average engine load and average exhaust temperature.

Real-time PN emissions results showed the presence of re-nucleated sub 10 nm particles, but negligible numbers of particles between 10 and 23 nm downstream of the PMP system, for both the UDDS and on-road tests. For the uphill driving conditions of the on-road test, the re-nucleated particles downstream of the PMP system can even grow to larger than 10 nm by condensation of volatile vapors. All the re-nucleated particles downstream of the PMP system were smaller than 10 nm for the UDDS and downhill driving conditions of the on-road test.

The total PM mass emissions for the UDDS test were between those for the uphill and downhill driving conditions. Uphill segments of the on-road test showed the highest PN emissions. PN emissions of particles larger than 23 nm for the UDDS were comparable in magnitude to those for the phase 3 downhill segment of the on-road test, and were 25% lower than those for the phase 4 downhill segment of the on-road test.

The presence of sub 23 nm particles downstream of the PMP poses challenges if the cut off diameter for the PMP protocol were to be reduced to count ash particles or if the PMP were to be applied more broadly to other sectors for measuring solid particles. This study provides evidence that the majority of sub 23 nm particles found in previous studies and the current study are artifact particles formed by renucleation of semivolatiles. Based on the current study, these artifact particles are mainly present below 10 nm, suggesting that artifact formation would not be as great if the cut off diameter of the PMP was only lowered to 10 nm. Overall, more study is needed to find

ways to further reduce or eliminate artifact formation under the PMP methodology for broader applications.

Bibliography

[1] M. Matti Maricq. Chemical characterization of particulate emissions from diesel engines: A review. *Journal of Aerosol Science*, 38(11):1079–1118, 2007.

[2] David B. Kittelson. Engines and nanoparticles: a review. *Journal of Aerosol Science*, 29(5-6):575–588, 1998.

[3] Barouch Giechaskiel, Athanasios Mamakos, Jon Andersson, Panagiota Dilara, Giorgio Martini, Wolfgang Schindler, and Alexander Bergmann. Measurement of automotive non-volatile particle number emissions within the european legislative framework: A review. *Aerosol Sci. Technol*, In press., 2012.

[4] EPA. Health assessment document for diesel engine exhaust. Technical report, 2002.

[5] C. A. Pope, B. Young, and D. W. Dockery. Health effects of fine particulate air pollution: lines that connect. *Journal of the Air & Waste Management Association*, 56(6):709–742, 2006.

[6] GÃijnter OberdÃűrster. Pulmonary effects of inhaled ultrafine particles. *International Archives of Occupational and Environmental Health*, 74(1):1–8, 2000.

[7] GÃijnter OberdÃűrster, Z. Sharp, V. Atudorei, A. Elder, R. Gelein, W. Kreyling, and C. Cox. Translocation of inhaled ultrafine particles to the brain. *Inhalation Toxicology*, 16(6-7):437–445, 2004.

[8] David B. Kittelson, Winthrop F. Watts, and Jason H. Johnson. Diesel aerosol sampling methodology - crc e-43. Technical report, 2002.

[9] EPA. 40 Code of Federal Regulations, part 1065., 2011.

[10] H. Burtscher. Physical characterization of particulate emissions from diesel engines: a review. *Journal of Aerosol Science*, 36(7):896–932, 2005.

[11] UNECE. Uniform provisions concerning the measures to be taken against the emission of gaseous and particulate pollutants from compressionignition engines for use in vehicles, and the emission of gaseous pollutants from positive-ignition engines fuelled with natural gas or liquefied petroleum gas for use in vehicle. Revision 5, Amendment 1, Addendum 48: Regulation No. 49, May 2011.

[12] UNECE. Uniform provisions concerning the approval of vehicles with regard to the emission of pollutants according to engine fuel requirements. Revision 4, Addendum 82: Regulation No. 83, April 2011.

[13] EC. Implementing and amending regulation (ec) no 715/2007 of the european parliament and of the council on type-approval of motor vehicles with respect to emissions from light passenger and commercial vehicles (euro 5 and euro 6) and on access to vehicle repair and maintenance information. Commission Regulation (EC) No 692/2008, July 2008.

[14] EC. Implementing and amending regulation (ec) no 595/2009 of the european parliament and of the council with respect to emissions from heavy duty vehicles (euro vi) and amending annexes i and iii to directive 2007/46/ec of the european parliament and of the council. Commission Regulation (EC) No 582/2011, 2011.

[15] J. P. Shi and R. M. Harrison. Investigation of ultrafine particle formation during diesel exhaust dilution. *Environmental Science & Technology*, 33(21):3730–3736, 1999.

[16] Andrea De Filippo and M. Matti Maricq. Diesel nucleation mode particles: semivolatile or solid? *Environmental Science & Technology*, 42(21):7957–7962, 2008.

[17] D. B. Kittelson, W. F. Watts, and J. P. Johnson. On-road and laboratory evaluation of combustion aerosols-part1: summary of diesel engine results. *Journal of Aerosol Science*, 37(8):913–930, 2006.

[18] Tero Lahde, Topi Ronkko, Annele Virtanen, Tanja J. Schuck, Liisa Pirjola, Kaarle Hameri, Markku Kulmala, Frank Arnold, Dieter Rothe, and Jorma Keskinen. Heavy duty diesel engine exhaust aerosol particle and ion measurements. *Environmental Science & Technology*, 43(1):163–168, 2009.

[19] Tero Lahde, Topi Ronkko, Annele Virtanen, Anu Solla, Matti Kyto, Christer Soderstrom, and Jorma Keskinen. Dependence between nonvolatile nucleation mode particle and soot number concentrations in an egr equipped heavy-duty diesel engine exhaust. *Environmental Science & Technology*, 44(8):3175–3180, 2010.

[20] T.Topi Ronkko, Annele Virtanen, Jonna Kannosto, Jorma Keskinen, Maija Lappi, and Liisa Pirjola. Nucleation mode particles with a nonvolatile core in the exhaust of a heavy duty diesel vehicle. *Environmental Science & Technology*, 41(18): 6384–6389, 2007.

[21] N Bukowiecki P Cohn C Huglin M Mohr U Matter S Nyeki V Schmatloch N Streit E Weingartner H Burtscher, U Baltensperger. Separation of volatile and non-volatile aerosol fractions by thermodesorption: instrumental development and applications. *Journal of Aerosol Science*, 32(4):427–442, 2001.

[22] Giorgio Martini, Barouch Giechaskiel, and Panagiota Dilara. Future european emission standards for vehicles: the importance of the un-ece particle measurement programme. *Biomarkers*, 14(s1):29–33, 2009.

[23] Barouch Giechaskiel, Martin Cresnoverh, Herwig JÃČÂűrgl, and Alexander Bergmann. Calibration and accuracy of a particle number measurement system. *Measurement Science and Technology*, 21(4):045102, 2010.

[24] J. T. Gidney, M. V. Twigg, and D. B. Kittelson. Effect of organometallic fuel additives on nanoparticle emissions from a gasoline passenger car. *Environmental Science & Technology*, 44(7):2562–2569, 2010.

[25] Jan Czerwinski, Pierre Comte, Bo Larsen, Giorgio Martini, and Andreas Mayer. Research on particle emissions of modern 2-stroke scooters. *SAE*, 2006-01-1078, 2006.

[26] J. D. Herner, W. H. Robertson, and A. Ayala. Investigation of ultrafine particle number measurements from a clean diesel truck using the european pmp protocol. *SAE*, 2007-01-1114, 2007.

[27] Kent C. Johnson, Thomas D. Durbin, Heejung Jung, Ajay Chaudhary, David R. Cocker, Jorn D. Herner, William H. Robertson, Tao Huai, Alberto Ayala, and David Kittelson. Evaluation of the european pmp methodologies during on-road and chassis dynamometer testing for dpf equipped heavy-duty diesel vehicles. *Aerosol Science and Technology*, 43(10):962 – 969, 2009.

[28] Barouch Giechaskiel, Massimo Carriero, Giorgio Martini, and Jon Andersson. Heavy duty particle measurement programme (pmp): exploratory work for the definition of the test protocol. *SAE*, 2009-01-1767, 2009.

[29] I. S. Abdul-Khalek and D. B. Kittelson. Real time measurement of volatile and solid exhaust particles using a catalytic stripper. *SAE*, 950236, 1995.

[30] D. B. Kittelson, W. F. Watts, J. C. Savstrom, and J. P. Johnson. Influence of a catalytic stripper on the response of real time aerosol instruments to diesel exhaust aerosol. *Journal of Aerosol Science*, 36(9):1089–1107, 2005.

[31] Kihong Park, David B. Kittelson, and Peter H. McMurry. A closure study of aerosol mass concentration measurements: comparison of values obtained with filters and by direct measurements of mass distributions. *Atmospheric Environment*, 37(9-10):1223–1230, 2003.

[32] Jacob Swanson and David Kittelson. Evaluation of thermal denuder and catalytic stripper methods for solid particle measurements. *Journal of Aerosol Science*, 41 (12):1113–1122, 2010.

[33] Jacob Swanson and David B. Kittelson. Alternatives to the gravimetric method for quantification of diesel particulate matter near the lower level of detection. *Journal of the Air & Waste Management Association (1995)*, 60(10):1177–1191, 2010.

[34] B. Giechaskiel, R. Chirico, P. F. DeCarlo, M. Clairotte, T. Adam, G. Martini, M. F. Heringa, R. Richter, A. S. H. Prevot, U. Baltensperger, and C. Astorga. Evaluation of the particle measurement programme (pmp) protocol to remove the vehicles' exhaust aerosol volatile phase. *Science of The Total Environment*, 408(21):5106–5116, 2010.

[35] M. Stenitzer. Nano particle formation in the exhaust of internal combustion engines. Master's thesis, Technischen UniversitÃČÂd'tWien, 2003.

[36] S. Biswas, V. Verma, J. J. Schauer, F. R. Cassee, A. K. Cho, and C. Sioutas. Oxidative potential of semi-volatile and non volatile particulate matter (pm) from heavy-duty vehicles retrofitted with emission control technologies. *Environmental Science & Technology*, 43(10):3905–3912, 2009.

[37] B. Giechaskiel and Y. Drossinos. Theoretical investigation of volatile removal efficiency of particle number measurement systems. *SAE*, 2010-01-1304, 2010.

[38] Robert L. Burwell, Robert B. Scott, Lucien G. Maury, and Allen S. Hussey. The action of 96*Journal of the American Chemical Society*, 76(22):5822–5827, 1954.

[39] David R. Cocker, Sandip D. Shah, Kent Johnson, J. Wayne Miller, and Joseph M. Norbeck. Development and application of a mobile laboratory for measuring emissions from diesel engines. 1. regulated gaseous emissions. *Environmental Science & Technology*, 38(7):2182–2189, 2004.

[40] Jorn Dinh Herner, Shaohua Hu, William H. Robertson, Tao Huai, M. C. Oliver Chang, Paul Rieger, and Alberto Ayala. Effect of advanced aftertreatment for pm and nox reduction on heavy-duty diesel engine ultrafine particle emissions. *Environmental Science & Technology*, 45(6):2413–2419, 2011.

[41] B. J. Cooper and J. E. Thoss. Role of no in diesel particulate emission control. *SAE*, 890404, 1989.

[42] Thomas D. Durbin, Heejung Jung, David R. Cocker, Kent Johnson, and Ajay Chaudhary. Evaluation of the proposed new european methodology for determination of particle number emissions and its potential in california for in-use screening. Technical report, California Air Resources Board, 2008.

[43] Zhongqing Zheng, Kent C. Johnson, Zhihua Liu, Thomas D. Durbin, Shaohua Hu, Tao Huai, David B. Kittelson, and Heejung S. Jung. Investigation of solid particle number measurement: Existence and nature of sub-23 nm particles under pmp methodology. *Journal of Aerosol Science*, 42(12):883–897, 2011.

[44] John H. Seinfeld and Spyros N. Pandis. *Atmospheric Chemistry and Physics: From Air Pollution to Climate Change*. John Wiley & Sons, Inc., second edition edition, 2006.

[45] Maik Bergmann, Volker Scheer, Rainer Vogt, and Thorsten Benter. Comparison of the performance of real-time pm mass and number instrumentation for vehicle exhaust measurements. *SAE International*, 2007-24-0116, 2007.

[46] S. Hu, J. D. Herner, M. Shafer, W. Robertson, J. J. Schauer, H. Dwyer, J. Collins, T. Huai, and A. Ayala. Metals emitted from heavy-duty diesel vehicles equipped with advanced pm and nox emission controls. *Atmospheric Environment*, 43(18): 2950–2959, 2009.

[47] M. Grose, H. Sakurai, J. Savstrom, M. R. Stolzenburg, W. F. Watts Jr, C. G. Morgan, I. P. Murray, M. V. Twigg, D. B. Kittelson, and P. H. McMurry. Chemical and

physical properties of ultrafine diesel exhaust particles sampled downstream of a catalytic trap. *Environmental Science & Technology*, 40(17):5502–5507, 2006.

[48] I. Abdul-Khalek, D. Kittelson, and F. Brear. The influence of dilution conditions on diesel exhaust particle size distribution measurements. *SAE transactions*, 108 (4):563–571, 1999.

[49] I. Abdul-Khalek, D. B. Kittelson, and F. Brear. Nanoparticle growth during dilution and cooling of diesel exhaust: Experimental investigation and theoretical assessment. 2000-01-0515, 2000.

[50] Q. Wei, D. B. Kittelson, and W. F. Watts. Single-stage dilution tunnel performance. *SAE Tech. Pap. Ser*, 2:001–01, 2001.

[51] TSI. Model 3025a ultrafine condensation particle counter instruction manual. Technical report, 2002.

[52] TSI, 2012. personal communication.

[53] Harry Dwyer, Alberto Ayala, Sherry Zhang, John Collins, Tao Huai, John Herner, and Wilson Chau. Emissions from a diesel car during regeneration of an active diesel particulate filter. *Journal of Aerosol Science*, 41(6):541–552, 2010.

[54] Athanasios Mamakos and Giorgio Martini. Particle number emissions during regeneration of dpf-quipped light duty diesel vehicles a literature survey. Technical report, European Commission Joint Research Centre, 2011.

[55] Zhongqing Zheng, Thomas D. Durbin, Georgios Karavalakis, Kent C. Johnson, Ajay Chaudhary, David R. Cocker III, Jorn D. Herner, William H. Robertson, Tao Huai, Alberto Ayala, David B. Kittelson, and Heejung S. Jung. Nature of sub 23 nm particles in the solid particle measurement method: a real time data perspective. *Aerosol Science & Technology*, In press., 2012.

[56] Z. G. Liu, V. N. Vasys, M. E. Dettmann, J. J. Schauer, D. B. Kittelson, and J. Swanson. Comparison of strategies for the measurement of mass emissions from diesel engines emitting ultra-low levels of particulate matter. *Aerosol Science and Technology*, 43(11):1142–1152, 2009.

[57] M. M. Maricq and N. Xu. The effective density and fractal dimension of soot particles from premixed flames and motor vehicle exhaust. *Journal of Aerosol Science*, 35(10):1251–1274, 2004.

[58] Vic Barnett and Toby Lewis. *Outliers in Statistical Data*. Wiley Series in Probability & Statistics. Wiley & Sons, third edition, 1994.

[59] Imad A. Khalek. 2007 diesel particulate measurement research. final report. crc project e-66-phase 1. Technical report, Coordinating Research Council, 2005.

[60] JRC. Particle measurement programme (pmp) heavy-duty inter-laboratory correlation exercise (ilce_hd) final report. Technical report, JRC, 2010.